Signaling pathways as linear transmitters

Harry Nunns and Lea Goentoro

Division of Biology and Biological Engineering

California Institute of Technology, Pasadena, CA 91125

Correspondence: hnunns@caltech.edu, goentoro@caltech.edu

Abstract

One challenge in biology is to make sense of the complexity of biological networks. A good system to approach this is signaling pathways, whose well-characterized molecular details allow us to relate the internal processes of each pathway to their input-output behavior. In this study, we analyzed mathematical models of three metazoan signaling pathways: the canonical Wnt, ERK, and Tgfβ pathways. We find an unexpected convergence: the three pathways behave in some physiological contexts as linear signal transmitters. Testing the results experimentally, we present direct measurements of linear input-output behavior in the Wnt and ERK pathways. Analytics from each model further reveal that linearity arises through different means in each pathway, which we tested experimentally in the Wnt and ERK pathways. Linearity is a desired property in engineering where it facilitates fidelity and superposition in signal transmission. Our findings illustrate how cells tune different complex networks to converge on the same behavior.

Introduction

Cells must continually sense, interpret, and respond to their environment. This is orchestrated by signaling pathways: networks of multiple proteins that transmit signals and initiate cellular response. Signaling pathways are critical to animal development and physiology, and yet there are fewer than 20 classes of metazoan signaling pathways (1). These signaling pathways evolved prior to the Cambrian, and remain highly conserved across animal phyla (1, 2). Each signaling pathway, therefore, governs a wide range of cellular events, both within and across organisms.

Insights into the versatility of signaling pathways may be gleaned from pathway architectures. Indeed, distinct architectural features define each pathway. Studies over the past several decades have revealed distinct signaling capabilities that arise from pathway architecture, *e.g.*, all-or-none response in the ERK pathway (3, 4), oscillations in the NFκB pathway (5), or asymmetrical cell signaling in the Notch/Delta pathway (6). Alternatively, analysis of pathway architectures may also reveal shared signaling capabilities that emerge from the distinct architectures, pointing to a fundamental property that pathways have converged upon despite their separate evolutionary trajectories. In this study, we sought to identify shared properties between conserved signaling pathways.

To this end, we examined three signaling pathways, the canonical Wnt, ERK and Tgfβ pathways. These pathways are activated by an extracellular ligand binding to a membrane receptor (Figure 1A). The ligand-receptor activation initiates a series of biochemical reactions

within the cell, culminating in a buildup of transcriptional regulator, which regulates transcription of broad gene targets. Since the ligand-receptor module is relatively plastic across organisms (*e.g.* flies have one EGF receptor whereas humans have four (7)), we focused on the conserved core pathway (Figure 1A). We define the input to the core pathway as the ligand-receptor activation, and the output as the level of transcriptional regulator.

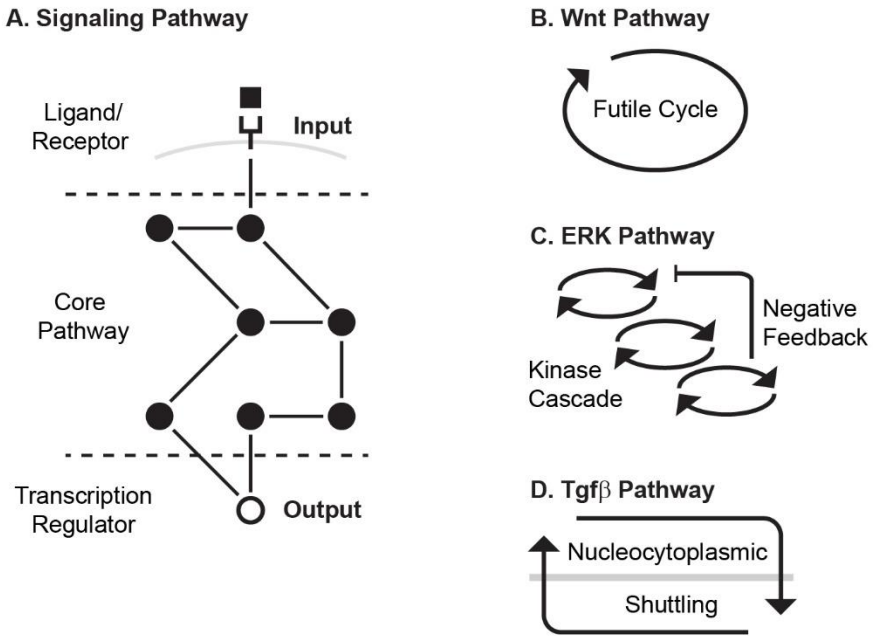

Figure 1. (A) Signaling pathways transmit inputs from ligand-receptor interaction to a change in output, the level of transcriptional regulator (white circle). **(B-D)** The core pathway for each metazoan signaling pathway is defined by distinct architectural features. In the Wnt pathway **(B)**, the output is regulated by a futile cycle of continual synthesis and rapid degradation. In the ERK pathway **(C)**, the output is regulated by a kinase cascade coupled to negative feedback. In the Tgfβ pathway **(D)**, the output is regulated through continual nucleocytoplasmic shuttling.

The Wnt, ERK, and Tgfβ pathways transmit input using different core transmission architecture (Figure 1B-D). In the Wnt pathway, signal transmission is characterized by a futile cycle of synthesis and rapid degradation (8-10). Ligand-receptor input diminishes the degradation arm of this cycle, leading to accumulation of β-catenin output (8, 11, 12). In the ERK pathway, signal transmission is characterized by a cascade of phosphorylation events coupled to feedbacks, leading to an increase in phosphorylated ERK output (13-16). Finally, signal transmission in the Tgfβ pathway is characterized by continual nucleocytoplasmic protein shuttling (17-21). Ligand-receptor input effectively increases the rate of nuclear import, leading to an increase in output, the nuclear Smad complex (22).

Importantly for our approach, the architectures of the three pathways are captured by mathematical models that have been refined by years of experiments. Although by no means complete, the mathematical models have track records of success in predicting systems-level behaviors across multiple biological systems. For instance, the Wnt model (23) captures the dynamics of destruction complex well enough as to enable prediction of robustness in fold-change response (24) and the differential roles of the two scaffolds in the pathway (23); the ERK model (3, 25-27) captures the ultrasensitivity in the phosphorylation cascade (3); and the Tgfβ model (22) reveals the roles of nucleocytoplasmic shuttling in transducing the duration and intensity of ligand stimulation (22).

We studied these mathematical models to identify what, if any, behaviors converge across pathways. The Wnt (23), ERK (27), and Tgfβ (22) models consist of 7, 26, and 10 coupled, nonlinear ODEs, respectively, with 22, 46, and 13 parameters. Because of their large

sizes, they are typically solved numerically to simulate experimental observations and generate new predictions. However, for the questions posed here, we found that numerical simulations are not sufficient. Rather, we needed analytics to uncover exactly how the pathway behaviors depend on the underlying biochemical processes. While we previously derived an analytical solution to the Wnt pathway (24), analytical treatment of the Tgfβ and ERK pathways has not been attempted due to the complex, nonlinear equations involved. To address this problem, we employed various analytical techniques, including graph theory-based variable elimination and dimensional analysis, to derive analytical or semi-analytical solutions to the steady-state output of each pathway. Our analysis, along with subsequent experimental verification, reveals a striking convergence across the Wnt, Tgfβ, and ERK pathways: cells operate in the parameter regime where the complex, nonlinear interactions in each pathway give rise to linear signal transmission.

Results

Mathematical analysis identifies the Wnt, ERK, and Tgfβ pathway as linear transmitters

We began our analysis using established models of the Wnt (23), ERK (27), and Tgfβ (22) pathways. These models capture the salient features of each pathway, and include biochemical details such as synthesis, degradation, binding, dissociation and post-translational modifications. In all the models, biochemical parameters have been directly measured or fitted to kinetic measurements from cell, embryo or extract systems. Numerical simulation of each model has predicted a wide range of pathway behaviors over the years (*e.g.* Wnt refs. (23, 24, 28); ERK

refs. (3, 4, 26, 27, 29); Tgfβ refs. (22, 30-33)). Below, we describe our analysis of each pathway and the unifying behavior that emerges from all three pathways.

Canonical Wnt Pathway. In this pathway, cells sense ligand-receptor input by monitoring β-catenin protein (8, 11, 12, 34, 35). β-catenin is continually synthesized and rapidly degraded by a large destruction complex, comprised of multiple proteins including APC, Axin, and GSK3β. The destruction complex binds and phosphorylates β-catenin, tagging it for degradation by the ubiquitin/proteosome machinery (8, 11). Wnt ligands, through binding to Frizzled and LRP receptors, inhibit the destruction complex, leading to accumulation of β-catenin. β-catenin then regulates the expression of broad target genes (11, 12).

The model of the Wnt pathway (Figure 2A) was published in 2003 by a collaboration between the Kirschner and Heinrich labs (23). The Wnt model consists of 7 nonlinear differential equations and 22 parameters. Applying dimensional analysis, we previously derived the analytical solution to β-catenin concentration at steady-state (24):

$$[\beta\mathrm{cat}]_{ss} = K_{17} \cdot \frac{1-\gamma+\frac{\alpha}{u}}{2}\left(\sqrt{1+\frac{4\gamma}{\left(1-\gamma+\frac{\alpha}{u}\right)^2}}-1\right) \quad 1]$$

$$\alpha = \frac{k_4 k_6 k_9 v_{14} \cdot GSK3_{tot} \cdot APC_{tot}}{k_5 k_{-6} K_7 K_8 k_{13} k_{15}} \quad 2]$$

$$\gamma = \frac{v_{12}}{k_{13} K_{17}} \quad 3]$$

where the input function $u = u(Wnt)$ is the rate of inhibition of the destruction complex via Dishevelled, a function of ligand-receptor activation. As illustrated in Figure 2A, K_i's are equilibrium dissociation constants, k_i's are rate constants, and v_i's are synthesis rates. α and γ in Eq. **1** are dimensionless parameter groups defined in Eqs. **2** and **3**: α characterizes β-catenin degradation by the destruction complex, and γ characterizes the extent to which β-catenin binds to APC independently of the destruction complex.

Eq. **1** demonstrates that, in general, β-catenin concentration is a nonlinear function of the input u. Many parameters of the model were directly measured in *Xenopus* extracts, and the remaining calculated from measurements in the same system (Appendix 1 - Table 1). In this study, we examined how the analytical solution (Eq. **1**) behaves with these measured parameters. The measured parameters (Appendix 1 - Table 1) indicate that $\alpha \sim 66$, $\gamma \sim 1.4$, and for maximal stimulation, $u \sim 6.0$. The large α reflects how β-catenin stability is primarily dictated by the destruction complex, *i.e.*, $\alpha/u \gg 1$ means that non-Axin dependent degradation is minimal, and $\alpha/u \gg \gamma$ means that the positive feedback from sequestration by APC is minimal. Indeed, the rapid action of the destruction complex in the Wnt pathway is a recurring observation across biological systems (8-10). With $\alpha/u \gg 1 + \gamma$, Eq. **1** simplifies to

$$[\beta cat]_{ss} \approx K_{17} \frac{\gamma}{\alpha} u \qquad 4]$$

with detailed derivations presented in the SI. Therefore, within physiologically relevant parameter values, the steady-state β-catenin concentration becomes a linear function of the input u (red line, Figure 2D). The linear input-output relationship holds for the entire dynamic range of the model, until the system saturates at maximal stimulation (u = 6). We confirmed that the

numerical solution of the full model matches the analytical solution in Eq. **4** (blue line, Figure 2D), and that the response becomes nonlinear when α is decreased, breaking the requirement $\alpha/u \gg 1 + \gamma$ (grey line, Figure 2D).

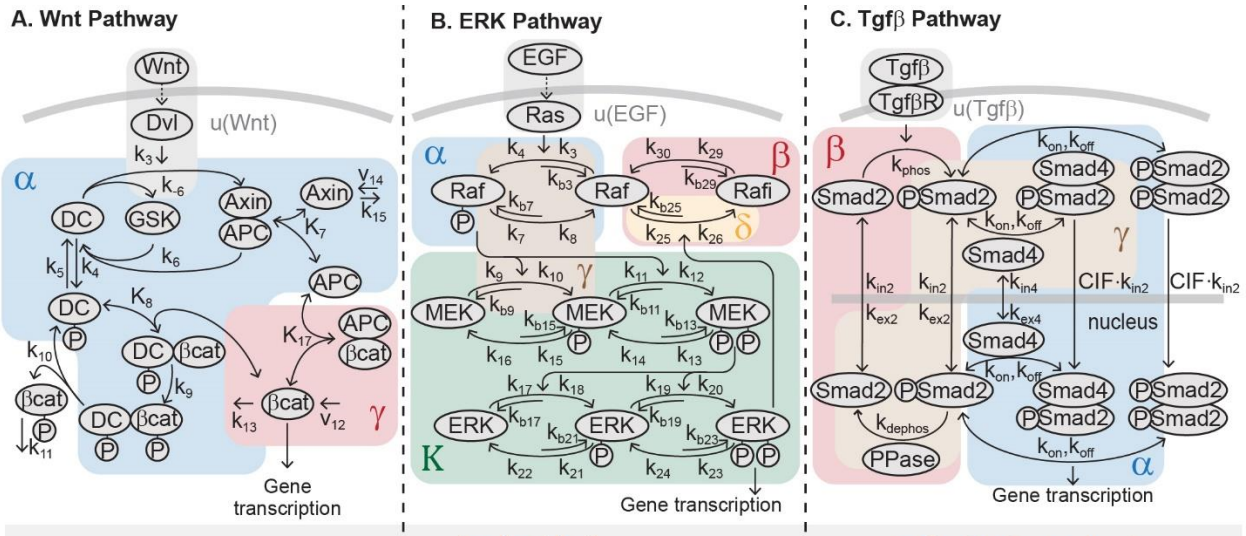

Parameter groups:

$$\alpha = \frac{k_4 k_6 k_9 v_{14} \cdot GSK3_{tot} \cdot APC_{tot}}{k_5 k_{-6} K_7 K_8 k_{13} k_{15}}$$

$$\gamma = \frac{v_{12}}{k_{13} K_{17}}$$

Linearity with:

futile cycle: $\frac{\alpha}{(1+\gamma)\cdot u} \gg 1$

$$[\beta cat]_{ss} \approx K_{17}\frac{\gamma}{\alpha}\cdot u(Wnt)$$

$$\alpha = \frac{k_3\cdot(k_8+k_{b7})}{k_7\cdot[P1]_{ss}\cdot k_8} + \cdots$$

$$\beta = \frac{k_{25}\cdot(k_{30}+k_{b29}+k_{29}\cdot[P4]_{ss})}{k_{29}\cdot[P4]_{ss}\cdot k_{30}} + \cdots$$

$$\gamma = \frac{k_3\cdot(k_8+k_{b7})\cdot k_9\cdot[MEK]_{ss}}{k_7\cdot[P1]_{ss}\cdot k_8\cdot k_{10}} + \cdots$$

$$\delta = \frac{k_{26}+k_{b25}}{k_{26}} + \cdots \quad K = \frac{d\ln([dpERK]_{ss})}{d\ln([pRaf]_{ss})}$$

ultrasensitivity & negative feedback:

$K \gg 1 \qquad \frac{\beta\cdot[dpERK]_{ss}}{(\alpha+\gamma)\cdot u+\delta} \sim 1$

$$[dpERK]_{ss} \approx \frac{\alpha}{\beta}\cdot\frac{Raf_{tot}}{R_s}\cdot u(EGF) - \frac{\delta}{\beta}$$

$$\alpha = \frac{a\cdot(k_{on}[S4n]_{ss} + a\cdot k_{ex2})}{k_{off}} + \cdots$$

$$\beta = \frac{PPase\cdot k_{dephos}}{k_{phos}\cdot R_{tot}\cdot\frac{k_{ex2}}{a\cdot k_{ex2}+k_{in2}}} + \cdots$$

$$\gamma = a\cdot(a\cdot k_{ex2} + PPase\cdot k_{dephos})\cdot\left(\frac{1}{a\cdot k_{ex2}}+\frac{1}{CIF\cdot k_{in2}}\right) + \cdots$$

continual shuttling: $\frac{\beta}{(\alpha+\gamma)\cdot u} \gg 1$

$$[S24n]_{ss} \approx a\cdot\frac{\alpha\cdot S2_{tot}}{\beta}\cdot u(Tgf\beta)$$

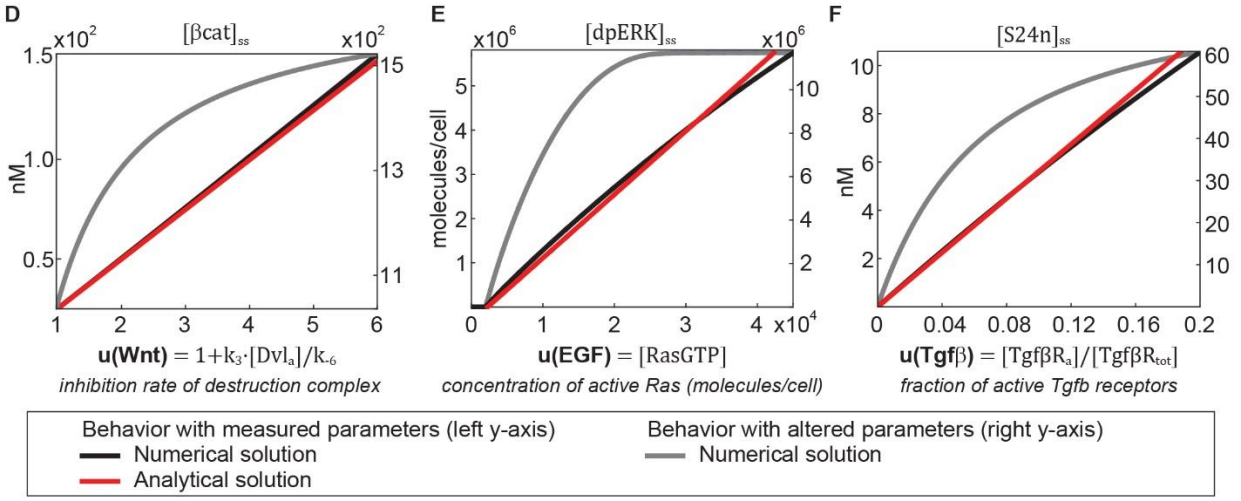

Figure 2. The Wnt, ERK, and Tgfβ pathways are linear signal transmitters. **(A-C)** Network diagrams of the signaling pathways. The Tgfβ diagram is modified from ref. (22). Below the network diagrams: the parameter groups and linearity equations we analytically derived in this study. Parameter groups and input functions are color-coded to the corresponding reactions in the network diagrams. Parameters that do not appear in the parameter groups either drop out due to irreversible reaction steps (such as k_{10} and k_{11} in the Wnt pathway) or negligible (as indicated by ellipses). **(D-F)** Our analysis reveals that in physiologically relevant parameter values, these pathways generate a linear input-output relationship. The outputs are β-catenin, dpERK, and nuclear Smad complex for the Wnt, ERK, and Tgfβ pathway, respectively. The input functions u describe the effect of ligand-receptor interactions on the core pathway. Specifically: u(Wnt) is the rate by which Dishevelled inhibits the destruction complex upon Wnt ligand activation, where k_3 and k_{-6} are defined in the figure and $[Dvl]_a$ is the concentration Wnt-activated Dishevelled (see Eqn. S2-4); u(EGF) is concentration of EGF-activated Ras (Ras-GTP); and u(Tgfβ) is the fraction of Tgfβ -activated receptors. Red and blue lines, respectively: analytical and numerical solutions with measured parameters (plotted against the left y-axis). Grey line: examples of numerical solutions outside measured parameters (plotted against the right y-axis).

Source codes for the numerical simulations in Figure 2D-F (grey and black lines) are available in Figure 2 – Source Code 1.

ERK Pathway. The unexpected linearity that emerges from the model of the Wnt pathway prompted us to wonder if such simplicity may be found in other pathways. Strikingly,

we observed the same linearity in the ERK and Tgfβ pathways. In the ERK pathway (Figure 2B), ligand-receptor input is transmitted via a cascade of protein phosphorylation (13, 14). In particular, ligand-receptor interactions activate Ras, which leads to membrane recruitment and phosphorylation of Raf. Phosphorylated Raf subsequently doubly-phosphorylates MEK, which in turn doubly-phosphorylates ERK (13). Doubly-phosphorylated ERK (dpERK) is a transcriptional regulator that affects a broad array of genes (14). The multi-step topology of the kinase cascade, combined with distributive phosphorylation of each kinase, gives rise to ultrasensitivity – first demonstrated in the seminal work by the Ferrell lab (3, 4). In other contexts, the pathway also exhibits a graded response (36-39) that is thought to arise from the incorporation of negative feedbacks (16), one of which is the inhibition of Raf by dpERK through hyper-phosphorylation of serine residues (27, 40, 41).

The ERK model (27) is the product of more than two decades of refinement (3, 4, 26, 27, 29). The model, which captures ultrasensitivity and Raf feedback, consists of 26 differential equations and 46 parameters. To derive an analytical expression for the ERK pathway, we used a variable elimination technique developed for networks of mass action kinetics (42). The technique utilizes an algebraic framework, linear elimination of variables, and mass conservation laws to parameterize steady-state in terms of core variables (described in SI). We derived an analytical relationship between the steady-state output of the pathway (dpERK) and the input to the phosphorylation cascade u:

$$[\mathrm{dpERK}]_{ss} = \frac{\alpha}{\beta} \cdot \left(\frac{\mathrm{Raf}_{tot}}{[\mathrm{pRaf}]_{ss}} - 1 - \frac{\gamma}{\alpha} \right) \cdot \mathrm{u} - \frac{\delta}{\beta} \qquad 5]$$

$$\alpha = \frac{k_3 \cdot (k_8 + k_{b7})}{k_7 \cdot [P1]_{ss} \cdot k_8} + \cdots \quad 6]$$

$$\beta = \frac{k_{25} \cdot (k_{30} + k_{b29} + k_{29} \cdot [P4]_{ss})}{k_{29} \cdot [P4]_{ss} \cdot k_{30}} + \cdots \quad 7]$$

$$\gamma = \frac{k_3 \cdot (k_8 + k_{b7}) \cdot k_9 \cdot [MEK]_{ss}}{k_7 \cdot [P1]_{ss} \cdot k_8 \cdot k_{10}} + \cdots \quad 8]$$

$$\delta = \frac{k_{26} + k_{b25}}{k_{26}} + \cdots \quad 9]$$

Detailed derivations of Eq. **5** are presented in the SI. The input $u = u(EGF)$ in Eq. **5** is the concentration of active Ras, which is activated via GTP loading at the ligand-receptor complex (13). The parameter groups α, β, γ, and δ in Eq. **5** are defined in Eqs. **6-9**, where the ellipses indicate additional small terms (expanded in SI). The relative magnitudes of α, β, γ, and δ indicate how the Raf pool partitions during signaling (Eqs. **S3.3, 11-13**). The dimensionless group $\alpha \cdot u$ relates to the amount of free, phosphorylated Raf (α, blue-shaded in Figure 2B), $\beta \cdot [dpERK]_{ss}$ describes the amount of Raf inhibited through negative feedback by dpERK (β, red-shaded in Figure 2B), δ relates to the amount of unphosphorylated (δ, blue-shaded in Figure 2B), and $\gamma \cdot u$ relates to the amount of phosphorylated Raf bound to other proteins (*e.g.*, to MEK, brown-shaded in Figure 2B). Eq. **5** is not a closed solution, as it includes the term $[pRaf]_{ss}$, and there are variables included in parameter groups α, β, γ. We confirmed that the parameter groups remain constant over the course of signaling (within 10%, Figure 2 – figure supplement 1), justifying treating the latter variables as parameters.

Next, we considered how the analytical expression (Eq. **5)** behaves within a specific parameter regime observed in experiments. First, experiments in several mammalian cell systems have shown that feedback is strong, such that a significant fraction of the Raf pool is inhibited (29, 40). This means that $\beta \cdot [\mathrm{dpERK}]_{ss} \sim (\alpha + \gamma) \cdot u + \delta$. Second, as has been observed in multiple contexts ((3, 4, 26, 27) Appendix 1 - Table 2), ERK phosphorylation is ultrasensitive to the amount of pRaf (the ultrasensitive cascade is shaded green in Figure 2B). Denoting K as the relative change of $[\mathrm{dpERK}]_{ss}$ with respect to $[\mathrm{pRaf}]_{ss}$, ultrasensitivity entails that $K \gg 1$. In this range, small changes in pRaf level have very large effects on dpERK level (*e.g.*, in model simulations, a 30% change in pRaf level results in a 900% change in dpERK level, Figure 2 – figure supplement 1). We find analytically that in the parameter regime where $\beta \cdot [\mathrm{dpERK}]_{ss} \sim (\alpha + \gamma) \cdot u + \delta$ and $K \gg 1$, the negative feedback holds the level of pRaf constant ($[\mathrm{pRaf}]_{ss} \approx R_s$, details in SI). With these two features, strong negative feedback and ultrasensitivity, dpERK becomes a linear function of the input u:

$$[\mathrm{dpERK}]_{ss} \approx \frac{\alpha}{\beta} \cdot \frac{\mathrm{Raf}_{tot}}{R_s} \cdot u - \frac{\delta}{\beta} \qquad 10]$$

The full derivation is given in the SI, and includes a toy model to illustrate the intuition for how ultrasensitivity combines with negative feedback to produce linearity. Eq. **10** is plotted in Figure 2E (red line). We confirmed that the numerical solution of the full model matches the analytics in Eq. **10**, and becomes nonlinear when the negative feedback is weakened (grey line, Figure 2E). Although the analytical expression describes up until 50% of ERK activation, we verified numerically that the predicted linearity extends to 93% of ERK activation (Figure 2 – figure supplement 2).

The linearity derived here applies across different dynamic ERK responses. The model we analyzed gives a sustained dpERK response. In some contexts, however, the ERK pathway shows a pulsatile response, which has been attributed to receptor desensitization (26). Using a larger model that includes details of receptor desensitization (26), we numerically verified that the linearity holds for pulsatile responses, *i.e.* the peak level of dpERK increases linearly with the peak level of u (Figure 2 - figure supplement 1).

Tgfβ Pathway. Finally, we examined signal transduction within the Tgfβ pathway (Figure 2C). In the Tgfβ pathway, input from ligand-receptor interactions is transmitted by the Smad proteins. There are several classes of Smad proteins, including the receptor-regulated Smads (R-Smads) and the common Smad (co-Smad or Smad4) (21). Ligand-activated receptors phosphorylate R-Smads. Phosphorylated R-Smads bind to the co-Smad, and shuttle into the nucleus and regulate broad target genes. In the nucleus, the Smad complex dissociates and R-Smads are constitutively de-phosphorylated and shuttled out to the cytoplasm, where the cycle of phosphorylation and complex formation begins again (22). This dynamic translocation in and out of the nucleus forms a continual nucleocytoplasmic shuttling of Smads, a known integral feature of the Tgfβ pathway (17-20).

The Tgfβ model (22) was published in 2008 by the Hill lab, and consists of 10 differential equations and 13 parameters. Even though the model was fitted to R-Smad2 data, the general architecture of signal transmission is conserved across all five R-Smads (21, 22). Using the variable elimination technique described before (42), we derived an analytical expression of the steady-state concentration of Smad complex in the nucleus:

$$[\mathrm{S24n}]_{ss} = \mathrm{a} \cdot \frac{\alpha \cdot \mathrm{u}}{(\alpha + \gamma) \cdot \mathrm{u} + \beta} \mathrm{S2}_{tot} \quad 11]$$

$$\alpha = \frac{\mathrm{a} \cdot (\mathrm{k}_{on}[\mathrm{S4n}]_{ss} + \mathrm{a} \cdot \mathrm{k}_{ex2})}{\mathrm{k}_{off}} + \cdots \quad 12]$$

$$\beta = \frac{\mathrm{PPase} \cdot \mathrm{k}_{dephos}}{\mathrm{k}_{phos} \cdot \mathrm{R}_{tot} \cdot \frac{\mathrm{k}_{ex2}}{\mathrm{a} \cdot \mathrm{k}_{ex2} + \mathrm{k}_{in2}}} + \cdots \quad 13]$$

$$\gamma = \mathrm{a} \cdot \left(\mathrm{a} \cdot \mathrm{k}_{ex2} + \mathrm{PPase} \cdot \mathrm{k}_{dephos}\right) \left(\frac{1}{\mathrm{a} \cdot \mathrm{k}_{ex2}} + \frac{1}{\mathrm{CIF} \cdot \mathrm{k}_{in2}}\right) + \cdots \quad 14]$$

In Eq. **11**, the input function $\mathrm{u} = \mathrm{u}(\mathrm{Tgf\beta})$ is the active fraction of Tgfβ receptors. The parameter a is the nucleocytoplasmic volume ratio. The dimensionless parameter groups α, β, and γ in Eq. **11** are defined in Eq. **12-14**, where the ellipses indicate additional small terms (expanded in SI). α, β, and γ describe how the Smad2 pool partitions during signaling (Eqs. **S4.2, 8, 9**): $\alpha \cdot \mathrm{u}$ relates to the amount of nuclear Smad complex (α, blue-shaded in Figure 2C, captures the parameters related to complex formation and translocation to the nucleus), β relates to the amount of free, unphosphorylated Smad2 (β, red-shaded in Figure 2C, captures the parameters related to complex dissociation and translocation to the cytoplasm), and $\gamma \cdot \mathrm{u}$ loosely relates to the remaining Smad2 pool (γ is brown-shaded in Figure 2C). Phosphorylated Smad2 quickly forms complex (43), so β essentially corresponds to total monomeric Smad2. Finally, Eq. **11** is not a closed solution, since variable $[\mathrm{S4n}]_{ss}$ appears in α. We numerically tested that it is constant within 2% for non-saturating inputs (Figure 2 – figure supplement 3), justifying treating it as a parameter.

As in the Wnt and ERK pathway, the analytical expression for nuclear Smad complex (Eq. **11)** allows us to see that the behavior dramatically simplifies with parameters observed in experiment. We consider the case for non-saturating inputs (u∼.1). Protein concentrations in the Tgfβ model were measured in human keratinocyte cells and the rate constants fitted to kinetic data measured in the cells (22). With the measured parameters (Appendix 1 - Table 3), we find that $\beta \sim 46$, $\alpha \cdot u \sim 1.5$, and $\gamma \cdot u \sim 0.7$. In this parameter regime, once Smad2 is imported to the nucleus, it is rapidly dephosphorylated and exported. Dynamic Smad2 translocation maintains monomeric Smad2 in excess to Smad complex ($\beta \gg (\alpha + \gamma) \cdot u$). and forms the continual nucleocytoplasmic shuttling that is characteristic of the Tgfβ pathway. Even under maximal Tgfβ stimulation, it has been estimated that phosphorylated Smad2 comprises only 36% of the Smad2 pool (20, 44). With $\beta \gg (\alpha + \gamma) \cdot u$, the first term in the denominator of Eq. **11** is small, and concentration of nuclear Smad complex becomes a linear function of input:

$$[S24n]_{ss} \approx a \cdot \frac{\alpha \cdot S2_{tot}}{\beta} \cdot u \qquad 15]$$

Eq. **15** is plotted in Figure 2F (red line), and we confirmed that numerical simulations recapitulates Eq. **15** (blue line, Figure 2F). Although the analytical solution is valid only for small values of u, we numerically verified that the predicted linearity holds for the entire range of input u (from 0 to 1, Figure 2 – figure supplement 2). We confirmed that the pathway becomes nonlinear when the R-Smad phosphatase is inhibited such that $\beta \sim (\alpha + \gamma) \cdot u$ (grey line, Figure 2F). While the model analyzed here gives a sustained Smad response, we verified numerically that the linearity holds for a larger model that includes receptor desensitization and gives a pulsatile Smad response (Figure 2 – figure supplement 3) (32).

Linearity in the Wnt and ERK pathways was observed experimentally

Analytical expressions for the Wnt, ERK, and Tgfβ pathways reveal that the three pathways behave as linear signal transmitters within parameter regimes measured in cells. To confirm the linearity, we directly measured the input-output relationships in human cell lines. We focused our efforts on the Wnt and ERK pathways, since we are limited by available antibodies in the Tgfβ pathway.

To analyze the canonical Wnt pathway, we performed quantitative Western blot measurements in RKO cells, a model system for Wnt signaling. To track the input, we measured the level of phosphorylated LRP5/6 receptors (on Ser1490), which increases within minutes of ligand-receptor complex formation (45). To track the output, we measured the level of β-catenin. We confirmed that the level of phosphorylated LRP5/6 and β-catenin increase upon Wnt simulation and reach steady-state within 6 hours (Figure 3 – figure supplement 1). Accordingly, all subsequent measurements were done at 6 hours after Wnt stimulation.

To measure the input-output relationship in the Wnt pathway, we treated RKO cells with varying doses of purified Wnt3A and measured how β-catenin (output) correlates with phosphorylated LRP (input). As shown in Figure 3A, the level of β-catenin increases linearly with the level of phosphorylated LRP. The linearity persists until saturation of the input, defined as 90% of maximal phosphorylated LRP response (blue circles, Figure 3A; Figure 3 – figure supplement 2). Notably, at high doses of Wnt3A, β-catenin continues to show incremental activation, despite saturation in phosphorylation of LRP (grey circles, Figure 3A). This can be

explained within some findings that, while Frizzled/LRP complex is the primary receptor input in β-catenin activation, β-catenin can be activated independently of LRP (*e.g.*, ref. (46)).

Consistent with the mathematical analysis, we observed in RKO cells that the Wnt pathway behaves as a linear transmitter throughout the dynamic range of the input. As a control that is expected from the Michaelis-Menten kinetics that describe ligand binding in the model, we confirmed that the linearity does not extend upstream to Wnt dose: both phospho-LRP5/6 and β-catenin show nonlinear response to Wnt dose (Figure 3 – figure supplement 2). Therefore, in the Wnt pathway, a nonlinear ligand-receptor processing step is followed by linear signal transmission through the core intracellular pathway.

Next, to measure the input-output relationship in the ERK pathway, we performed quantitative Western blots in H1299 cells, one of the model systems used in the field. Detecting the input level, EGF-activated Ras-GTP, requires a pull-down step that makes it less quantifiable. We therefore tested the dose of EGF ligand itself, since a previous study indicates there could be linearity in ligand-receptor processing (47). To track the output, we measured the level of doubly-phosphorylated ERK1/2 (on Thr202/Tyr204), dpERK. We first characterized the kinetics of response: dpERK peaks 5 minutes after EGF stimulation (Figure 3 – figure supplement 3), and saturates at 4ng/ml EGF (grey circles, Figure 3B). Accordingly, all subsequent measurements were performed at 5 minutes after EGF stimulation, and linearity was assessed over the input range of 0-4 ng/mL EGF (blue circles, Figure 3B).

We observed linearity in the input-output relationship of the ERK pathway, with the level of dpERK increasing linearly with EGF dose (Figure 3B). The linearity holds throughout the dynamic range of the system, over at least 12-fold activation of dpERK. As the ERK pathway is

sometime observed to show bimodal response that would be masked by bulk measurements, we confirmed that the H1299 cells indeed show to graded dpERK response in single-cell level (Figure 3 – figure supplement 4), in agreement with a previous single-cell, live imaging study (38). Therefore, as in the Wnt pathway, signals are transmitted linearly in the ERK pathway throughout the dynamic range of the cell. Moreover, the linearity in the ERK pathway is more extensive than in the Wnt pathway, as linearity extends all the way upstream, such that the level of dpERK directly reflects the dose of extracellular EGF ligand.

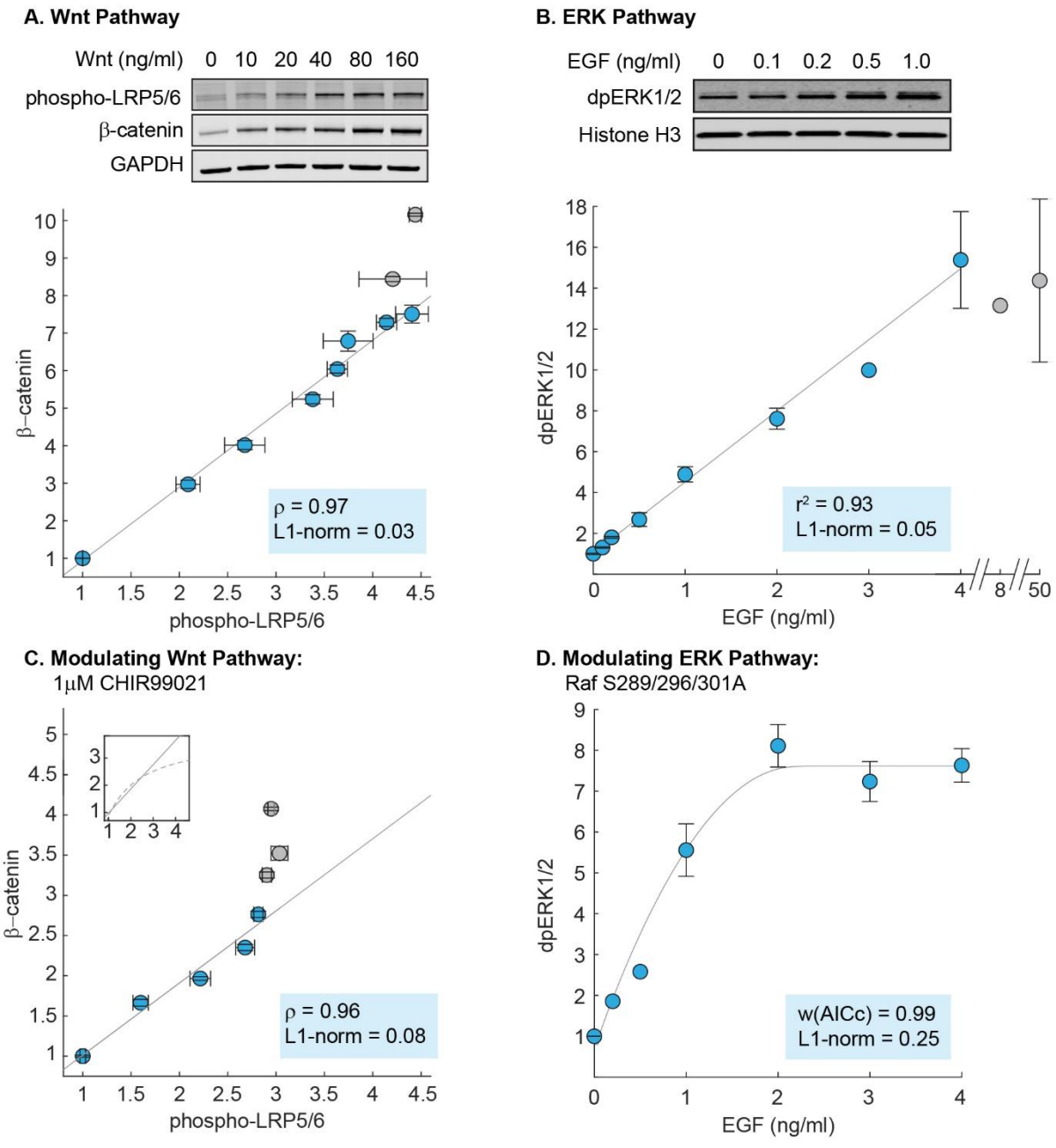

317

318 **Figure 3. (A)** Measurements of the input-output relationship in the Wnt pathway. In
319 these experiments, RKO cells were stimulated with 0-1280 ng/mL purified Wnt3A ligand,
320 harvested at 6 hours after ligand stimulation, and lysed for Western blot analyses. Shown on top
321 is a representative Western blot. The data plotted come from 7 independent experiments (total N

= 66). Each circle indicate the mean intensities of the phospho-LRP5/6 (x-axis) and β-catenin (y-axis) bands for all Western blot biological replicates, and error bars indicate the standard error of the mean. For each gel, we normalize the unstimulated sample (*i.e.*, 0 ng/mL of Wnt3A) to one, and scale the magnitude of the dose response to the average of all gels (described in Methods). The grey line is a least squares regression line, and ρ is the Pearson's coefficient, where ρ = 1 is a perfect positive linear correlation.

(B) Measurements of the input-output relationship in the ERK pathway. In these experiments, H1299 cells were stimulated with 0-50 ng/mL purified EGF ligand, harvested at 5 minutes after ligand stimulation, and lysed for Western blot analyses. Shown on top is a representative Western blot. The data plotted here come from 5 independent experiments (total N = 30). Each circle indicates the mean intensities of dpERK1/2 bands across Western blot biological replicates, and the error bars indicate standard error of the mean. Single replicates are plotted without error bars. All data is plotted relative to unstimulated sample. The grey line is a least squares regression line, and r^2 is the coefficient of correlation where $r^2 = 1$ is a perfect linear correlation.

(C) As in **(A)**, except that cells were treated with 1μM CHIR99021 (detailed in Methods). The data plotted here come from 5 independent experiments (total N=59). The grey line is a least squares regression , and ρ is the Pearson's coefficient, where ρ = 1 is a perfect positive linear correlation. Shown in the subplot are the same least squares regression line (solid line), overlaid with the model prediction (dashed line).

(D) As in **(B)**, but measurements were performed in H1299 cells expressing mutant Raf S289/296/301A. The data plotted here come from 3 independent experiments (total N = 15). The

grey line is a fit using the ERK model. We first fitted the gain of the model to the data (*i.e.*, the y-range), and afterward, varied the strength of dpERK feedback (k_{25}) to find the best fit. We used the weighted Akaike Information Criterion, w(AICc), to verify that the nonlinear fit from the ERK model outperforms a linear least squares fit (see Methods). $0 < w(AICc) < 1$, with higher w(AICc) indicates better performance by the non-linear fit.

In all figures, linearity was additionally assessed using the least absolute deviations, L1-norm (see Methods). L1-norm can range from 0 to 0.5, with L1-norm < 0.1 indicate a linear relationship. Blue vs grey circles in each figure are explained in the main text.

Source files of all Western blot gel images and numerical quantitation data are available in Figure 3 – Source Data 1.

Linearity in the Wnt and ERK pathways is modulated by perturbation to parameters

Finally, the analytical expressions we derived in this study not only reveal linear signal transmission, but also the mechanisms by which it arises. In the model of the Wnt pathway, linear transmission occurs due to the futile cycle of β-catenin, in the parameter regime where β-catenin is continually synthesized and rapidly degraded (*i.e.* $\alpha/u \gg 1 + \gamma$). This regime is not infinite: for instance, a ten-fold decrease in α (*e.g.* by inhibiting the destruction complex) will break the futile cycle (grey line, Figure 2D).

To test if the futile cycle is indeed required for linear signal transmission, we inhibited the destruction complex using CHIR99021, an inhibitor of GSK3β kinase. As before, we measured the input-output relationship, β-catenin vs. phospho-LRP5/6 level, up to 90% of

maximal phospho-LRP5/6 input (blue circles, Figure 3C). As expected, we found that inhibiting the destruction complex (decreasing α in the model) reduced the range of linearity. The non-treated cells (blue circles, Figure 3A) exhibit a linear input-output relationship over a 4.4-fold range of LRP input, whereas the CHIR-treated cells show a linear input-output relationship over only a 2.8-fold range of LRP input (blue circles, Figure 3C).

Further, our measurements also reveal an unexpected feature of the Wnt pathway. In the model, inhibiting GSK3β causes β-catenin response to become nonlinear for larger inputs (dashed line, Figure 3C subplot). In CHIR-treated RKO cells, however, this nonlinearity cannot be reached, as the maximal amount of phosphorylated LRP (input) is reduced by 50% (grey circles, Figure 3; Figure 3 – supplement figure 2), consistent with the dual-function of GSK3β identified by Zeng *et al.* (48, 49) in phosphorylating β-catenin for degradation as well as phosphorylation LRP for activation. Incorporating this dual-role of GSK3β into the model, we found that this expanded model can indeed recapitulate the data (Figure 2 –figure supplement 4) . Therefore, our data indicate two findings: first, that inhibiting GSK3β reduces the range of linear input-output behavior in the Wnt pathway, as predicted by our analytics, and second, that GSK3β co-regulation of β-catenin and LRP unexpectedly constrains the system within the linear regime.

Next, we examine the requirements for linearity in the ERK pathway. Eq. **10** reveals that linearity in the ERK pathway depends upon the coupling of strong nonlinearities – ultrasensitivity and negative feedback. As in the Wnt pathway, this regime is not infinite, *e.g.*, decreasing the strength of feedback β enables the system to exit the ultrasensitive regime, and therefore reduces linearity (grey line, Figure 2E).

To test this requirement, we examined the effects of weakening the negative feedback. We created a stable H1299 cell line expressing Raf S289/296/301A, a Raf-1 mutant in which three serine residues that are phosphorylated by dpERK are mutated to alanine (40, 41). Assessing the dynamic range of the input as before (0-4 ng/mL EGF), we now found that dpERK responds nonlinearly to EGF dose (blue circles, Figure 3D), consistent with model predictions (grey line, Figure 3D). As a control, we found that overexpressing WT Raf-1 to a similar level does not perturb linearity (experiments, Figure 3 – figure supplement 5; modeling, Figure 2 – figure supplement 1). Lastly, mutating all 5 direct ERK feedback sites on Raf-1 to alanine had a similar effect to Raf S289/296/301A (Figure 3 – figure supplement 6). Our results support the model requirement that strong negative feedback is critical to linear signal transmission in the ERK pathway.

Discussion

Our study suggests that the canonical Wnt pathway, the ERK pathway, and the Tgfβ pathway have converged upon a shared strategy of linear signal transmission. Our mathematical analysis reveals that, despite their distinct architectures, the three signaling pathways behave in some physiological contexts as linear transmitters. Not only is linearity is predicted within measured parameter regimes, the analysis shows that linearity is a property of the systems that occurs through a considerable range of parameters (Figure 2 – figure supplement 5, 6). We then showed direct measurements of the linear input-output relationship in the canonical Wnt and ERK pathway.

It would be interesting to further probe the generality of linear signal transmission. Linear behavior requires that single cells responds to ligand in a graded manner. Although there are reports of oscillatory or bimodality in signaling pathways, there are also multiple observations across biological contexts of single cells responding to ligand in a graded manner (Appendix 1 - Table 4). Besides the systems analyzed here, NF-κB is another signaling pathway that has been modeled rigorously (5, 50, 51). Numerical simulations of a well-established NF-κB model (50) over the range of nuclear NF-κB translocation observed in human epithelial cells (51) reveal that the peak of the nuclear NF-κB pulse correlates linearly with ligand concentration (Figure 2 – figure supplement 7). Finally, linearity extends beyond metazoan signaling pathways. In the yeast pheromone sensing pathway, a homolog of the ERK cascade, transcriptional output correlates linearly with receptor occupancy (52). The linearity is mediated by negative feedback by Fus3 acting on Sst2, a feedback that is not conserved in the mammalian ERK system. These further argue for linear signal transmission as a convergent property across independently evolving signaling pathways, as well as between conserved pathways that diverged 1.5 billion years ago.

What are potential advantages to linear signal transmission? Linearity is a feature of many engineering systems, where it serves several practical purposes. In particular, linear signal transmission enables the superposition of multiple signals, where the output of two simultaneous inputs is equal to the sum of the outputs for each input separately. Superposition enables multiple, dynamic signals to be faithfully transmitted and processed independently. Thus, for instance, linearity enables people to listen to a phone call and interpret speech amongst background noise, and allows a car radio to tune into one station out of multiple broadcasting on separate carrier frequencies. Notably, linearity is also a desired goal in synthetic biology, where

it is often implemented using negative feedback (53, 54). Analogous to engineered circuits, linearity in biological signaling pathways may facilitate multiplexing inputs into a single pathway (Figure 4A).

A second benefit is that linearity might underlie two phenomena that are increasingly found across signaling pathways. First, a linear transmitter naturally gives rise to dose-response alignment (55), where one or more downstream responses of a pathway closely follows the fraction of occupied receptor (Figure 4B). Dose response alignment appears in many biological systems and is thought to improve the fidelity of information transfer through signaling pathways (47, 52, 55, 56). Second, linearity facilitates fold change detection, where cells sense fold changes in signal, rather than absolute level, to buffer cellular noise (24, 38, 51, 57, 58). In linear input-output systems, the stimulated output correlates linearly to the basal output; thus, the fold-change in output is robust to variations in cellular parameters (Figure 4C). Indeed, for the signaling pathways studied here, it has been shown experimentally that the robust outcome of ligand stimulation is the fold-change in the level of transcriptional regulator (24, 38, 51, 58). Therefore, selecting for linearity may naturally confer the benefits of superposition, dose-response alignment, and a robust fold-change in output.

Interestingly, unlike synthetic circuits whose linearity is often designed to extend across multiple orders of magnitude (53, 59), the linearity we observed in the three natural pathways extends only one order of magnitude, which is also the dynamic range of the pathways. However, we know that natural pathways can convey inputs varying across multiple orders of magnitude, e.g., vision. Thus, an advantage of linearity in natural pathways may be

that, in conjunction with fold-change detection at the receptor-level (60), the system as a whole can continually adapt to a given input, hence maintaining sensitivity to future signals.

Why evolve complexity in signaling pathways only to produce seemingly simple behavior? We offer two thoughts. First, complexity of each pathway might afford tunability, in the sense that parameters can be tuned to produce different behaviors in different contexts. For instance, the ERK pathway produces digital, all-or-none response in some contexts (3), and analog response in others (36, 37). Second - to take an example from engineering - in order to utilize physical processes that are not naturally linear, engineers must implement complex design features to approximate linearity. Similarly, many biochemical processes are inherently nonlinear, meaning that linearity does not arise from a reduction in complexity. Indeed, in each pathway we analyzed here, linearity emerges *from* complex interactions: a futile cycle in the Wnt pathway, ultrasensitivity coupled to feedback in the ERK pathway, and continual nucleocytoplasmic shuttling in the Tgfβ pathway. Therefore, analogous to engineered systems, complexity in the biochemical pathways we analyzed here might have evolved in part to produce linearity.

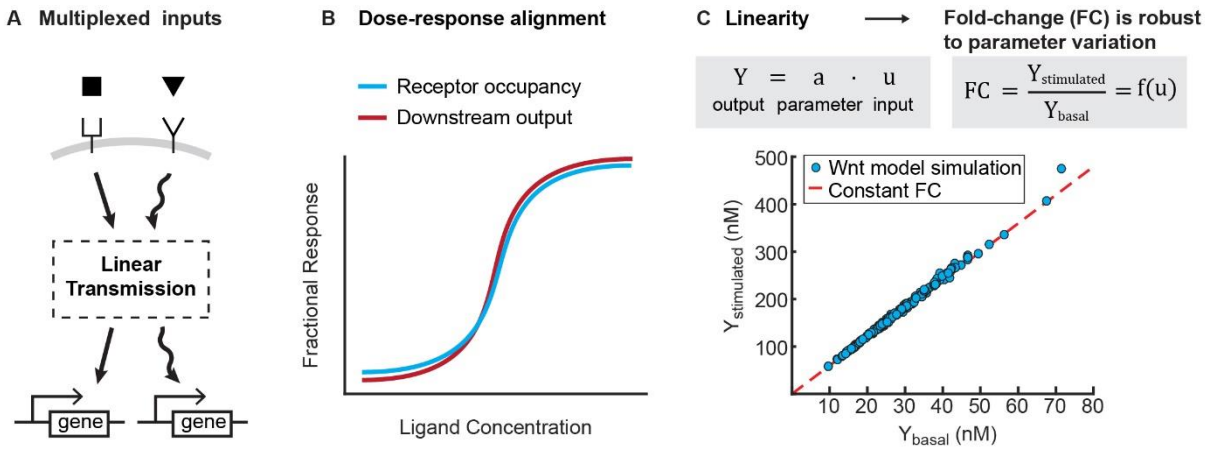

Figure 4. Benefits of linearity. (A) Linearity enables multiplexing of inputs to a signaling pathway. Multiplexed signals can be independently decoded downstream, and therefore regulate distinct transcriptional events. **(B)** Illustration for how linearity between the receptor occupancy and downstream outputs gives rise to dose-response alignment (55). **(C)** Linearity can produce fold-changes in output that are robust to variation in cellular parameters. To illustrate this, we added lognormal noise (0.1 CV) to all parameters of the Wnt model, and simulated the level of β-catenin before and after Wnt stimulation (blue circles). As long as the model operates in the regime of linear signal transmission (*i.e.*, $Y = a \cdot u$, where Y is output, u is input, and a is a scalar that is a function of parameters), variation in parameters affects stimulated and basal level of β-catenin equally, and we get a constant fold change in β-catenin (*i.e.*, red line, where $FC = Y_{stimulated}/Y_{basal}$ is independent of parameter variations).

Materials and Methods

Expression Constructs. pBABEpuro-CRAF that contains the wt human Raf-1 clone was a gift from Matthew Meyerson (Addgene plasmid # 51124). Mutant Raf (S289/296/301A) and

(S29/289/296/301/642A) were generated using the Q5 site-directed mutagenesis kit (New England Biolabs, E0554S). The mutant and wt Raf-1 were then placed downstream of a CMV promoter.

Cell Lines and Cell Culture. RKO cells (ATCC, CRL-2577) and H1299 cells (ATCC, CRL-5803) were authenticated by STR profiling and supplied by ATCC. RKO cells were cultured at 37°C and 5% (vol/vol) CO2 in DMEM (ThermoFisher Scientific; 11995) supplemented with 10% (vol/vol) FBS (Invitrogen; A13622DJ), 100 U/mL penicillin, 100µg/mL streptomycin, 0.25µg/mL amphotericin, and 2 mML-glutamine (Invitrogen). H1299 cells were cultured at 37C and 5% (vol/vol) CO2 in RPMI (ThermoFisher Scientific; 11875) supplemented with 10% (vol/vol) FBS (Invitrogen; A13622DJ), 100 U/mL penicillin, 100µg/mL streptomycin, 0.25µg/mL amphotericin, and 2 mML-glutamine (Invitrogen). Both cell lines tested negative for mycoplasma contamination.

Transfection of Raf-1 constructs. H1299 cells were transfected with the mutant and wt Raf-1 constructs using Lipofectamine 3000 (ThermoFisher Scientific, L3000). Stable expression was selected using puromycin at a concentration of 1.5 µg/mL for two weeks.

Reagents and Antibodies. The following antibodies were purchased from Cell Signaling Technologies: anti-Phospho-p44/42 MAPK (Erk1/2) (Thr202/Tyr204) (E10) Mouse mAb #9106, anti-histone H3 (D1H2) XP® Rabbit mAb #4499, anti-c-Raf Antibody #9422, anti-phospho-LRP6 (Ser1490) Antibody #2568, anti-GAPDH (D4C6R) Mouse mAb #97166. Anti-Beta-catenin mouse mAb was purchased from BD Transduction Laboratories (#610153) and anti-GAPDH rabbit antibody was purchased from Abcam (ab9485). The following fluorescent

secondary antibodies were purchased from Fisher Scientific: IRDye 800CW Goat anti-Mouse IgG (926-32210) and IRDye 680LT Goat anti-Rabbit IgG (926-68021).

Recombinant human Wnt3A was purchased from Fisher Scientific (5036WN), and recombinant human EGF was purchased from Sigma (E9644). CHIR99021 was purchased from Sigma (SML1046). Halt™ Protease and Phosphatase Inhibitor Cocktail (100X) was purchased from Fisher Scientific (78440).

CHIR99021 Treatment. RKO cells were pre-treated with 1μM CHIR99021 for 24 hours before adding replacement media containing 1μM CHIR99021 and Wnt3A for six hours.

Cell Lysis. RKO cells at 70% confluency were scraped in PBS, pelleted, and snap-frozen, and then thawed in NP-40 lysis buffer containing Halt inhibitor cocktail. Samples were spun down, and the supernatants were transferred to Laemmli sample buffer and boiled. The samples were then run onto a Bolt™ 4-12% Bis-Tris Plus Gel (Thermofisher, NW04120BOX). H1299 cells at 70% confluence were scraped in NP-40 lysis buffer containing Halt inhibitor cocktail, and further lysed in Laemmli sample buffer. Samples were spun down, and the supernatants were boiled. The samples were then run onto a Novex™ 4-20% Tris-Glycine Mini Gel (ThermoFisher, XP04200BOX).

Quantitative Western blots. Proteins were transferred onto nitrocellulose membranes, blocked for one hour at RT with blocking buffer (Odyssey® Blocking Buffer (TBS) (927-50000) or 5% milk powder in TBS) and stained overnight at 4°C with primary antibody diluted in blocking buffer. The membranes were then stained with fluorescent IR secondary antibodies diluted in blocking buffer for one hour at RT. The fluorescent signal was then imaged using the LiCOR Odyssey Imager and quantified using Odyssey Application software version 3.0. The

background-subtracted intensity of the protein bands were normalized to the loading control, GAPDH and/or Histone H3 (for RKO) or Histone H3 (for H1299). These values were then normalized to the reference lanes within each gel, to allow comparison across gels. For β-catenin and phospho-LRP, variation in the fold-activation from experiment to experiment could artificially stretch the data along the x- and y-axis, and introduce artifacts into the relationship between phospho-LRP5/6 and β-catenin. Therefore, for Wnt3A dose responses, the data from each gel was scaled such that the mean of 80ng/mL and 160ng/mL samples was equal to the mean across all gels. Finally, for each antibody used in the study, we did careful characterization of the linear range, and verified that our measurement conditions were within the linear range of the antibody. **Technical variability of Western blot quantitation.** To confirm the effects reported, we verified that quantitation of the same sample loaded in multiple lanes in a gel gives CV < 10%, and quantitation of the same sample across multiple independent gels gives CV < 10% (Figure 3 – figure supplement 7). As further control, we verified that normalization with loading control did not produce artificial distortion of the input-output relationship: linearity was observed without normalization in cases where loading was already uniform (Figure 3 – figure supplement 8).

L-1 and L2-norm analysis. L1-norm analysis was performed as described in ref. (59). Briefly, the data is fitted with a cubic Hermite polynomial, and rescaled along the x and y axis to [0, 1]. The L1-norm is computed as the area between the polynomial fit and the diagonal. Linearity is defined in this context as L1-norm<0.1. L2-norm analysis for Wnt pathway data was performed using a Pearson's coefficient, and L2-norm analysis for ERK pathway data was performed using the coefficient of correlation, r^2.

Akaike Information Criterion. To score the validity of nonlinear model fits for Figure 3D, we used the bias-corrected Akaike Information Criterion as described in ref. (60), which assesses goodness-of-fit and model parsimony. The weighted Aikaike w(AIC) provides a comparison of all considered models, which in our case is the nonlinear ERK pathway model fit and a linear fit, with the higher score indicating a more valid model.

Acknowledgments

We would like to thank Rob Oania for providing advice on experiments, Michael Abrams, Christopher Frick, Kibeom Kim, and Noah Olsman for comments on the manuscript, and Michael Elowitz and Richard Murray for discussions on the study.

Competing Interests

The authors declare that no competing interests exist.

References

1. Gerhart J. 1998 Warkany lecture: signaling pathways in development. Teratology. 1999;60(4):226-39.

2. Pires-daSilva A, Sommer RJ. The evolution of signalling pathways in animal development. Nature Reviews Genetics. 2003;4(1):39-49.

3. Huang C-Y, Ferrell JE. Ultrasensitivity in the mitogen-activated protein kinase cascade. Proceedings of the National Academy of Sciences. 1996;93(19):10078-83.

4. Ferrell JE, Machleder EM. The biochemical basis of an all-or-none cell fate switch in Xenopus oocytes. Science. 1998;280(5365):895-8.

5. Hoffmann A, Levchenko A, Scott ML, Baltimore D. The IκB-NF-κB signaling module: temporal control and selective gene activation. Science. 2002;298(5596):1241-5.

6. Sprinzak D, Lakhanpal A, LeBon L, Santat LA, Fontes ME, Anderson GA, et al. Cis-interactions between Notch and Delta generate mutually exclusive signalling states. Nature. 2010;465(7294):86-90.

7. Citri A, Skaria KB, Yarden Y. The deaf and the dumb: the biology of ErbB-2 and ErbB-3. Experimental cell research. 2003;284(1):54-65.

8. Kimelman D, Xu W. β-Catenin destruction complex: insights and questions from a structural perspective. Oncogene. 2006;25(57):7482-91.

9. Saito-Diaz K, Chen TW, Wang X, Thorne CA, Wallace HA, Page-McCaw A, et al. The way Wnt works: components and mechanism. Growth factors. 2013;31(1):1-31.

10. Hoppler SP, Moon RT. Wnt signaling in development and disease: molecular mechanisms and biological functions: John Wiley & Sons; 2014.

11. Stamos JL, Weis WI. The β-catenin destruction complex. Cold Spring Harbor perspectives in biology. 2013;5(1):a007898.

12. Nusse R, Clevers H. Wnt/β-Catenin Signaling, Disease, and Emerging Therapeutic Modalities. Cell. 2017;169(6):985-99.

13. Kolch W. Coordinating ERK/MAPK signalling through scaffolds and inhibitors. Nature reviews Molecular cell biology. 2005;6(11):827-37.

14. Yoon S, Seger R. The extracellular signal-regulated kinase: multiple substrates regulate diverse cellular functions. Growth factors. 2006;24(1):21-44.

15. Avraham R, Yarden Y. Feedback regulation of EGFR signalling: decision making by early and delayed loops. Nature reviews Molecular cell biology. 2011;12(2):104-17.

16. Lake D, Corrêa SAL, Müller J. Negative feedback regulation of the ERK1/2 MAPK pathway. Cellular and Molecular Life Sciences. 2016;73(23):4397-413.

17. Inman GJ, Nicolás FJ, Hill CS. Nucleocytoplasmic shuttling of Smads 2, 3, and 4 permits sensing of TGF-β receptor activity. Molecular cell. 2002;10(2):283-94.

18. Nicolás FJ, De Bosscher K, Schmierer B, Hill CS. Analysis of Smad nucleocytoplasmic shuttling in living cells. Journal of cell science. 2004;117(18):4113-25.

19. Xu L, Massagué J. Nucleocytoplasmic shuttling of signal transducers. Nature Reviews Molecular Cell Biology. 2004;5(3):209-19.

20. Schmierer B, Hill CS. Kinetic analysis of Smad nucleocytoplasmic shuttling reveals a mechanism for transforming growth factor β-dependent nuclear accumulation of Smads. Molecular and cellular biology. 2005;25(22):9845-58.

21. Massagué J, Seoane J, Wotton D. Smad transcription factors. Genes & development. 2005;19(23):2783-810.

22. Schmierer B, Tournier AL, Bates PA, Hill CS. Mathematical modeling identifies Smad nucleocytoplasmic shuttling as a dynamic signal-interpreting system. Proceedings of the National Academy of Sciences. 2008;105(18):6608-13.

23. Lee E, Salic A, Krüger R, Heinrich R, Kirschner MW. The roles of APC and Axin derived from experimental and theoretical analysis of the Wnt pathway. PLoS Biol. 2003;1(1):e10.

24. Goentoro L, Kirschner MW. Evidence that fold-change, and not absolute level, of β-catenin dictates Wnt signaling. Molecular cell. 2009;36(5):872-84.

25. Ferrell JE, Bhatt RR. Mechanistic studies of the dual phosphorylation of mitogen-activated protein kinase. Journal of Biological Chemistry. 1997;272(30):19008-16.

26. Schoeberl B, Eichler-Jonsson C, Gilles ED, Müller G. Computational modeling of the dynamics of the MAP kinase cascade activated by surface and internalized EGF receptors. Nature biotechnology. 2002;20(4):370-5.

27. Sturm OE, Orton R, Grindlay J, Birtwistle M, Vyshemirsky V, Gilbert D, et al. The mammalian MAPK/ERK pathway exhibits properties of a negative feedback amplifier. Science signaling. 2010;3(153):ra90.

28. Hernández AR, Klein AM, Kirschner MW. Kinetic responses of β-catenin specify the sites of Wnt control. Science. 2012;338(6112):1337-40.

29. Fritsche-Guenther R, Witzel F, Sieber A, Herr R, Schmidt N, Braun S, et al. Strong negative feedback from Erk to Raf confers robustness to MAPK signalling. Molecular systems biology. 2011;7(1):489.

30. González-Pérez V, Schmierer B, Hill CS, Sear RP. Studying Smad2 intranuclear diffusion dynamics by mathematical modelling of FRAP experiments. Integrative Biology. 2011;3(3):197-207.

31. Andrieux G, Fattet L, Le Borgne M, Rimokh R, Théret N. Dynamic regulation of Tgf-B signaling by Tif1γ: a computational approach. PloS one. 2012;7(3):e33761.

32. Vizán P, Miller DS, Gori I, Das D, Schmierer B, Hill CS. Controlling long-term signaling: receptor dynamics determine attenuation and refractory behavior of the TGF-β pathway. Science signaling. 2013;6(305):ra106.

33. Wang J, Tucker-Kellogg L, Ng IC, Jia R, Thiagarajan PS, White JK, et al. The Self-Limiting Dynamics of TGF-β Signaling In Silico and In Vitro, with Negative Feedback through PPM1A Upregulation. PLoS computational biology. 2014;10(6):e1003573.

34. MacDonald BT, Tamai K, He X. Wnt/β-catenin signaling: components, mechanisms, and diseases. Developmental cell. 2009;17(1):9-26.

35. Clevers H, Nusse R. Wnt/β-catenin signaling and disease. Cell. 2012;149(6):1192-205.

36. Whitehurst A, Cobb MH, White MA. Stimulus-coupled spatial restriction of extracellular signal-regulated kinase 1/2 activity contributes to the specificity of signal-response pathways. Molecular and cellular biology. 2004;24(23):10145-50.

37. MacKeigan JP, Murphy LO, Dimitri CA, Blenis J. Graded mitogen-activated protein kinase activity precedes switch-like c-Fos induction in mammalian cells. Molecular and cellular biology. 2005;25(11):4676-82.

38. Cohen-Saidon C, Cohen AA, Sigal A, Liron Y, Alon U. Dynamics and variability of ERK2 response to EGF in individual living cells. Molecular cell. 2009;36(5):885-93.

39. Ahmed S, Grant KG, Edwards LE, Rahman A, Cirit M, Goshe MB, et al. Data-driven modeling reconciles kinetics of ERK phosphorylation, localization, and activity states. Molecular systems biology. 2014;10(1):718.

40. Dougherty MK, Müller J, Ritt DA, Zhou M, Zhou XZ, Copeland TD, et al. Regulation of Raf-1 by direct feedback phosphorylation. Molecular cell. 2005;17(2):215-24.

41. Hekman M, Fischer A, Wennogle LP, Wang YK, Campbell SL, Rapp UR. Novel C-Raf phosphorylation sites: serine 296 and 301 participate in Raf regulation. FEBS letters. 2005;579(2):464-8.

42. Feliu E, Wiuf C. Variable elimination in chemical reaction networks with mass-action kinetics. SIAM Journal on Applied Mathematics. 2012;72(4):959-81.

43. Lagna G, Hata A, Hemmati-Brivanlou A, Massagué J. Partnership between DPC4 and SMAD proteins in TGF-β signalling pathways. 1996.

44. Gao S, Alarcón C, Sapkota G, Rahman S, Chen P-Y, Goerner N, et al. Ubiquitin ligase Nedd4L targets activated Smad2/3 to limit TGF-β signaling. Molecular cell. 2009;36(3):457-68.

45. Tamai K, Zeng X, Liu C, Zhang X, Harada Y, Chang Z, et al. A mechanism for Wnt coreceptor activation. Molecular cell. 2004;13(1):149-56.

46. Rotherham M, El Haj AJ. Remote activation of the Wnt/β-catenin signalling pathway using functionalised magnetic particles. PloS one. 2015;10(3):e0121761.

672 47. Oyarzún DA, Bramhall JL, López-Caamal F, Richards FM, Jodrell DI, Krippendorff
673 B-F. The EGFR demonstrates linear signal transmission. Integrative Biology. 2014;6(8):736-42.

674 48. Zeng X, Tamai K, Doble B, Li S, Huang H, Habas R, et al. A dual-kinase mechanism
675 for Wnt co-receptor phosphorylation and activation. Nature. 2005;438(7069):873-7.

676 49. Zeng X, Huang H, Tamai K, Zhang X, Harada Y, Yokota C, et al. Initiation of Wnt
677 signaling: control of Wnt coreceptor Lrp6 phosphorylation/activation via frizzled, dishevelled
678 and axin functions. Development. 2008;135(2):367-75.

679 50. Ashall L, Horton CA, Nelson DE, Paszek P, Harper CV, Sillitoe K, et al. Pulsatile
680 stimulation determines timing and specificity of NF-κB-dependent transcription. Science.
681 2009;324(5924):242-6.

682 51. Lee REC, Walker SR, Savery K, Frank DA, Gaudet S. Fold change of nuclear NF-κB
683 determines TNF-induced transcription in single cells. Molecular cell. 2014;53(6):867-79.

684 52. Richard CY, Pesce CG, Colman-Lerner A, Lok L, Pincus D, Serra E, et al. Negative
685 feedback that improves information transmission in yeast signalling. Nature.
686 2008;456(7223):755-61.

687 53. Nevozhay D, Adams RM, Murphy KF, Josić K, Balázsi G. Negative autoregulation
688 linearizes the dose–response and suppresses the heterogeneity of gene expression.
689 Proceedings of the National Academy of Sciences. 2009;106(13):5123-8.

690 54. Del Vecchio D, Dy AJ, Qian Y. Control theory meets synthetic biology. Journal of
691 The Royal Society Interface. 2016;13(120):20160380.

692 55. Andrews SS, Peria WJ, Richard CY, Colman-Lerner A, Brent R. Push-pull and
693 feedback mechanisms can align signaling system outputs with inputs. Cell systems.
694 2016;3(5):444-55. e2.

695 56. Becker V, Schilling M, Bachmann J, Baumann U, Raue A, Maiwald T, et al.
696 Covering a broad dynamic range: information processing at the erythropoietin receptor.
697 Science. 2010;328(5984):1404-8.

698 57. Thurley K, Tovey SC, Moenke G, Prince VL, Meena A, Thomas AP, et al. Reliable
699 encoding of stimulus intensities within random sequences of intracellular Ca2+ spikes. Science
700 signaling. 2014;7(331):ra59.

701 58. Frick CL, Yarka C, Nunns H, Goentoro L. Sensing relative signal in the Tgf-β/Smad
702 pathway. Proceedings of the National Academy of Sciences. 2017:201611428.

703 59. Nevozhay D, Zal T, Balázsi G. Transferring a synthetic gene circuit from yeast to
704 mammalian cells. Nature communications. 2013;4:1451.

705 60. Spiess A-N, Neumeyer N. An evaluation of R 2 as an inadequate measure for
706 nonlinear models in pharmacological and biochemical research: a Monte Carlo approach. BMC
707 pharmacology. 2010;10(1):6.

61. Vizán P, Miller D, Gori I, Das D, Schmierer B, Hill C. Controlling long-term signaling: receptor dynamics determine attenuation and refractory behavior of the TGF-β pathway. Sci Signal. 2013;6(305):ra106.

62. Warmflash A, Zhang Q, Sorre B, Vonica A, Siggia ED, Brivanlou AH. Dynamics of TGF-β signaling reveal adaptive and pulsatile behaviors reflected in the nuclear localization of transcription factor Smad4. Proceedings of the National Academy of Sciences. 2012;109(28):E1947-E56.

63. Strasen J, Sarma U, Jentsch M, Bohn S, Sheng C, Horbelt D, et al. Cell-specific responses to the cytokine TGFβ are determined by variability in protein levels. Molecular systems biology. 2018;14(1):e7733.

64. Kafri P, Hasenson SE, Kanter I, Sheinberger J, Kinor N, Yunger S, et al. Quantifying β-catenin subcellular dynamics and cyclin D1 mRNA transcription during Wnt signaling in single living cells. Elife. 2016;5:e16748.

65. Toettcher JE, Weiner OD, Lim WA. Using optogenetics to interrogate the dynamic control of signal transmission by the Ras/Erk module. Cell. 2013;155(6):1422-34.

66. Cheong R, Rhee A, Wang CJ, Nemenman I, Levchenko A. Information transduction capacity of noisy biochemical signaling networks. science. 2011:1204553.

67. Selimkhanov J, Taylor B, Yao J, Pilko A, Albeck J, Hoffmann A, et al. Accurate information transmission through dynamic biochemical signaling networks. Science. 2014;346(6215):1370-3.

68. Perrett RM, Fowkes RC, Caunt CJ, Tsaneva-Atanasova K, Bowsher CG, McArdle CA. Signaling to ERK from ErbB1 and PKC: Feedback, Heterogeneity and Gating. Journal of Biological Chemistry. 2013:jbc. M113. 455345.

69. Voliotis M, Perrett RM, McWilliams C, McArdle CA, Bowsher CG. Information transfer by leaky, heterogeneous, protein kinase signaling systems. Proceedings of the National Academy of Sciences. 2014;111(3):E326-E33.

70. Schohl A, Fagotto F. β-catenin, MAPK and Smad signaling during early Xenopus development. Development. 2002;129(1):37-52.

71. Itman C, Small C, Griswold M, Nagaraja AK, Matzuk MM, Brown CW, et al. Developmentally regulated SMAD2 and SMAD3 utilization directs activin signaling outcomes. Developmental dynamics: an official publication of the American Association of Anatomists. 2009;238(7):1688-700.

72. Dubrulle J, Jordan BM, Akhmetova L, Farrell JA, Kim S-H, Solnica-Krezel L, et al. Response to Nodal morphogen gradient is determined by the kinetics of target gene induction. Elife. 2015;4:e05042.

73. Schneider S, Steinbeisser H, Warga RM, Hausen P. β-catenin translocation into nuclei demarcates the dorsalizing centers in frog and fish embryos. Mechanisms of development. 1996;57(2):191-8.

74. Fagotto F, Gumbiner BM. Beta-catenin localization during Xenopus embryogenesis: accumulation at tissue and somite boundaries. Development. 1994;120(12):3667-79.

75. Aulehla A, Wiegraebe W, Baubet V, Wahl MB, Deng C, Taketo M, et al. A β-catenin gradient links the clock and wavefront systems in mouse embryo segmentation. Nature cell biology. 2008;10(2):186.

76. Sureda-Gómez M, Martín-Durán JM, Adell T. Localization of planarian βCATENIN-1 reveals multiple roles during anterior-posterior regeneration and organogenesis. Development. 2016:dev. 135152.

77. Wikramanayake AH, Hong M, Lee PN, Pang K, Byrum CA, Bince JM, et al. An ancient role for nuclear β-catenin in the evolution of axial polarity and germ layer segregation. Nature. 2003;426(6965):446.

78. Delfini M-C, Dubrulle J, Malapert P, Chal J, Pourquié O. Control of the segmentation process by graded MAPK/ERK activation in the chick embryo. Proceedings of the National Academy of Sciences. 2005;102(32):11343-8.

79. Lin J, Harding A, Giurisato E, Shaw AS. KSR1 modulates the sensitivity of mitogen-activated protein kinase pathway activation in T cells without altering fundamental system outputs. Molecular and cellular biology. 2009;29(8):2082-91.

80. Santos SD, Verveer PJ, Bastiaens PI. Growth factor-induced MAPK network topology shapes Erk response determining PC-12 cell fate. Nature cell biology. 2007;9(3):324.

Figure 2 – figure supplement 1. Model simulations for the ERK pathway. (A) Parameter groups in the ERK model are constant to within 10%, over the physiologically relevant range of u considered here, justifying the inclusion of variables into the parameter groups. **(B-C)** The dpERK output is an ultrasensitive function of both free and total phosphorylated Raf. The values E_s and R_s are illustrated in (B), and are defined in SI Section 3. **(D-F)** Numerical simulation of pulsatile response in the ERK pathway. **(D)** A pulse of input, RasGTP, is generated by EGF addition in an ERK model that includes details of receptor desensitization (26). Basal activity of Ras is included to ensure constitutive negative feedback (29). **(E)** dpERK output also exhibits a pulsatile response, peaking within 10 minutes. **(F)** We plot the peak dpERK output against peak input for a range of physiologically relevant u(EGF) doses, and find that it matches our steady-state predictions for linear input-output behavior. **(G)** Five-fold Raf overexpression does not break the linear input-output behavior.

Figure 2 – figure supplement 2. The predicted linearity extends throughout the dynamic range of the ERK and Tgfβ pathways. (A-B) Numerical simulation of the ERK and Tgfβ models. (A) The ERK model shows linear input-output relationship up to 93% of dpERK activation. (B) The Tgfβ pathway shows linear input-output relationship throughout the entire input range (from 0 to 1). Linearity was analyzed using the L1-norm or least absolute deviation (see Method). The blue range indicates where L1-norm was computed.

Figure 2 – figure supplement 3. Model simulations for the Tgfβ pathway. (A) Nuclear Smad4 concentration is constant to within 2%, over a physiologically relevant range of u(Tgfβ) considered here, justifying its inclusion into parameter group α. **(B-D)** Numerical simulation of pulsatile response in the Tgfβ pathway. **(B)** A pulse of input, active Tgfβ receptor, is generated by Tgfβ addition in a model that includes details of receptor desensitization (61). **(C)** S24n output also exhibits a pulsatile response. **(D)** We plot the peak S24n output against peak input, and find that it matches our steady-state predictions for linear input-output behavior.

Figure 2 – figure supplement 4. Incorporating into the Wnt model the dual function of GSK3β in phosphorylating β-catenin and LRP5/6. We include the role of GSK3β in phosphorylating LRP5/6 into the input function u(Wnt), such that u(Wnt) is a function of GSK3β and the phosphorylation rate k_9 (for simplicity, the same rate as GSK3β phosphorylation of β-catenin), and the reverse rate k_r. In both models, β-catenin increases in response to GSK3β inhibition (*e.g.*, by CHIR99021). However, only the model with the dual function of GSK3β shows a decrease in input range that we observed experimentally.

Figure 2 – figure supplement 5. The requirements for linear signal transmission in the Wnt, Tgfβ, and ERK pathway. In each plot, we varied S, defined in the equation shown on the x-axis, and simulated the input-output curve over the dynamic range of the model. The parameters in the equations are as defined in the main text. For the ERK and Tgfβ pathway, α and γ are linked in such a way that they could not easily be varied independently. Linearity was assessed using the L-1 norm, which ranges from 0 to 0.5, with L-1 norm < 0.1 indicating linearity. L1-norm analysis was performed over the full dynamic range of the system, *i.e.*, u(Wnt) = 1- 6, u(ERK) = 0 to 110,000 molecules of Ras-GTP, which gave 90% activation of [dpERK] in unperturbed cells, and u(Tgfβ) = 0 to 1.

Figure 2 – figure supplement 6. Linear signal transmission occurs over a range of parameters in the model. In this analysis, the parameter groups in each model were varied as indicated *e.g.*, 3x is 3-fold increase, 0.3x is 3-fold decrease. 1x corresponds to the measured parameters. Plotted in each box is the input-output relationship, numerically simulated over the full dynamic range of the models, *i.e.*, 1-6 for u(Wnt), 0-10^5 for u(EGF), and 0-1 for u(Tgfβ). For simplicity, all outputs are normalized from 0 to 1. Grey shade: the unperturbed state. Purple shade: linear input-output response, as defined by L-1 norm < 0.1.

Figure 2 - supplement figure 7. Numerical simulation of the input-output relationship of the NF-κB pathway. We used the model first built by Hoffman *et al.* in 2002 (46) and later revised by Ashall *et al.* in 2009 (47). The parameters in the model have been measured or fitted to single-cell dynamics in multiple cell types (46-48). We simulated the model here over a physiologically observed dynamic range, *i.e.*, Lee *et al.*, 2014 (48) observed in HeLa cells that at saturating ligand dose (10 ng/mL TNFα, set to 1 in the model), ~25% of NF-κB pool is nuclear. Linearity is assessed using the L1-norm, where L1-norm <1 indicates linear relationship (see Method).

Figure 3 – figure supplement 1. LRP5/6 phosphorylation and β-catenin accumulation are already at steady state at 6 hours after Wnt stimulation. RKO cells were treated with 160 ng/mL Wnt3A for the specified times, and then assayed for phospho-LRP5/6 and β-catenin level by Western blot. Error bars are standard error of the mean from 2-4 biological replicates. Data are plotted relative to the sample at time zero, and normalized to the average maximal activation across experiments. The grey lines connect the mean of each time point.

Figure 3 – figure supplement 2. The dynamic range of Wnt signaling in RKO cells. RKO cells were treated with the specified dose of Wnt3A for six hours, and then assayed for phospho-LRP5/6 and β-catenin by quantitative Western blot. Data are plotted relative to unstimulated samples. **(A-B)** In wt cells, phospho-LRP5/6 **(A)** shows >90% of maximal response at 200 ng/mL Wnt3A, while β-catenin **(B)** shows 70% of maximal response at 200 ng/mL, and subsequently incremental response until 640 ng/mL Wnt3A. **(C-D)** In cells pre-treated with 1μM CHIR99021, phospho-LRP5/6 **(C)** shows >90% of maximal response at 80ng/mL Wnt3A, while β-catenin **(D)** shows 70% of maximal response at 80 ng/mL and continues incremental activation at higher doses. **(E).** Cells were treated with 160 ng/mL Wnt3A and assayed for phospho-LRP5/6. Cells pre-treated with 1μM CHIR99021 (N = 3) exhibited 50% the level of phospho-LRP5/6 as untreated cells (N = 3). The grey lines simply connect the means of data.

Figure 3 – figure supplement 3. ERK activation peaks at 5 minutes after EGF stimulation. H1299 cells were treated with 1 ng/mL EGF for the specified times, and then assayed for dpERK1/2 by Western blot. Data is plotted relative to the samples at time zero, with at least three biological replicates per time point.

Figure 3 – figure supplement 4. In these experiments, H1299 cells were treated with varying doses of EGF for 5 minutes, and then fixed and analyzed for immunofluorescence against doubly phosphorylated ERK (dpERK). **(A)** Representative images of cells treated with the indicated doses of EGF. **(B)** The intensity of nuclear level of dpERK staining across individual cells. Cell nuclei were delineated using DAPI staining (for EGF doses 0, 0.3, 1.3, and 2.0 ng/mL, N = 453, 381, 373, and 413 cells, respectively).

Figure 3 – figure supplement 5. WT Raf-1 overexpression does not affect linear dose-response. H1299 cells over-expressing Raf-1 were treated with the indicated dose of EGF for 5 minutes, and then assayed for dpERK1/2 by Western blot. The grey line is a fit from a linear model with $r^2 = 0.99$. Data is plotted relative to unstimulated samples, with total N = 9.

Figure 3 – figure supplement 6. Expression of Raf S29/289/296/301/642A induces non-linear dose-response. H1299 cells expressing the Raf mutant Raf S29/289/296/301/642 were treated with the indicated dose of EGF for five minutes, and then assayed for dpERK1/2 by Western blot. Data is plotted relative to unstimulated samples, with total N = 5.

Figure 3 – figure supplement 7. (A) The level of β-catenin and phosphorylated LRP, measured across different lanes. **(B)** Ligand-stimulated change in β-catenin and phophorylated LRP level, measured in 6 independent Western blots. CV is coefficient of variation, defined as standard deviation/mean.

Figure 3- figure supplement 8. In these two independent experiments, RKO cells were stimulated with a range of Wnt3A dose (0-160 ng/mL), the cells lysed after 6 hours, and analyzed for Western blot against β-catenin and phosphorylated LRP5/6 (pLRP5/6). **Top row:** In each experiment, GAPDH intensity varies with <10% CV across samples. **Bottom row:** Raw β-catenin and LRP intensity data without normalization with GAPDH loading control. The measurements are plotted relative to unstimulated cells. Grey lines are least squares regression lines, and ρ is the Pearson correlation coefficient.

Figure 3 – figure supplement 9. Linearity was observed across independent experiments. (A) In these 2 independent experiments, RKO cells were stimulated with a range of Wnt3A doses, lysed after 6 hours, and analyzed for Western blot against β-catenin and phospho-LRP5/6. **(B)** In these 4 independent experiments, H1299 cells were stimulated with a range of EGF doses, lysed after 5 minutes, and analyzed for Western blot against doubly-phosphorylated ERK. All measurements are plotted relative to unstimulated cells. Grey lines are least squares regression, ρ is Pearson correlation coefficient, and r^2 is correlation coefficient.

Appendix 1

1. Variable Elimination

We use a variable elimination technique from Feliu *et al.* (42) to derive analytic expressions for the steady-states of the Tgfβ and ERK pathways. This technique was developed to handle the complexity of large chemical reaction networks. By eliminating variables from the steady-state solution, we can express the steady-state of the system in terms of a smaller subset of variables. This is a useful tool for analyzing the Tgfβ and ERK models, as the steady-state solution consists of a large set of variables, each with a polynomial equation describing its steady-state.

The technique works as follows: if we can identify **a cut set** within the reaction network, we can reduce the system to a set of first-order homogeneous equations with respect to that cut. This set of equations can then be solved using linear algebra.

A cut is a set of species such that for every reaction involving those species, there is exactly one reactant and one product that falls within that cut. For example, let us consider a network of 4 interacting species, A, B, C, and D.

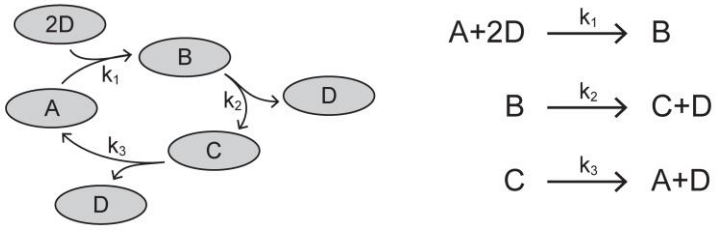

In this network, there is a cut $\{A, B, C\}$ that contains exactly one product and one reactant for each reaction. We have highlighted this cut in the reaction set:

$$A+2D \xrightarrow{k_1} B$$

$$B \xrightarrow{k_2} C+D$$

$$C \xrightarrow{k_3} A+D$$

The species D cannot belong in the cut, since it appears twice as a reactant in the first reaction. The behavior of this network is described by four differential equations,

$$[\dot{A}] = -k_1[A] \cdot [D]^2 + k_3[C] = 0 \quad \textbf{[S1.1]}$$

$$[\dot{B}] = k_1[A] \cdot [D]^2 - k_2[B] = 0 \quad \textbf{[S1.2]}$$

$$[\dot{C}] = k_2[B] - k_3[C] = 0 \quad \textbf{[S1.3]}$$

$$[\dot{D}] = -2k_1[A] \cdot [D]^2 + k_2[B] + k_3[C] = 0 \quad \textbf{[S1.4]}$$

which are set to zero at steady-state, and two additional conservation equations:

$$T_1 = [A] + [B] + [C] \quad \textbf{[S1.5]}$$

$$T_2 = 2[B] + [C] + [D] \quad \textbf{[S1.6]}$$

The variable elimination technique allows us to reduce the steady-state system of equations by four (three equations for the cut set, and one conservation equation). We do this by expressing each member of the cut set as a dependent variable of D, shown below. We utilize the fact that the differential equations for A, B, and C are first-order and homogenous with respect to our cut, and rewrite them in matrix form. We use the subscript “ss” to denote steady-state:

$$\begin{pmatrix} -k_1[D]_{ss}^2 & 0 & k_3 \\ k_1[D]_{ss}^2 & -k_2 & 0 \\ 0 & k_2 & -k_3 \end{pmatrix} \begin{pmatrix} [A]_{ss} \\ [B]_{ss} \\ [C]_{ss} \end{pmatrix} = 0 \qquad \textbf{[S1.7]}$$

Feliu *et al.* (42) provides a proof of why a cut set guarantees that we can rewrite the corresponding equations in matrix form. It can be understood intuitively from the fact that a cut contains exactly one reactant of each reaction, and therefore each rate is first-order with respect to the cut. Homogeneity also follows from this, since there are no rate terms that do not include members of the cut.

For a complex model, there is no guarantee that we can derive closed-form analytical solutions for steady-state. The matrix formulation and variable elimination technique immediately provides us with a set of solvable variables. The solution to the matrix equation above is:

$$[A]_{ss} = c \cdot k_2 k_3 \qquad \textbf{[S1.8]}$$

$$[B]_{ss} = c \cdot k_1 k_3 D_{ss}^2 \qquad \textbf{[S1.9]}$$

$$[C]_{ss} = c \cdot k_1 k_2 D_{ss}^2 \qquad \textbf{[S1.10]}$$

c is a scaling factor not constrained by the matrix equation. With the use of the conservation equation **S1.5**, we can calculate c and express the steady state of all three species solely in terms of the parameters of the network, and $[D]_{ss}$. For instance, the solution for $[C]_{ss}$ is below.

$$[C]_{ss} = \frac{k_1 k_2 [D]_{ss}^2}{k_2 k_3 + k_1 [D]_{ss}^2 (k_2 + k_3)} T_1 \qquad \textbf{[S1.11]}$$

The solutions for $[A]_{ss}$, $[B]_{ss}$, and $[C]_{ss}$ derived from the variable elimination technique still depend on $[D]_{ss}$. If we plug in the solutions for the cut species, we can obtain polynomial equations for the remaining species (in this case $[D]_{ss}$), but closed form expressions are not necessarily obtainable. In all the cases analyzed in this paper, variables that appear in the analytical solutions for the cut set happen to be approximately constant across a wide range of input values, as they are present in excess relative to other species.

Finally, each parameter group is physically meaningful. For instance, k_2k_3, $k_1k_3[D]_{ss}^2$, and $k_1k_2[D]_{ss}^2$ represent the un-normalized fraction of T_1 that exists as A, B, and C, respectively. The normalization factor for these fractions is c/T_1, or in this case, simply the sum of all parameter groups. This provides an intuitive way of analyzing how parameter groups affect the overall distribution of T_1. For instance, increasing the value of k_1 will increase the amount of T_1 that exists as B and C, while necessarily decreasing the amount of A (assuming $[D]_{ss}$ does not change significantly)

2. Wnt Model

We analyzed a mathematical model of the canonical Wnt pathway built by Lee *et al.* (23). The model is illustrated in Fig. 2A, and consists of 7 ODEs and 22 parameters, reproduced in Appendix 1 - Table 1.

Solving the Wnt model at steady-state

We previously derived an expression for β-catenin in steady-state (24):

$$[\beta\mathrm{cat}]_{ss} = K_{17}\frac{1-\gamma+\frac{\alpha}{u(\mathrm{Wnt})}}{2}\left(\sqrt{1+\frac{4\gamma}{\left(1-\gamma+\frac{\alpha}{u(\mathrm{Wnt})}\right)^2}}-1\right) \qquad \textbf{[S2.1]}$$

where the parameters are dimensionless groups of the binding rate constants and protein concentrations:

$$\alpha = \frac{k_4 \cdot k_6 \cdot k_9 \cdot v_{14} \cdot \mathrm{GSK3_{tot}} \cdot \mathrm{APC_{tot}}}{k_5 \cdot k_{-6} \cdot K_7 \cdot K_8 \cdot k_{13} \cdot k_{15}} \qquad \textbf{[S2.2]}$$

$$\gamma = \frac{v_{12}}{k_{13} \cdot K_{17}} \qquad \textbf{[S2.3]}$$

$$u(\mathrm{Wnt}) = 1 + \frac{k_3 \cdot \mathrm{Dvl_{tot}}}{k_{-6}} \cdot \frac{k_1 \cdot \mathrm{Wnt}}{k_2 + k_1 \cdot \mathrm{Wnt}} \qquad \textbf{[S2.4]}$$

The input function $u = u(\mathrm{Wnt})$ corresponds to the rate at which Wnt stimulation inhibits the destruction complex, normalized by k_{-6}. The value of Wnt ranges from 0 to 1 in the model. Please refer to Goentoro *et al.* (24) for the physical intuition of each parameter group.

Derivation of Linear Behavior

We calculate the value of the parameter groups, as well as the value of the input function at saturating Wnt stimulation:

$$\alpha = 66$$

$$\gamma = 1.4$$

$$u(\mathrm{Wnt} = 1) = 6.0$$

Within the parameter regime measured in cells, the analytical expression for β-catenin dramatically simplifies. We can perform the following first-order Taylor expansion:

$$\sqrt{1+\epsilon} \approx 1 + \frac{1}{2}\epsilon, \qquad \epsilon \ll 1 \qquad \textbf{[S2.5]}$$

$$\epsilon = \frac{4\gamma}{\left(1 - \gamma + \frac{\alpha}{u}\right)^2} \qquad \textbf{[S2.6]}$$

This holds true for $\alpha/u \gg \gamma$. Furthermore, we can make the approximation $1 - \gamma + \alpha/u \approx \alpha/u$ as long as $\alpha/u \gg 1$ also holds. We can encompass these two inequalities within $\alpha/u \gg 1 + \gamma$. The equation simplifies to:

$$[\beta\mathrm{cat}]_{ss} \approx K_{17}\frac{\gamma}{\alpha}u \qquad \textbf{[S2.7]}$$

3. ERK Model

We analyzed a mathematical model built by Huang *et al.* (3), and revised by Sturm *et al.* (27). The model is illustrated in Figure 2B, and contains 26 ODEs and 46 parameters, reproduced in Appendix 1 - Table 2.

We changed two parameters from the original model, which are highlighted in Appendix 1 - Table 2. k_{25} characterizes the negative feedback from dpERK to unphosphorylated Raf, and k_{27} characterizes the negative feedback from dpERK to phosphorylated Raf. In Sturm *et al.* (27), the values of these parameters were estimated, rather than measured. Experimental measurements indicate that dpERK mostly interacts with Raf, and that this feedback causes strong repression of Raf (40). We therefore increased the value of k_{25}, and set k_{27} to zero.

Solving the ERK model at steady-state

In the ERK pathway, doubly-phosphorylated ERK is produced by the Raf/MEK/ERK cascade of phosphorylation,

$$[\mathrm{dpERK}]_{ss} = g\left([\mathrm{pRaf}]_{ss}\right) \qquad \textbf{[S3.1]}$$

There is a negative feedback within the pathway, such that,

$$[\mathrm{pRaf}]_{ss} = f\left(u, [\mathrm{dpERK}]_{ss}\right) \qquad \textbf{[S3.2]}$$

where u is the input function, the concentration of RasGTP (a function of ligand dose).

We first focus on deriving the negative feedback function in Eq. **S3.2**. Using the variable elimination techniques in section “Variable Elimination”, we identify the following cut set:

$$\{\text{Raf, Raf: RasGTP, pRaf, pRaf: P1, MEK: pRaf, pMEK: pRaf, Raf: ppERK, Rafi, Rafi: P4}\}$$

This allows us to express the steady-state concentration of pRaf as a function of parameters, and the remaining species in the ERK pathway. Specifically, members of this cut interact directly with, and have dependencies on, the following set:

$$\{\text{P1, MEK, pMEK, dpERK, P4}\}$$

With this, we derive the expression for $[\text{pRaf}]_{ss}$,

$$[\text{pRaf}]_{ss} = \frac{\alpha \cdot u}{\beta \cdot [\text{dpERK}]_{ss} + (\alpha + \gamma) \cdot u + \delta} \cdot \text{Raf}_{tot} \qquad \textbf{[S3.3]}$$

where the parameter groups are:

$$\alpha = \frac{k_3 \cdot (k_8 + k_{b7})}{k_7 \cdot [P1]_{ss} \cdot k_8} + \cdots \qquad \textbf{[S3.4]}$$

$$\beta = \frac{k_{25} \cdot (k_{30} + k_{b29} + k_{29} \cdot [P4]_{ss})}{k_{29} \cdot [P4]_{ss} \cdot k_{30}} + \cdots \qquad \textbf{[S3.5]}$$

$$\gamma = \frac{k_3 \cdot (k_8 + k_{b7}) \cdot (k_9 \cdot [MEK]_{ss})}{k_7 \cdot [P1]_{ss} \cdot k_8 \cdot k_{10}} + \cdots \qquad \textbf{[S3.6]}$$

$$\delta = \frac{k_{26} + k_{b25}}{k_{26}} + \cdots \qquad \textbf{[S3.7]}$$

The ellipses indicate additional small terms (*i.e.*, <10% of the previous terms, numerically calculated using the model parameters and u = 4.5e4). All the calculations for this paper use these truncated parameter groups. The complete parameter groups are written below:

$$\alpha = (k_3 \cdot (k_8 + k_{b7}) \cdot (k_{10} + k_{b9}) \cdot (k_{12} + k_{b11}) \cdot (k_{26} + k_{b25}))/([P1]_{ss} \cdot k_7 \cdot k_8 \cdot k_{10} \cdot k_{12} \cdot k_{26})$$

$$\beta = (k_{25} \cdot (k_4 + k_{b3}) \cdot (k_{10} + k_{b9}) \cdot (k_{12} + k_{b11}) \cdot (k_{26} \cdot k_{30} + k_{26} \cdot k_{b29} + [P4]_{ss} \cdot k_{26} \cdot k_{29} + [P4]_{ss} \cdot k_{29} \cdot k_{30}))/([P4]_{ss} \cdot k_4 \cdot k_{10} \cdot k_{12} \cdot k_{26} \cdot k_{29} \cdot k_{30})$$

$$\gamma = (k_3 \cdot (k_{26} + k_{b25}) \cdot (k_4 \cdot k_8 \cdot k_{10} \cdot k_{12} + k_4 \cdot k_8 \cdot k_{10} \cdot k_{b11} + k_4 \cdot k_8 \cdot k_{12} \cdot k_{b9} + k_4 \cdot k_{10} \cdot k_{12} \cdot k_{b7} + k_4 \cdot k_8 \cdot k_{b9} \cdot k_{b11} + k_4 \cdot k_{10} \cdot k_{b7} \cdot k_{b11} + k_4 \cdot k_{12} \cdot k_{b7} \cdot k_{b9} + k_4 \cdot k_{b7} \cdot k_{b9} \cdot k_{b11} + [MEK]_{ss} \cdot k_4 \cdot k_8 \cdot k_9 \cdot k_{12} + [MEK]_{ss} \cdot k_4 \cdot k_8 \cdot k_9 \cdot k_{b11} + [MEK]_{ss} \cdot k_4 \cdot k_9 \cdot k_{12} \cdot k_{b7} + [MEK]_{ss} \cdot k_4 \cdot k_9 \cdot k_{b7} \cdot k_{b11} + [P1]_{ss} \cdot k_4 \cdot k_7 \cdot k_{10} \cdot k_{12} + [P1]_{ss} \cdot k_7 \cdot k_8 \cdot k_{10} \cdot k_{12} + [P1]_{ss} \cdot k_4 \cdot k_7 \cdot k_{10} \cdot k_{b11} + [P1]_{ss} \cdot k_4 \cdot k_7 \cdot k_{12} \cdot k_{b9} + [P1]_{ss} \cdot k_7 \cdot k_8 \cdot k_{10} \cdot k_{b11} + [P1]_{ss} \cdot k_7 \cdot k_8 \cdot k_{12} \cdot k_{b9} + [P1]_{ss} \cdot k_4 * k_7 \cdot k_{b9} \cdot k_{b11} + [P1]_{ss} \cdot k_7 \cdot k_8 \cdot k_{b9} \cdot k_{b11} + k_4 \cdot k_8 \cdot k_{10} \cdot k_{11} \cdot [pMEK]_{ss} + k_4 \cdot k_8 \cdot k_{11} \cdot k_{b9} \cdot [pMEK]_{ss} + k_4 \cdot k_{10} \cdot k_{11} \cdot k_{b7} \cdot [pMEK]_{ss} + k_4 \cdot k_{11} \cdot k_{b7} \cdot k_{b9} \cdot [pMEK]_{ss}))/([P1]_{ss} \cdot k_4 \cdot k_7 \cdot k_8 \cdot k_{10} \cdot k_{12} \cdot k_{26})$$

$$\delta = ((k_4 + k_{b3}) \cdot (k_{10} + k_{b9}) \cdot (k_{12} + k_{b11}) \cdot (k_{26} + k_{b25}))/(k_4 \cdot k_{10} \cdot k_{12} \cdot k_{26})$$

Physical significance of parameter groups

Next, we would like to develop an intuition for the physical significance of these parameter groups. As discussed in section 1, $\alpha \cdot u$ relates to the amount of free, phosphorylated Raf since $\alpha \cdot u/\left((\alpha+\gamma)\cdot u+\beta[\mathrm{dpERK}]_{ss}+\delta\right)$ is the fraction of Raf present as pRaf. Thus, as $\alpha \cdot u$ increases relative to $\gamma \cdot u+\beta[\mathrm{dpERK}]_{ss}+\delta$, the amount of pRaf also increases.

We can define three subpopulations of Raf: Raf inhibited by dpERK, $[R_i]$; Raf activated by RasGTP (input), $[R_a]$; and unphosphorylated Raf $[R_n]$. Specifically:

$$[R_i] = [\mathrm{Raf{:}\,dpERK}] + [\mathrm{Rafi}] + [\mathrm{Raf{:}\,P4}] \quad \textbf{[S3.8]}$$

$$[R_a] = [\mathrm{pRaf}] + [\mathrm{pRaf{:}\,P1}] + [\mathrm{MEK{:}\,pRaf}] + [\mathrm{pMEK{:}\,pRaf}] + \mathrm{Raf{:}\,RasGTP}] \quad \textbf{[S3.9]}$$

$$[R_n] = [\mathrm{Raf}] \quad \textbf{[S3.10]}$$

We can calculate the steady-state of each subpopulation as:

$$[R_i]_{ss} = \frac{\beta \cdot [\mathrm{dpERK}]_{ss}}{\left((\alpha+\gamma)\cdot u+\beta[\mathrm{dpERK}]_{ss}+\delta\right)}\mathrm{Raf}_{tot} \quad \textbf{[S3.11]}$$

$$[R_a]_{ss} = \frac{\gamma \cdot u}{\left((\alpha+\gamma)\cdot u+\beta[\mathrm{dpERK}]_{ss}+\delta\right)}\mathrm{Raf}_{tot} + [\mathrm{pRaf}]_{ss} \quad \textbf{[S3.12]}$$

$$[R_n]_{ss} = \frac{\delta}{\left((\alpha+\gamma)\cdot u+\beta[\mathrm{dpERK}]_{ss}+\delta\right)} \cdot \mathrm{Raf}_{tot} \quad \textbf{[S3.13]}$$

Thus, in the same sense that $\alpha \cdot u$ relates to the amount of free phosphorylated Raf, $\beta \cdot [\mathrm{dpERK}]_{ss}$ relates to the amount of inhibited Raf, $\gamma \cdot u$ relates to the amount of phosphorylated Raf bound to other proteins (not free), and δ relates to the amount of unphosphorylated Raf.

Derivation of linear behavior

Now that we have derived the negative feedback function from Eq. S**3.2**, we examine Eq. S**3.1**. The relationship $[\mathrm{dpERK}]_{ss} = g\,([\mathrm{pRaf}]_{ss})$ is analytically intractable, because of the complexity of the phosphorylation cascade. But we know from simulations and experimental observations that it is an ultrasensitive function. From simulations, we find that a 1.3 fold change in pRaf leads to a 9-fold change in dpERK (from 10% to 90% of max, Fig. S1B-C).

We therefore approximate $[\mathrm{pRaf}]_{ss}$ by a value R_s within this range, as indicated by the dashed line in Figure 2 – figure supplement 1B. Substituting this into the equation above and rearranging, we find that $[\mathrm{dpERK}]_{ss}$ becomes a linear function of input:

$$[\mathrm{dpERK}]_{ss} \approx \frac{\alpha}{\beta} \cdot \left(\frac{\mathrm{Raf_{tot}}}{R_s} - 1 - \frac{\gamma}{\alpha}\right) \cdot u - \frac{\delta}{\beta} \qquad \textbf{[S3.14]}$$

Lastly, we write the value of two terms in Eq. **S3.14** below, numerically calculated using the parameter values of the model:

$$\frac{\alpha}{\beta} \cdot \frac{\mathrm{Raf_{tot}}}{R_s} = 140$$

$$\frac{\alpha}{\beta}\left(1 + \frac{\gamma}{\alpha}\right) = 13$$

We can neglect the second term, yielding:

$$[\mathrm{dpERK}]_{ss} \approx \frac{\alpha_1}{\beta} \cdot \frac{\mathrm{Raf_{tot}}}{R_s} \cdot u - \frac{\delta}{\beta} \qquad \textbf{[S3.15]}$$

Derivation for treating pRaf as a constant

Next, we analyze exactly how the level of pRaf changes with the input u. From earlier, we have that

$$[\mathrm{dpERK}]_{ss} = g([\mathrm{pRaf}]_{ss}) \qquad \textbf{[S3.1]}$$

$$[\mathrm{pRaf_{tot}}]_{ss} = f(u, [\mathrm{dpERK}]_{ss}) \qquad \textbf{[S3.2]}$$

We can now derive a general expression for the relative change of $[\mathrm{pRaf}]_{ss}$ with respect to a relative change in u. We use the notation $d\hat{x} = d\ln x = dx/x$.

$$\frac{d\hat{f}}{d\hat{u}} = \frac{\partial f}{\partial u}\cdot\frac{u}{f}\cdot\left(1 - \frac{\partial f}{\partial [\mathrm{dpERK}]_{ss}}\cdot\frac{dg}{d[\mathrm{pRaf}]_{ss}}\right)^{-1} \qquad \textbf{[S3.16]}$$

Next, we define the response coefficient K between $[\mathrm{dpERK}]_{ss}$ and $[\mathrm{pRaf}]_{ss}$:

$$K \triangleq \frac{dg}{d[\mathrm{pRaf}]_{ss}}\cdot\frac{[\mathrm{pRaf}]_{ss}}{[\mathrm{dpERK}]_{ss}} \qquad \textbf{[S3.17]}$$

From Eq. **S3.3**, we get the partial derivatives:

$$\frac{\partial f}{\partial u} = \frac{f}{u}\cdot\frac{\beta[\mathrm{dpERK}]_{ss} + \delta}{\beta[\mathrm{dpERK}]_{ss} + (\alpha+\gamma)u + \delta} \qquad \textbf{[S3.18]}$$

$$\frac{\partial f}{\partial [\mathrm{dpERK}]_{ss}} = -f\cdot\frac{\beta}{\beta[\mathrm{dpERK}]_{ss} + (\alpha+\gamma)u + \delta} \qquad \textbf{[S3.19]}$$

Using these two equations, we find that:

$$\frac{d\hat{f}}{d\hat{u}} = \frac{\beta[\mathrm{dpERK}]_{ss} + \delta}{(1+k)\cdot\beta[\mathrm{dpERK}]_{ss} + \alpha u + \delta} \qquad \textbf{[S3.20]}$$

When $K \gg 1$ and $\beta[\mathrm{dpERK}]_{ss} \sim (\alpha + \gamma) \cdot u + \delta$, we see that

$$\frac{d\hat{f}}{d\hat{u}} \approx K^{-1} \qquad \textbf{[S3.21]}$$

Therefore, $[\mathrm{pRaf}]_{ss}$ is held constant in the region where the kinase cascade is ultrasensitive and feedback is strong. In this region, it is easy to show that $[\mathrm{dpERK}]_{ss}$ becomes a linear function of input.

$$\frac{d\hat{g}}{d\hat{u}} \approx 1; \qquad g_0 = -\frac{\delta}{\beta} \qquad \textbf{[S3.22]}$$

It is not guaranteed that the system is stable as K increases, but we see from simulations that our parameter regime provides a stable output.

Toy Model of the ERK pathway

Here we utilize a toy model to illustrate how ultrasensitivity and strong negative feedback combine to generate input-output linearity. In this model, induction of the output species E is a two-step process:

1. An input u increases the amount of species R, which in turn influences E as $E = g(R)$. There is negative feedback from E to R, which in the limit of strong negative feedback is inversely proportional to E.
2. Next, we specify the function g(R) such that $K = K_0$, where K is the relative change of E with respect to R. As K_0 increases, therefore, the function g(R) becomes more ultrasensitive.

Solving for E, we see that in the limit of $K = K_0 \gg 1$, E becomes a linear function of u, and R is held constant at R_s.

While we do not have an explicit function for g(R) for the full ERK model, we include derivations in section "**Derivation for treating pRaf as a constant**" that show that these results hold for any function g(R) in the region where $K \gg 1$. We also show that these results hold outside the limit of strong negative feedback, as long as the feedback-inhibited pool of R is comparable to the remaining pool.

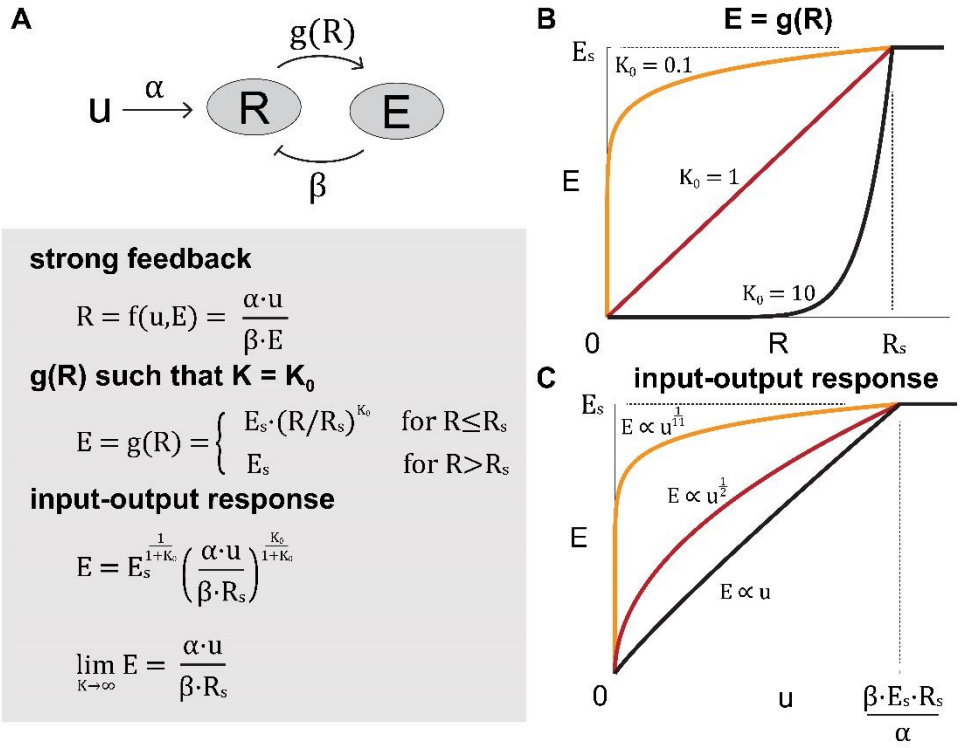

4. Tgfβ Model

We analyzed a mathematical model built by Schmierer *et al.* (22). The model is illustrated in Fig. 2C, and consists of 10 ODEs and 14 parameters, reproduced in Appendix 1 – Tables 3.

Solving the Tgfβ model at steady-state

We use the variable elimination technique described in section “Variable Elimination” to derive an analytical expression for the steady-state concentration of nuclear Smad complex. First, based on the measured parameter values, and as confirmed by simulations, the extent of Smad2-Smad2 binding is limited. We therefore neglect this reaction in subsequent analysis. We identify the following cut of the Tgfβ model:

$$\{\mathrm{S2c}, \mathrm{pS2c}, \mathrm{S24c}, \mathrm{S2n}, \mathrm{pS2n}, \mathrm{S24n}\}$$

which is subject to the conservation equation:

$$([\mathrm{S2c}] + [\mathrm{pS2c}] + [\mathrm{S24c}]) + \frac{1}{\mathrm{a}}([\mathrm{S2n}] + [\mathrm{pS2n}] + [\mathrm{S24n}]) = \mathrm{S2_{tot}} \qquad \textbf{[S4.1]}$$

Thus, we can eliminate these variables from the steady-state polynomial solution, with dependence only on variables outside this cut:

$$\{\mathrm{S4c}, \mathrm{S4n}\}$$

Using this relationship, we derive an expression for the nuclear Smad complex (S24n) at steady-state,

$$[\mathrm{S24n}]_{\mathrm{ss}} = \frac{\mathrm{a} \cdot \alpha \cdot \mathrm{u}}{(\alpha + \gamma) \cdot \mathrm{u} + \beta}\, \mathrm{S2_{tot}} \qquad \textbf{[S4.2]}$$

where the parameter groups are:

$$\alpha = \frac{\mathrm{a} \cdot (\mathrm{k_{on}}[\mathrm{S4n}]_{\mathrm{ss}} + \mathrm{a} \cdot \mathrm{k_{ex2}})}{\mathrm{k_{off}}} + \cdots \qquad \textbf{[S4.3]}$$

$$\beta = \mathrm{PPase} \cdot \frac{\mathrm{k_{dephos}}}{\mathrm{k_{phos}} \cdot \mathrm{R_{tot}} \cdot \frac{\mathrm{k_{ex2}}}{\mathrm{a} \cdot \mathrm{k_{ex2}} + \mathrm{k_{in2}}}} + \cdots \qquad \textbf{[S4.4]}$$

$$\gamma = a \cdot \left(a \cdot k_{ex2} + PPase \cdot k_{dephos}\right)\left(\frac{1}{a \cdot k_{ex2}} + \frac{1}{CIF \cdot k_{in2}}\right) + \cdots \qquad \textbf{[S4.5]}$$

Here the input function $u = u(Tgf\beta)$ is the fraction of receptors activated by Tgfβ ligands. The ellipses indicate additional small terms (*i.e.*, <10% of the previous terms, as calculated using the model parameters, with the variables $[S4c]_{ss}$ and $[S4n]_{ss}$ calculated for $u = 0$). All calculations for the paper use these truncated parameter groups. The complete parameter groups are written below:

$$\alpha = (a \cdot ([S4n]_{ss} \cdot k_{off} + CIF \cdot [S4n]_{ss} \cdot k_{in2} + CIF \cdot PPase \cdot [S4c]_{ss} \cdot k_{dephos} + CIF \cdot [S4c]_{ss} \cdot [S4n]_{ss} \cdot k_{on} + CIF \cdot [S4c]_{ss} \cdot a \cdot k_{ex2}))/(CIF \cdot [S4c]_{ss} \cdot k_{off})$$

$$\beta = (PPase \cdot k_{dephos} \cdot (k_{in2} + a \cdot k_{ex2}) \cdot (k_{off} + CIF \cdot k_{in2} + CIF \cdot [S4c]_{ss} \cdot k_{on}))/(CIF \cdot R_{tot} \cdot [S4c]_{ss} \cdot k_{ex2} \cdot k_{on} \cdot k_{phos})$$

$$\gamma = ((PPase \cdot k_{dephos} + a \cdot k_{ex2}) \cdot (k_{in2} \cdot k_{off} + CIF \cdot k_{in2}^2 + a \cdot k_{ex2} \cdot k_{off} + CIF \cdot [S4c]_{ss} \cdot k_{in2} \cdot k_{on} + CIF \cdot a \cdot k_{ex2} \cdot k_{in2} + [S4c]_{ss} \cdot a \cdot k_{ex2} \cdot k_{on}))/(CIF \cdot [S4c]_{ss} \cdot k_{ex2} \cdot k_{in2} \cdot k_{on})$$

Physical significance of parameter groups

Next, we would like to develop an intuition for the physical significance of these parameter groups. As discussed in section 1, $\alpha \cdot u$ relates to the amount of nuclear Smad complex since $\alpha \cdot u/\left((\alpha + \gamma) \cdot u + \beta\right)$ is the fraction of Smad2 present as S24n. Thus, as $\alpha \cdot u$ increases relative to $\gamma \cdot u + \beta$, the amount of S24n also increases.

By definition, the parameter groups β and $\gamma \cdot u$ capture the remaining input-independent and input-dependent polynomials, respectively. Nevertheless, we would like to understand the physical significance of the parameter groups. We can calculate the amount of unphosphorylated Smad2 as:

$$[S2c]_{ss} + \frac{1}{a}[S2n]_{ss} = \frac{\beta + \delta \cdot u}{\beta + (\alpha + \gamma) \cdot u} S2_{tot} \quad \textbf{[S4.6]}$$

$$\delta = PPase \cdot k_{dephos} \cdot \frac{k_{off} + CIF \cdot k_{in2} + CIF \cdot [S4c]_{ss} \cdot k_{on}}{CIF \cdot [S4c]_{ss} \cdot k_{ex2} \cdot k_{on}} \quad \textbf{[S4.7]}$$

δ captures the dependence of nuclear, unphosphorylated Smad on the input. With the measured parameters, $\beta \gg \delta \cdot u$, so we have

$$[S2c]_{ss} + \frac{1}{a}[S2n]_{ss} \approx \frac{\beta}{\beta + (\alpha + \gamma) \cdot u} S2_{tot} \quad \textbf{[S4.8]}$$

This means that β relates to the amount of unphosphorylated Smad2 in the same sense that $\alpha \cdot u$ relates to nuclear Smad complex. We can also express the remaining Smad2 species as:

$$[pS2c]_{ss} + [S24c]_{ss} + \frac{1}{a}[pS2n]_{ss} = \frac{(\gamma - \delta) \cdot u}{\left((\alpha + \gamma) \cdot u + \beta\right)} \cdot S2_{tot} \quad \textbf{[S4.9]}$$

However, as δ is of the same order of magnitude as γ, the parameter group γ only loosely relates to these remaining species of Smad2.

Derivation of linear behavior

Within the parameter values measured in cells, the behavior of Smad complex dramatically simplifies. Using the measured values (Appendix 1 - Table 3), the parameter groups are

$$\alpha \cdot u = 3.1$$

$$\gamma \cdot u = 1.3$$

$$\beta = 46$$

where we have used a non-saturating input ($u = 0.2$). Therefore, within the physiological regime of parameters, $\beta \gg (\alpha + \gamma) \cdot u$. With this, the denominator in the $[S4n]_{ss}$ equation simplifies, and the concentration of Smad complex becomes a linear function of the input:

$$[S24n]_{ss} \approx \frac{\alpha \cdot S2_{tot}}{\beta} \cdot u \qquad \textbf{[S4.10]}$$

Appendix 1 - Table 1.

Parameters, variables, and equations of the Wnt model.

Parameter	Label	Value	
Activation rate of Dvl by Wnt	k_1	$.182$	min^{-1}
Inactivation rate of Dvl	k_2	$1.82 \cdot 10^{-2}$	min^{-1}
Dissociation of DC by active Dvl	k_3	$5.00 \cdot 10^{-2}$	$nM^{-1}\ min^{-1}$
Phosphorylation of DC	k_4	0.267	min^{-1}
Dephosphorylation of DC	k_5	0.133	min^{-1}
Forward rate for DC binding	k_6	$9.09 \cdot 10^{-2}$	$nM^{-1}\ min^{-1}$
Reverse rate for DC binding	k_{-6}	0.909	min^{-1}
Dissociation constant for APC:axin binding	K_7	50	nM
Dissociation constant for β-catenin:DC binding	K_8	120	nM
Phosphorylation rate of β-catenin	k_9	206	min^{-1}
Rate of phosphorylated β-catenin release from DC	k_{10}	206	min^{-1}
Degradation rate of phosphorylated β-catenin	k_{11}	0.417	min^{-1}
Synthesis rate of β-catenin	v_{12}	0.423	$nM\ min^{-1}$
Degradation rate of β-catenin	k_{13}	$2.57 \cdot 10^{-4}$	min^{-1}
Synthesis rate of axin	v_{14}	$8.22 \cdot 10^{-5}$	$nM\ min^{-1}$
Degradation rate of axin	k_{15}	0.167	min^{-1}
Dissociation constant for β-catenin:TCF binding	K_{16}	30	nM
Dissociation constant for β-catenin:APC binding	K_{17}	1200	nM
Total concentration of Disheveled	Dvl_{tot}	100	nM
Total concentration of adenomatous polyposis coli	APC_{tot}	100	nM

Total concentration of T-cell factor	TCF_{tot}	15	nM
Total concentration of glycogen synthase kinase 3β	$GSK3_{tot}$	50	nM

Independent Variable	Label
Active Disheveled	X_2
APC*/axin*/GSK3	X_3
APC/axin/GSK3	X_4
β-catenin*/APC*/axin*/GSK3	X_9
β-catenin*	X_{10}
β-catenin	X_{11} (βcat)
axin	X_{12}

Dependent Variable	Label
Inactive Disheveled	X_1
GSK3	X_5
APC/axin	X_6
APC	X_7
β-catenin/APC*/axin*/GSK3	X_8
TCF	X_{13}
β-catenin/TCF	X_{14}
β-catenin/APC	X_{15}

Differential Equations

$$[\dot{X_2}] = k_1 \cdot Wnt \cdot (Dvl_{tot} - [X_2]) - k_2 \cdot [X_2]$$

$$\left(1 + \frac{[X_{11}]}{K_8}\right) \cdot [\dot{X_3}] + \frac{[X_3]}{K_8} \cdot [\dot{X_{11}}] = k_4 \cdot [X_4] - k_5 \cdot [X_3] - \frac{k_9 \cdot [X_3] \cdot [X_{11}]}{K_8} + k_{10} \cdot [X_9]$$

$$[\dot{X_4}] = -(k_3 \cdot [X_2] + k_4 + k_{-6}) \cdot [X_4] + k_5 \cdot [X_3] + k_6 \cdot GSK3_{tot} \cdot \frac{K_{17} \cdot [X_{12}] \cdot APC_{tot}}{K_7 \cdot (K_{17} + [X_{11}])}$$

$$[\dot{X_9}] = \frac{k_9 \cdot [X_3] \cdot [X_{11}]}{K_8} - k_{10} \cdot [X_9]$$

$\dot{[X_{10}]} = k_{10} \cdot [X_9] - k_{11} \cdot [X_{10}]$
$\left(1 + \frac{[X_3]}{K_8} + \frac{K_{16} \cdot TCF_{tot}}{(K_{16} + [X_{11}])^2} + \frac{K_{17} \cdot APC_{tot}}{(K_{17} + [X_{11}])^2}\right) \cdot \dot{[X_{11}]} + \frac{[X_{11}]}{K_8} \cdot \dot{[X_3]} = v_{12} - \left(\frac{k_9 \cdot [X_3]}{K_8} + k_{13}\right) \cdot [X_{11}]$
$\left(1 + \frac{K_{17} \cdot APC_{tot}}{K_7 \cdot (K_{17} + [X_{11}])}\right) \cdot \dot{[X_{12}]} - \frac{K_{17} \cdot [X_{12}] \cdot APC_{tot}}{K_7 \cdot (K_{17} + [X_{11}])^2} \cdot \dot{[X_{11}]} = k_3 \cdot [X_2] \cdot [X_4] - k_6 \cdot GSK3_{tot} \cdot \frac{K_{17} \cdot [X_{12}] \cdot APC_{tot}}{K_7 \cdot (K_{17} + [X_{11}])} + k_{-6} \cdot [X_4] + v_{14} - k_{15} \cdot [X_{12}]$
Equations for fast equilibrium reactions
$[X_1] = Dvl_{tot} - [X_2]$
$[X_5] = GSK3_{tot}$
$[X_6] = \frac{K_{17} \cdot [X_{12}] \cdot APC_{tot}}{K_7 \cdot (K_{17} + [X_{11}])}$
$[X_7] = \frac{K_{17} \cdot APC_{tot}}{K_{17} + [X_{11}]}$
$[X_8] = \frac{[X_3] \cdot [X_{11}]}{K_8}$
$[X_{13}] = \frac{K_{16} \cdot TCF_{tot}}{K_{16} + [X_{11}]}$
$[X_{14}] = \frac{[X_{11}] \cdot TCF_{tot}}{K_{16} + [X_{11}]}$
$[X_{15}] = \frac{[X_{11}] \cdot APC_{tot}}{K_{17} + [X_{11}]}$

211
212

Appendix 1 - Table 2. Parameters, variables, and equations of the ERK model. Values highlighted in yellow have been changed from the original model (explained in section "ERK Model").

Parameter	Label	Value	
Forward rate for Raf:RasGTP binding	k_3	$1.67 \cdot 10^{-6}$	$molecule^{-1}s^{-1}$
Reverse rate for Raf:RasGTP binding	k_{b3}	$5.3 \cdot 10^{-3}$	s^{-1}
Phosphorylation rate for Raf by RasGTP	k_4	1	s^{-1}
Forward rate of pRaf:P1 binding	k_7	$1.18 \cdot 10^{-4}$	$molecule^{-1}s^{-1}$
Reverse rate of pRaf:P1 binding	k_{b7}	0.2	s^{-1}
Dephosphorylation rate of pRaf by P1	k_8	1	s^{-1}
Forward rate of MEK:pRaf binding	k_9	$1.95 \cdot 10^{-5}$	$molecule^{-1}s^{-1}$
Reverse rate of MEK:pRaf binding	k_{b9}	$3.3 \cdot 10^{-2}$	s^{-1}
Phosphorylation rate of MEK by pRaf	k_{10}	3.5	s^{-1}
Forward rate of pMEK:pRaf binding	k_{11}	$1.95 \cdot 10^{-5}$	$molecule^{-1}s^{-1}$
Reverse rate of pMEK:pRaf binding	k_{b11}	$3.3 \cdot 10^{-2}$	s^{-1}
Phosphorylation rate of pMEK by pRaf	k_{12}	2.9	s^{-1}
Forward rate of dpMEK:P2 binding	k_{13}	$2.38 \cdot 10^{-5}$	$molecule^{-1}s^{-1}$
Reverse rate of dpMEK:P2 binding	k_{b13}	0.8	s^{-1}
Dephosphorylation rate of dpMEK by P2	k_{14}	$5.8 \cdot 10^{-2}$	s^{-1}
Forward rate of pMEK:P2 binding	k_{15}	$4.5 \cdot 10^{-7}$	$molecule^{-1}s^{-1}$
Reverse rate of pMEK:P2 binding	k_{b15}	0.5	s^{-1}
Dephosphorylation rate of pMEK by P2	k_{16}	$5.8 \cdot 10^{-2}$	s^{-1}
Forward rate of ERK:dpMEK binding	k_{17}	$8.9 \cdot 10^{-5}$	$molecule^{-1}s^{-1}$
Reverse rate of ERK:dpMEK binding	k_{b17}	$1.83 \cdot 10^{-2}$	s^{-1}
Phosphorylation rate of ERK by dpMEK	k_{18}	16	s^{-1}
Forward rate of pERK:dpMEK binding	k_{19}	$8.9 \cdot 10^{-5}$	$molecule^{-1}s^{-1}$
Reverse rate of pERK:dpMEK binding	k_{b19}	$1.83 \cdot 10^{-2}$	s^{-1}

Phosphorylation rate of pERK by dpMEK	k_{20}	5.7	s^{-1}
Forward rate of pERK:P3 binding	k_{21}	$8.33 \cdot 10^{-6}$	$molecule^{-1}s^{-1}$
Reverse rate of pERK:P3 binding	k_{b21}	0.5	s^{-1}
Dephosphorylation rate of pERK by P3	k_{22}	0.246	s^{-1}
Forward rate of dpERK:P3 binding	k_{23}	$2.35 \cdot 10^{-5}$	$molecule^{-1}s^{-1}$
Reverse rate of dpERK:P3 binding	k_{b23}	0.6	s^{-1}
Dephosphorylation rate of dpERK by P3	k_{24}	0.246	s^{-1}
Forward rate of Raf:dpERK binding	k_{25}	$1 \cdot 10^{-6}$	$molecule^{-1}s^{-1}$
Reverse rate of Raf:dpERK binding	k_{b25}	1	s^{-1}
Hyper-phosphorylation rate of Raf by ppERK	k_{26}	10	s^{-1}
Forward rate of pRaf:dpERK binding	k_{27}	0	$molecule^{-1}s^{-1}$
Reverse rate of pRaf:dpERK binding	k_{b27}	1	s^{-1}
Hyper-phosphorylation rate of phosphorylated Raf by dpERK	k_{28}	10	s^{-1}
Forward rate of Rafi:P4 binding	k_{29}	$5 \cdot 10^{-5}$	$molecule^{-1}s^{-1}$
Reverse rate of Rafi:P4 binding	k_{b29}	0.2	s^{-1}
Dephosphorylation rate of Rafi by P4	k_{30}	0.5	s^{-1}
Total Raf	Raf_{tot}	$4 \cdot 10^4$	molecules
Total MEK	MEK_{tot}	$2.1 \cdot 10^7$	molecules
Total ERK	ERK_{tot}	$2.21 \cdot 10^7$	molecules
Total phosphatase P1	$P1_{tot}$	$4 \cdot 10^4$	molecules
Total phosphatase P2	$P2_{tot}$	$4 \cdot 10^5$	molecules
Total phosphatase P3	$P3_{tot}$	$1 \cdot 10^7$	molecules
Total phosphatase P4	$P4_{tot}$	$4 \cdot 10^4$	molecules

Variable	Label
Unphosphorylated Raf	Raf
Raf bound to RasGTP	Raf: RasGTP

Phosphorylated Raf	pRaf
Phosphatase for phosphorylated Raf	P1
Phosphorylated Raf bound to its phosphatase	pRaf: P1
Unphosphorylated MEK	MEK
MEK bound to its kinase	MEK: pRaf
Phosphorylated MEK	pMEK
Phosphorylated MEK bound to its kinase	pMEK: pRaf
Doubly-phosphorylated MEK	dpMEK
MEK phosphatase	P2
Doubly-phosphorylated MEK bound to its phosphatase	dpMEK: P2
Phosphorylated MEK bound to its phosphatase	pMEK: P2
Unphosphorylated ERK	ERK
ERK bound to its kinase	ERK: dpMEK
Phosphorylated ERK	pERK
Phosphorylated ERK bound to its kinase	pERK: dpMEK
Doubly-phosphorylated ERK	dpERK
ERK phosphatase	P3
Phosphorylated ERK bound to its phosphatase	pERK: P3
Doubly-phosphorylated ERK bound to its phosphatase	dpERK: P3
Raf bound to doubly-phosphorylated ERK	Raf: dpERK
Hyper-phosphorylated, “inactive” Raf	Rafi
Phosphorylated Raf bound to doubly-phosphorylated ERK	pRaf: dpERK
Phosphatase for hyper-phosphorylated Raf	P4
Hyper-phosphorylated Raf bound to its phosphatase	Rafi: P4

Differential Equations
$[\dot{\text{Raf}}] = -k_3 \cdot [\text{Raf}] \cdot u(\text{EGF}) + k_{b3} \cdot [\text{Raf: RasGTP}] + k_8 \cdot [\text{pRaf: P1}] - k_{25} \cdot [\text{Raf}] \cdot [\text{dpERK}] + k_{b25} \cdot [\text{Raf: dpERK}] + k_{30} \cdot [\text{Rafi: P4}]$
$[\text{Raf: } \dot{\text{RasGTP}}] = k_3 \cdot [\text{Raf}] \cdot u(\text{EGF}) - (k_{b3} + k_4) \cdot [\text{Raf: RasGTP}]$
$[\dot{\text{pRaf}}] = k_4 \cdot [\text{Raf: RasGTP}] - k_7 \cdot [\text{pRaf}] \cdot [\text{P1}] + k_{b7} \cdot [\text{pRaf: P1}] - k_9 \cdot [\text{MEK}] \cdot [\text{pRaf}] + (k_{b9} + k_{10}) \cdot [\text{MEK: pRaf}] - k_{11} \cdot [\text{pMEK}] \cdot [\text{pRaf}] + (k_{b11} + k_{12}) \cdot [\text{pMEK: pRaf}] - k_{27} \cdot [\text{pRaf}] \cdot [\text{dpERK}] + k_{b27} \cdot [\text{pRaf: dpERK}]$
$[\dot{\text{P1}}] = -k_7 \cdot [\text{pRaf}] \cdot [\text{P1}] + (k_{b7} + k_8) \cdot [\text{pRaf: P1}]$
$[\text{pRaf: } \dot{\text{P1}}] = k_7 \cdot [\text{pRaf}] \cdot [\text{P1}] - (k_{b7} + k_8) \cdot [\text{pRaf: P1}]$
$[\dot{\text{MEK}}] = -k_9 \cdot [\text{MEK}] \cdot [\text{pRaf}] + k_{b9} \cdot [\text{MEK: pRaf}] + k_{16} \cdot [\text{pMEK: P2}]$
$[\text{MEK: } \dot{\text{pRaf}}] = k_9 \cdot [\text{MEK}] \cdot [\text{pRaf}] - (k_{b9} + k_{10}) \cdot [\text{MEK: pRaf}]$
$[\dot{\text{pMEK}}] = k_{10} \cdot [\text{MEK: pRaf}] - k_{11} \cdot [\text{pMEK}] \cdot [\text{pRaf}] + k_{b11} \cdot [\text{pMEK: pRaf}] + k_{14} \cdot [\text{dpMEK: P2}] - k_{15} \cdot [\text{pMEK}] \cdot [\text{P2}] + k_{b15} \cdot [\text{pMEK: P2}]$
$[\text{pMEK: } \dot{\text{pRaf}}] = k_{11} \cdot [\text{pMEK}] \cdot [\text{pRaf}] - (k_{b11} + k_{12}) \cdot [\text{pMEK: pRaf}]$
$[\dot{\text{dpMEK}}] = k_{12} \cdot [\text{pMEK: pRaf}] - k_{13} \cdot [\text{dpMEK}] \cdot [\text{P2}] + k_{b13} \cdot [\text{dpMEK: P2}] - k_{17} \cdot [\text{ERK}] \cdot [\text{dpMEK}] + (k_{b17} + k_{18}) \cdot [\text{ERK: dpMEK}] - k_{19} \cdot [\text{pERK}] \cdot [\text{dpMEK}] + (k_{b19} + k_{20}) \cdot [\text{pERK: dpMEK}]$
$[\dot{\text{P2}}] = -k_{13} \cdot [\text{dpMEK}] \cdot [\text{P2}] + (k_{b13} + k_{14}) \cdot [\text{dpMEK: P2}] - k_{15} \cdot [\text{pMEK}] \cdot [\text{P2}] + (k_{b15} + k_{16}) \cdot [\text{pMEK: P2}]$
$[\text{dpMEK: } \dot{\text{P2}}] = k_{13} \cdot [\text{dpMEK}] \cdot [\text{P2}] - (k_{b13} + k_{14}) \cdot [\text{dpMEK: P2}]$
$[\text{pMEK: } \dot{\text{P2}}] = k_{15} \cdot [\text{pMEK}] \cdot [\text{P2}] - (k_{b15} + k_{16}) \cdot [\text{pMEK: P2}]$
$[\dot{\text{ERK}}] = -k_{17} \cdot [\text{ERK}] \cdot [\text{dpMEK}] + k_{b17} \cdot [\text{ERK: dpMEK}] + k_{22} \cdot [\text{pERK: P3}]$
$[\text{ERK: } \dot{\text{dpMEK}}] = k_{17} \cdot [\text{ERK}] \cdot [\text{dpMEK}] - (k_{b17} + k_{18}) \cdot [\text{ERK: dpMEK}]$
$[\dot{\text{pERK}}] = k_{18} \cdot [\text{ERK: dpMEK}] - k_{19} \cdot [\text{pERK}] \cdot [\text{dpMEK}] + k_{b19} \cdot [\text{pERK: dpMEK}] - k_{21} \cdot [\text{pERK}] \cdot [\text{P3}] + k_{b21} \cdot [\text{pERK: P3}] + k_{24} \cdot [\text{dpERK: P3}]$
$[\text{pERK: } \dot{\text{dpMEK}}] = k_{19} \cdot [\text{pERK}] \cdot [\text{dpMEK}] - (k_{b19} + k_{20}) \cdot [\text{pERK: dpMEK}]$
$[\dot{\text{dpERK}}] = k_{20} \cdot [\text{pERK: dpMEK}] - k_{23} \cdot [\text{dpERK}] \cdot [\text{P3}] + k_{b23} \cdot [\text{dpERK: P3}] - k_{25} \cdot [\text{Raf}] \cdot [\text{dpERK}] + (k_{b25} + k_{26}) \cdot [\text{Raf: dpERK}] - k_{27} \cdot [\text{pRaf}] \cdot [\text{dpERK}] + (k_{b27} + k_{28}) \cdot [\text{pRaf: dpERK}]$

$[\dot{P3}] = -k_{21} \cdot [pERK] \cdot [P3] + (k_{b21} + k_{22}) \cdot [pERK: P3] - k_{23} \cdot [dpERK] \cdot [P3] + (k_{b23} + k_{24}) \cdot [dpERK: P3]$
$[pER\dot{K}: P3] = k_{21} \cdot [pERK] \cdot [P3] - (k_{b21} + k_{22}) \cdot [pERK: P3]$
$[dpER\dot{K}: P3] = k_{23} \cdot [dpERK] \cdot [P3] - (k_{b23} + k_{24}) \cdot [dpERK: P3]$
$[Raf: \dot{dp}ERK] = k_{25} \cdot [Raf] \cdot [dpERK] - (k_{b25} + k_{26}) \cdot [Raf: dpERK]$
$[\dot{Rafi}] = k_{26} \cdot [Raf: dpERK] + k_{28} \cdot [pRaf: dpERK] - k_{29} \cdot [Rafi] \cdot [P4] + k_{b29} \cdot [Rafi: P4]$
$[pRaf: \dot{dp}ERK] = k_{27} \cdot [pRaf] \cdot [dpERK] - (k_{b27} + k_{28}) \cdot [pRaf: dpERK]$
$[\dot{P4}] = -k_{29} \cdot [Rafi] \cdot [P4] + (k_{b29} + k_{30}) \cdot [Rafi: P4]$
$[\dot{Rafi}: P4] = k_{29} \cdot [Rafi] \cdot [P4] - (k_{b29} + k_{30}) \cdot [Rafi: P4]$
Algebraic Equations for conserved species
$Raf_{tot} = [Raf] + [Raf: RasGTP] + [pRaf] + [pRaf: P1] + [MEK: pRaf] + [pMEK: pRaf] + [Raf: dpERK] + [Rafi] + [pRaf: dpERK] + [Rafi: P4]$
$MEK_{tot} = [MEK] + [MEK: pRaf] + [pMEK] + [pMEK: pRaf] + [dpMEK] + [dpMEK: P2] + [pMEK: P2] + [ERK: dpMEK] + [pERK: dpMEK]$
$ERK_{tot} = [ERK] + [ERK: dpMEK] + [pERK] + [pERK: dpMEK] + [dpERK] + [pERK: P3] + [dpERK: P3] + [Raf: dpERK] + [pRaf: dpERK]$
$P1_{tot} = [P1] + [pRaf: P1]$
$P2_{tot} = [P2] + [dpMEK: P2] + [pMEK: P2]$
$P3_{tot} = [P3] + [pERK: P3] + [dpERK: P3]$
$P4_{tot} = [P4] + [Rafi: P4]$

216

Appendix 1 - Table 3. Parameters, variables and equations of the Tgfβ model.

Parameter	Label	Value
Phosphorylation rate of Smad2	k_{phos}	$4.0 \cdot 10^{-4}$ $nM^{-1}s^{-1}$
Dephosphorylation rate of Smad2	k_{dephos}	$6.6 \cdot 10^{-3}$ $nM^{-1}s^{-1}$
Nuclear import rate of Smad2	k_{in2}	$2.6 \cdot 10^{-3}$ s^{-1}
Nuclear export rate of Smad2	k_{ex2}	$5.6 \cdot 10^{-3}$ s^{-1}
Nuclear import rate of Smad4	k_{in4}	$2.6 \cdot 10^{-3}$ s^{-1}
Nuclear export rate of Smad4	k_{ex4}	$2.6 \cdot 10^{-3}$ s^{-1}
Smad complex import factor	CIF	5.7
Forward rate for Smad complex binding	k_{on}	$1.8 \cdot 10^{-3}$ $nM^{-1}s^{-1}$
Reverse rate for Smad complex binding	k_{off}	$1.6 \cdot 10^{-2}$ s^{-1}
Cytoplasmic to nuclear volume ratio	a	2.3
Total Smad2 (initialized to cytoplasm)	$S2_{tot}$	73.0 nM
Total Smad4 (initialized to cytoplasm)	$S4_{tot}$	73.0 nM
Total phosphatase in nucleus	PPase	1 nM
Total Receptors	R_{tot}	1 nM

Variable	Label
Cytoplasmic Smad2	S2c
Cytoplasmic phosphorylated Smad2	pS2c
Cytoplasmic Smad4	S4c
Cytoplasmic Smad2:Smad4 complex	S24c
Cytoplasmic Smad2:Smad2 complex	S22c
Nuclear Smad2	S2n
Nuclear phosphorylated Smad2	pS2n
Nuclear Smad4	S4n
Nuclear Smad2:Smad4 complex	S24n

Nuclear Smad2:Smad2 complex	S22n

Differential Equations
$[\dot{S2c}] = -k_{phos} \cdot u(Tgf\beta) \cdot [S2c] - k_{in2} \cdot [S2c] + k_{ex2} \cdot [S2n]$
$[\dot{pS2c}] = k_{phos} \cdot u(Tfg\beta) \cdot [S2c] - k_{in2} \cdot [pS2c] - k_{on} \cdot [pS2c] \cdot ([S4c] + 2 \cdot [pS2c]) + k_{off} \cdot ([S24c] + 2 \cdot [S22c]) + k_{ex2} \cdot [pS2n]$
$[\dot{S4c}] = -k_{in4} \cdot [S4c] - k_{on} \cdot [pS2c] \cdot [S4c] + k_{off} \cdot [S24c] + k_{ex4} \cdot [S4n]$
$[\dot{S24c}] = k_{on} \cdot [pS2c] \cdot [S4c] - k_{off} \cdot [S24c] - k_{in2} \cdot CIF \cdot [S24c]$
$[\dot{S22c}] = k_{on} \cdot [pS2c]^2 - k_{off} \cdot [S22c] - k_{in2} \cdot CIF \cdot [S22c]$
$[\dot{S2n}] = a \cdot k_{in2} \cdot [S2c] - a \cdot k_{ex2} \cdot [S2n] + k_{dephos} \cdot PPase \cdot [pS2n]$
$[\dot{pS2n}] = a \cdot k_{in2} \cdot [pS2c] - a \cdot k_{ex2} \cdot [pS2n] - k_{dephos} \cdot PPase \cdot [pS2n] - k_{on} \cdot [pS2n] \cdot ([S4n] + 2 \cdot [pS2n]) + k_{off} \cdot ([S24n] + 2 \cdot [S22n])$
$[\dot{S4n}] = a \cdot k_{in4} \cdot [S4c] - a \cdot k_{ex4} \cdot [S4n] - k_{on} \cdot [pS2n] \cdot [S4n] + k_{off} \cdot [S24n]$
$[\dot{S24n}] = a \cdot k_{in2} \cdot CIF \cdot [S24c] + k_{on} \cdot [pS2n] \cdot [S4n] - k_{off} \cdot [S24n]$
$[\dot{S22n}] = a \cdot k_{in2} \cdot CIF \cdot [S22c] + k_{on} \cdot [pS2n]^2 - k_{off} \cdot [S22n]$
Algebraic Equations for conserved species
$S2_{tot} = [S2c] + [pS2c] + [S24c] + 2 \cdot [S22c] + \frac{1}{a}(2 \cdot [S22n] + [S24n] + [pS2n] + [S2n])$
$S4_{tot} = [S4c] + [S24c] + \frac{1}{a}([S24n] + [S4n])$

218

Appendix 1 - Table 4. Examples of biological systems where the Wnt, ERK, and Tgfβ pathways have been shown to produce graded response in single-cell level.

Pathway	**Systems where graded response has been observed**	**References**
Live imaging of single cells		
Tgfβ pathway	Mouse myoblasts	Frick *et al.*, 2017 (58); Warmflash *et al.*, 2012 (62)
	Human epidermal keratinocytes	Nicolas *et al.*, 2004 (18); Warmflash *et al.* 2012 (62); Schmierer *et al.*, 2008 (22); Vizan *et al.*, 2013 (32)
	Human cervical epithelial cells	Nicolas *et al.*, 2004 (18)
	Human breast epithelial cells	Strasen *et al.*, 2018 (63)
Canonical Wnt pathway	Human embryonic kidney cells	Kafri *et al.*, 2016 (64) (this is the only published live single-cell imaging study in the Wnt pathway so far)
ERK pathway	Mouse fibroblasts	Toettcher *et al.*, 2013 (65)
	Mouse embryonic fibroblasts	MacKeigan *et al.*, 2005 (37)
	Human non-small cell lung carcinoma	Cheong *et al.*, 2011 (66)
	Human mammary gland cells	Selimkhanov *et al.*, 2014 (67); Perrett *et al.*, 2013 (68)
	Human cervical epithelial cells	Voliotis *et al.*, 2014 (69); Whitehursts *et al.*, 2004 (36); Perrett *et al.*, 2013 (68)
	Human foreskin fibroblasts	Whitehursts *et al.*, 2004 (36)
Immunofluorescence and FACS studies		
Tgfβ pathway	*Xenopus* embryo	Schohl and Fagotto, 2002 (70)
	Mouse testes	Itman *et al.*, 2009 (71)
	Zebrafish embryo	Dubrulle *et al.*, 2015 (72)
Canonical Wnt pathway	*Xenopus* embryo	Schneider et al., 1996 (73); Fagotto and Gumbiner, 1994 (74); Schohl and Fagotto, 2002 (70)
	Mouse embyo	Auhlela *et al.*, 2008 (75)
	Planaria	Sureda-Gomez *et al.*, 2016 (76)
	Sea anemone embryo	Wikramanayake *et al.*, 2003 (77)
ERK pathway	Chick embryo	Delfini *et al.*, 2005 (78)
	Xenopus embryo	Schohl and Fagotto, 2002 (70)
	Human T lymphocyte cells	Lin *et al.*, 2009 (79)
	Rat adrenal gland cells	Santos *et al.*, 2007 (80)

A. Parameter group are constant across inputs

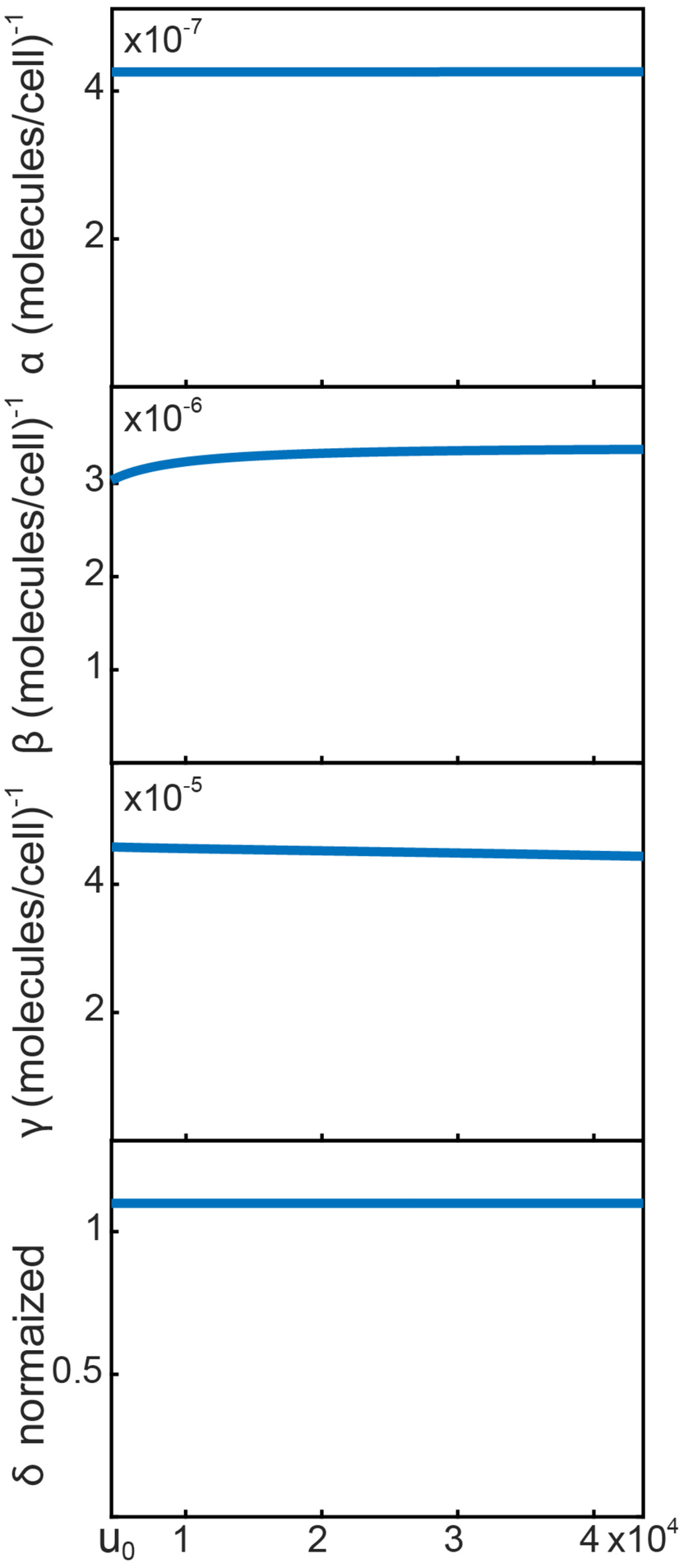

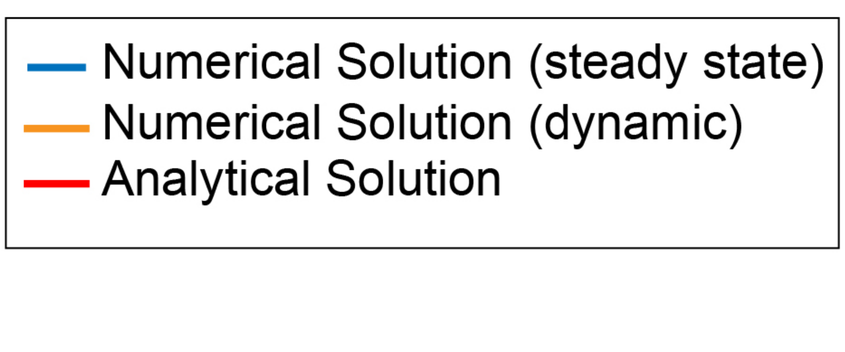

B. Ultrasensitivity for free pRaf

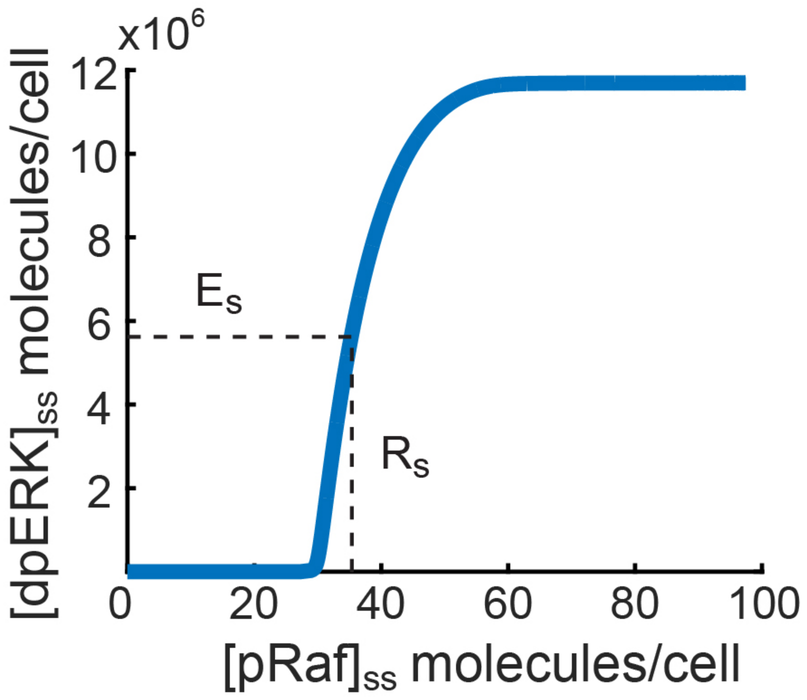

C. Ultrasensitivity for total pRaf

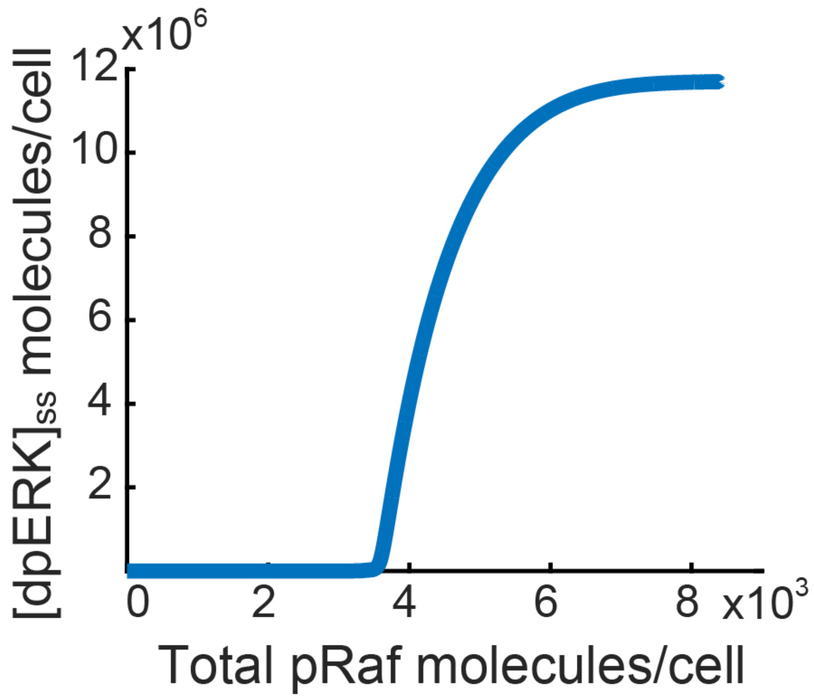

D. Dynamic input u(EGF)

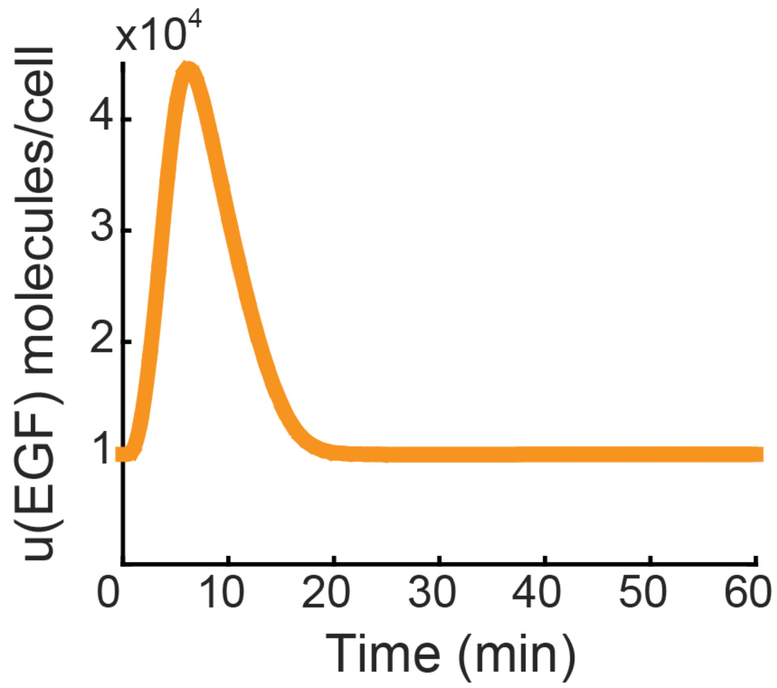

E. Dynamic output [dpERK]

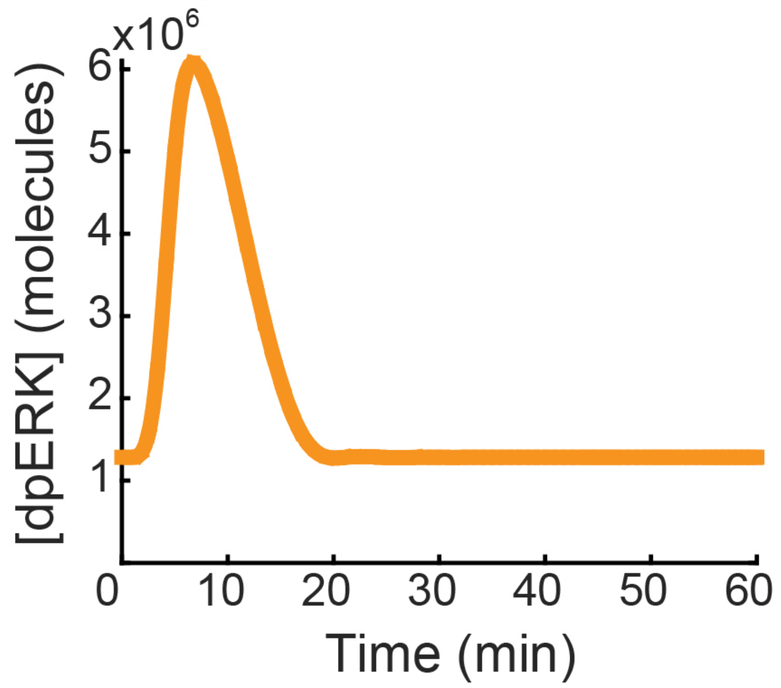

F. Linearity for pulsatile ERK

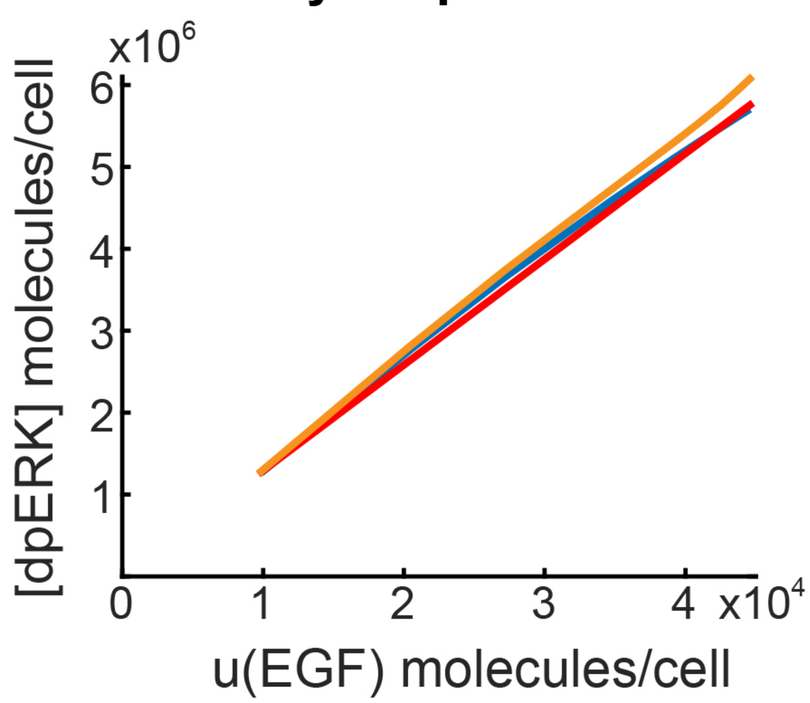

G. Linearity for Raf overexp

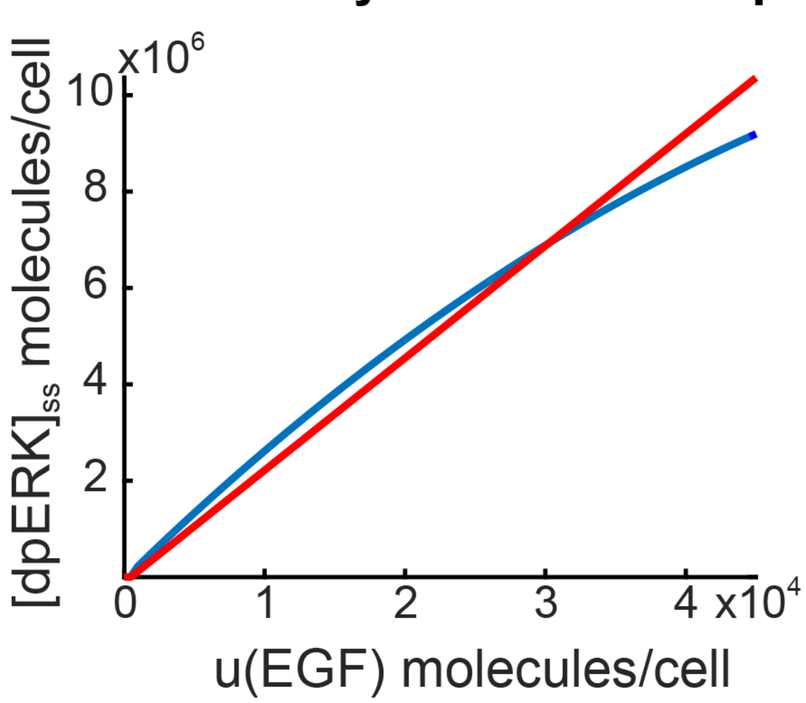

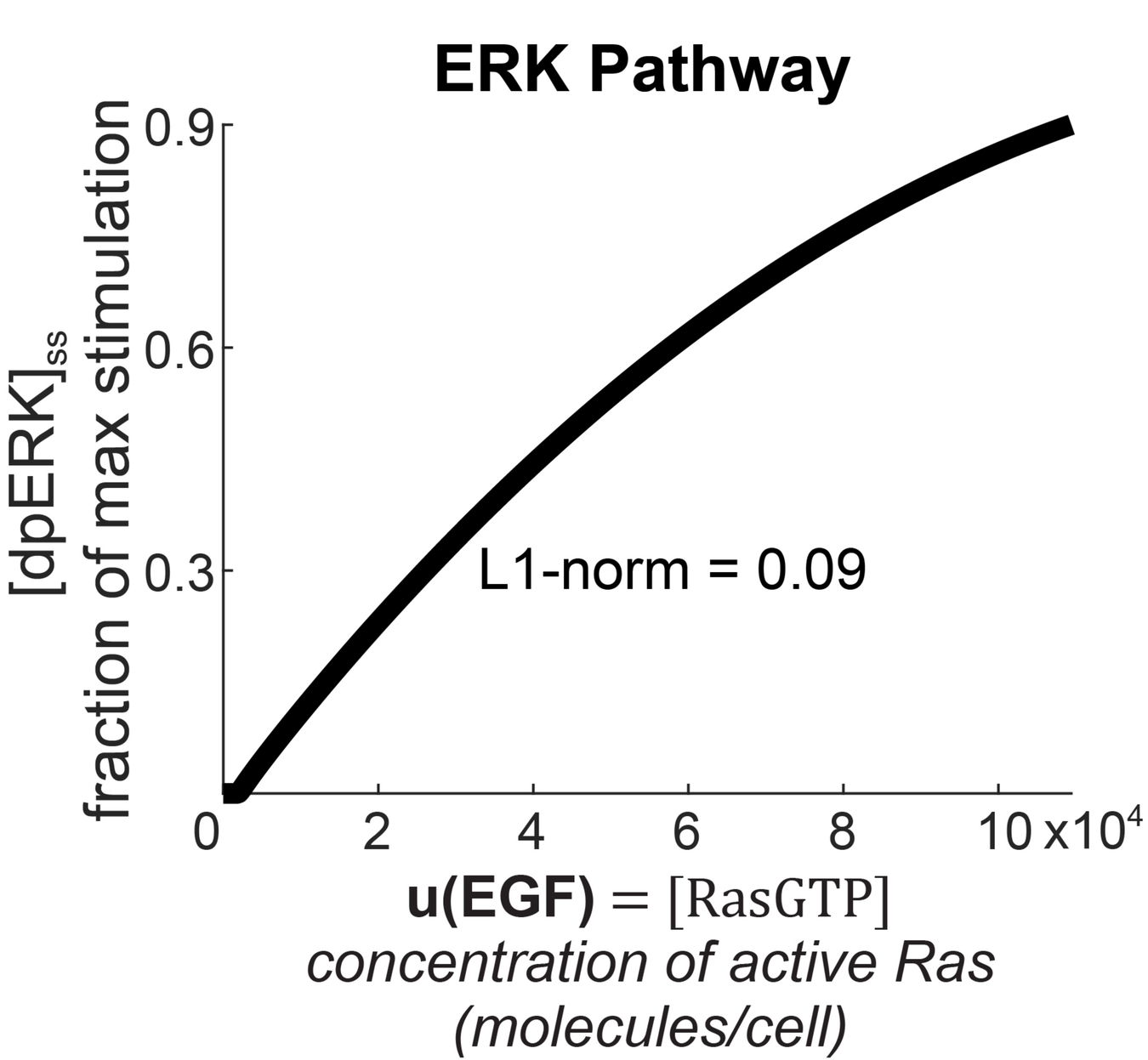
ERK Pathway
[dpERK]ss
fraction of max stimulation
0.9
0.6
0.3
0
L1-norm = 0.09
0
2
4
6
8
10 x10^4
u(EGF) = [RasGTP]
concentration of active Ras
(molecules/cell)

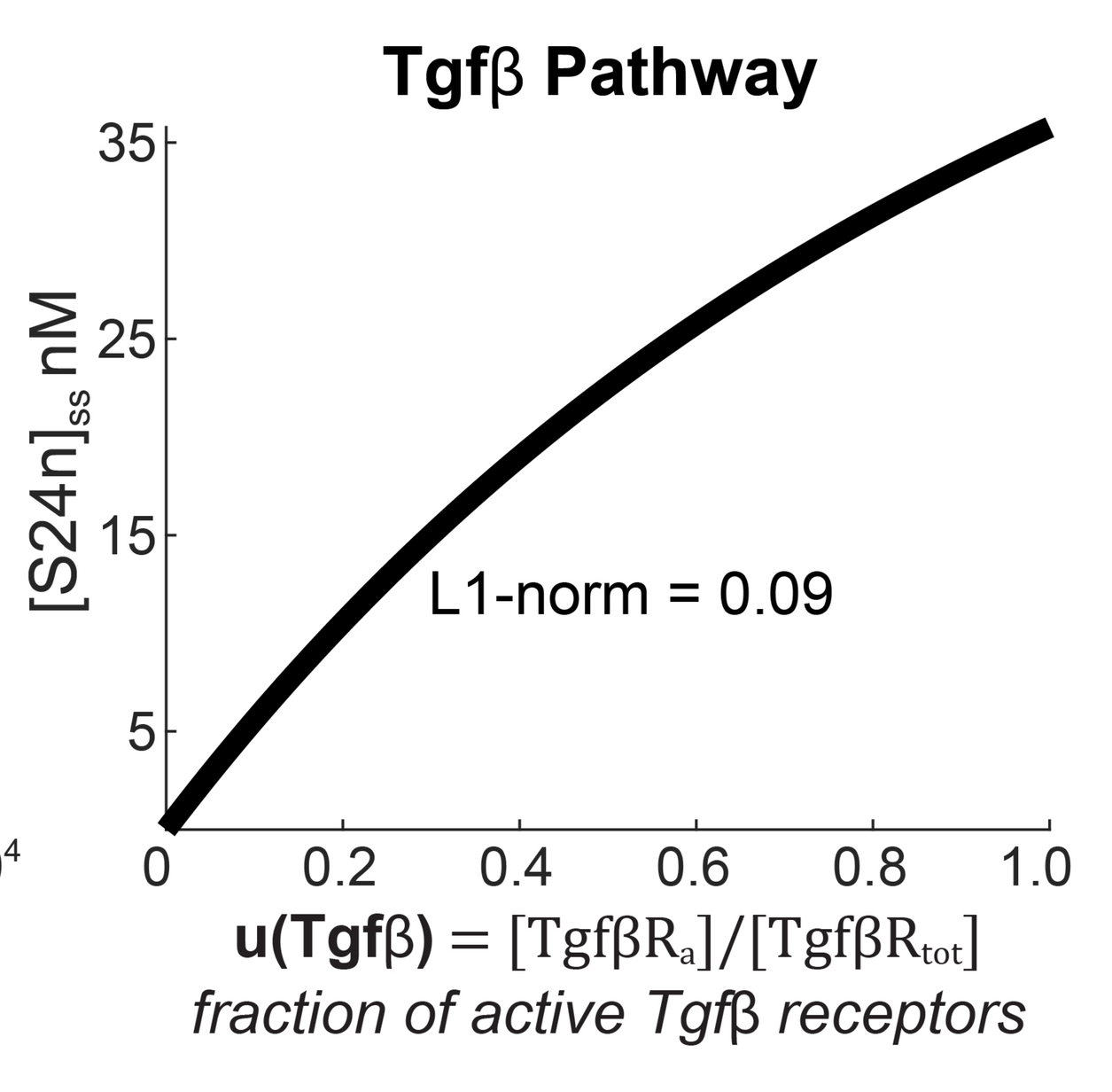
Tgfβ Pathway
[S24n]ss nM
35
25
15
5
L1-norm = 0.09
0
0.2
0.4
0.6
0.8
1.0
u(Tgfβ) = [TgfβRa]/[TgfβRtot]
fraction of active Tgfβ receptors

A. $[S4n]_{ss}$ is constant across inputs

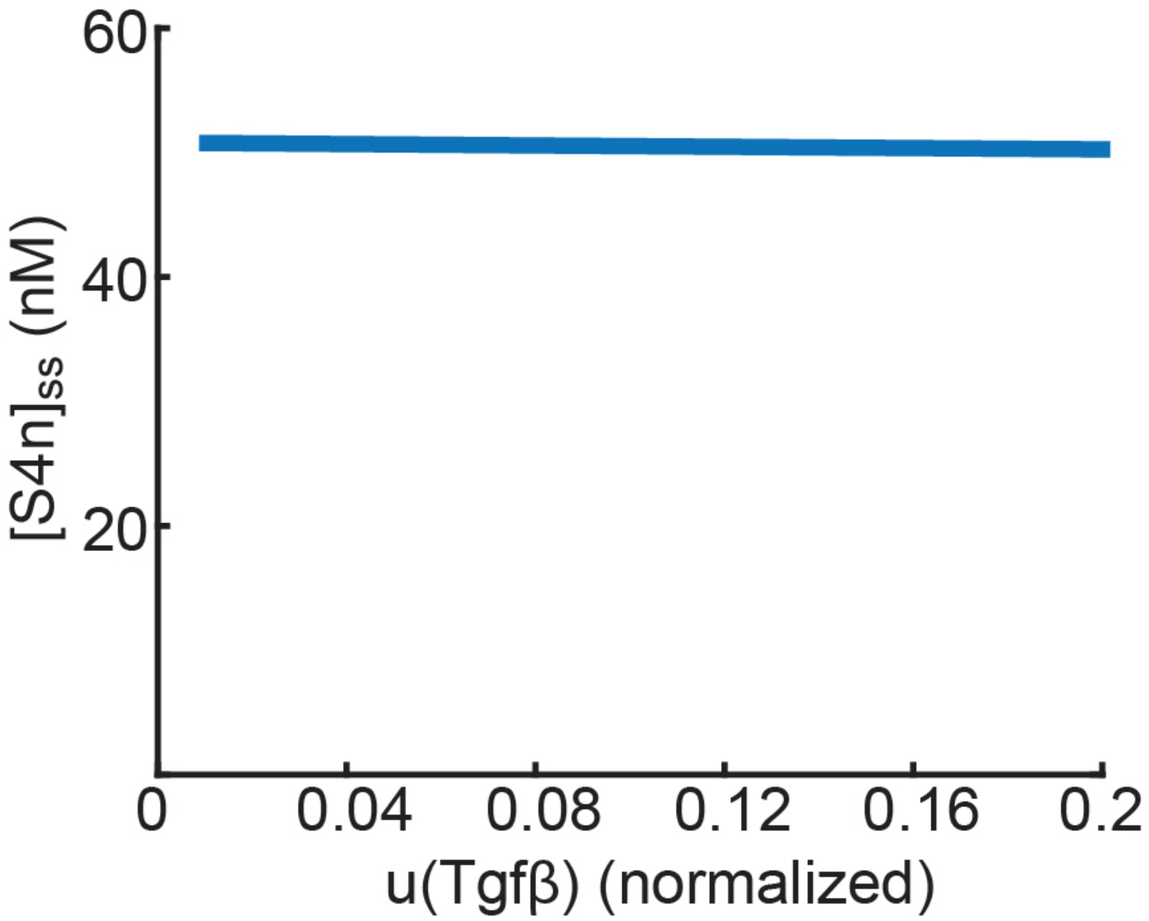

B. Dynamic input u(Tgfβ)

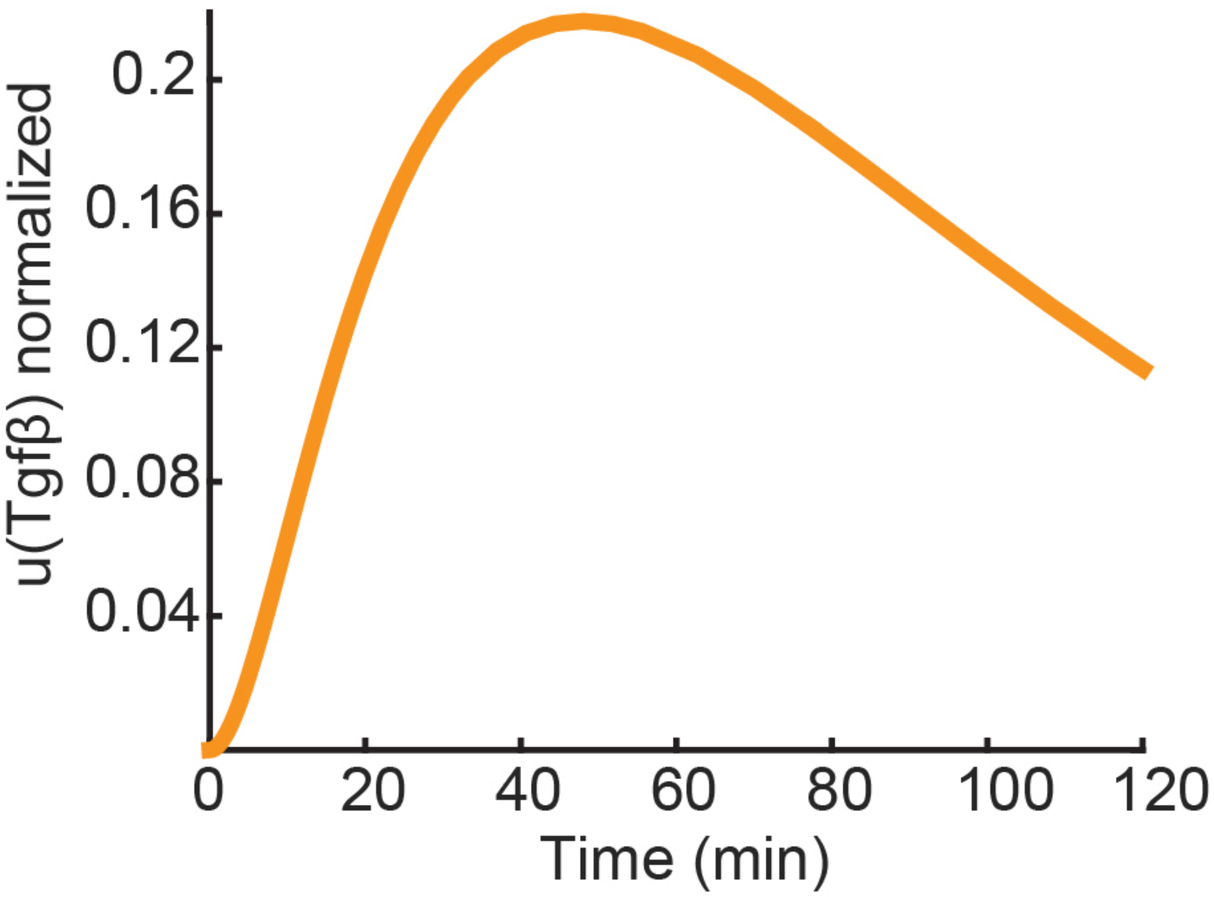

C. Dynamic output [S24n]

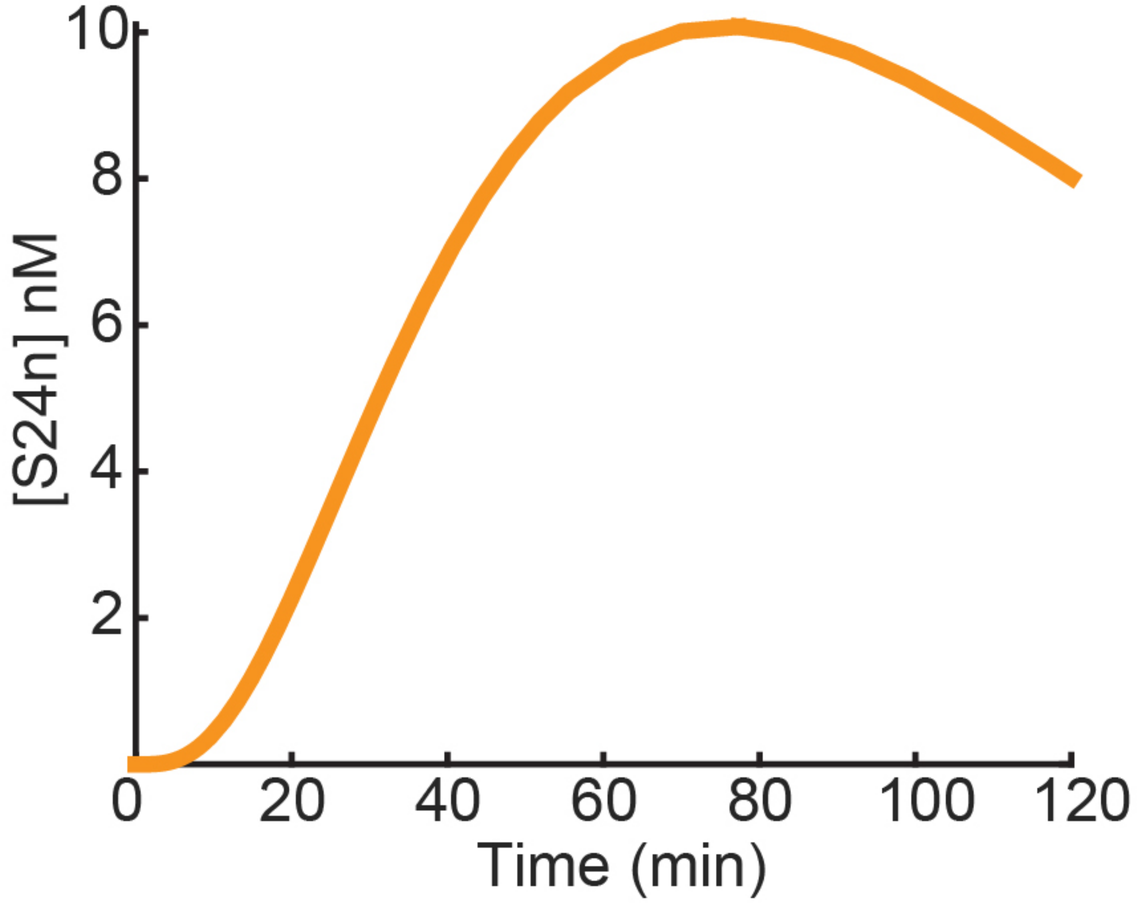

D. Linearity for pulsatile Smad

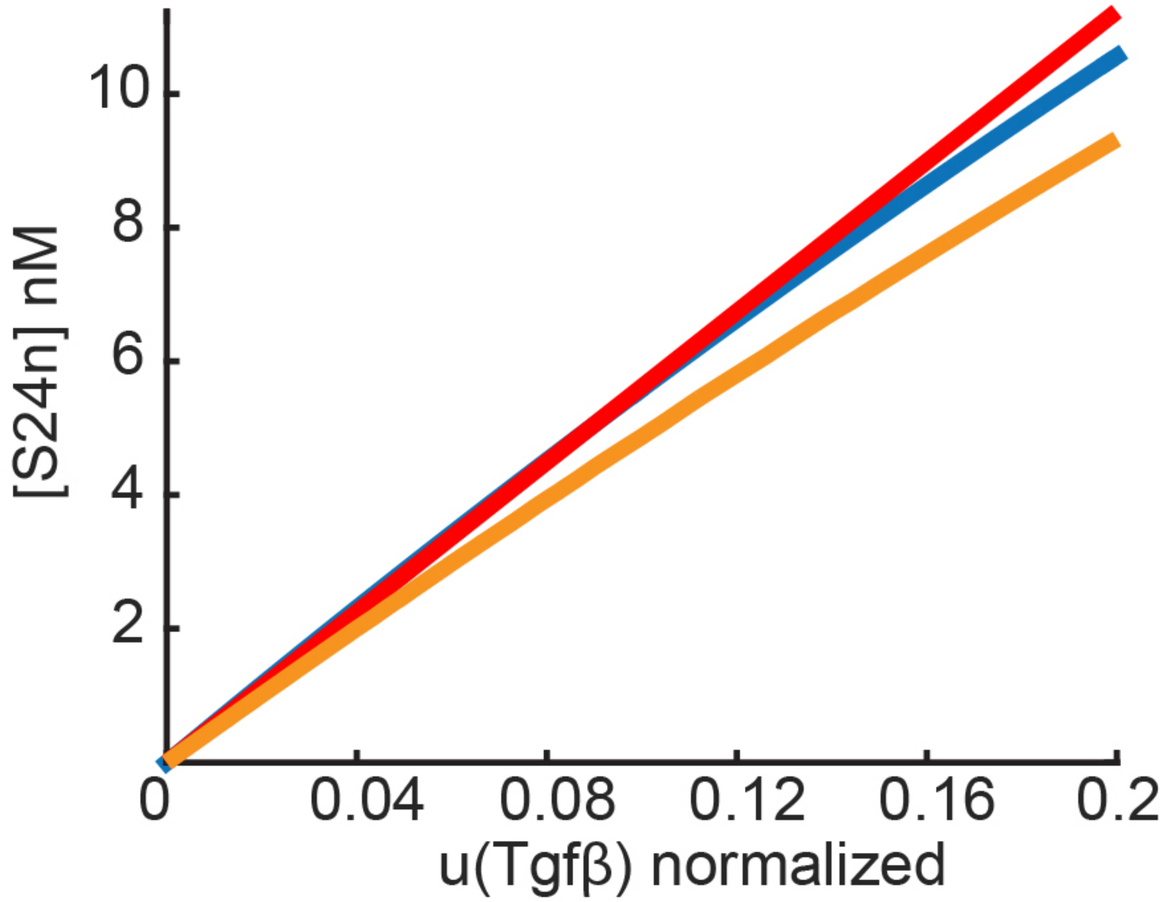

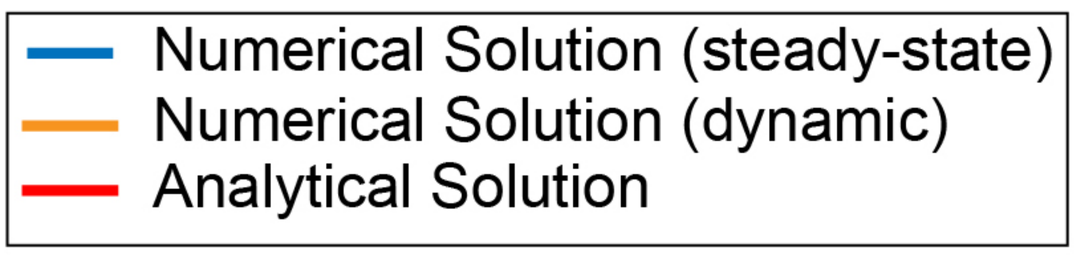

Incorporating the dual function of GSK3β: Inhibiting β-catenin and activating LRP

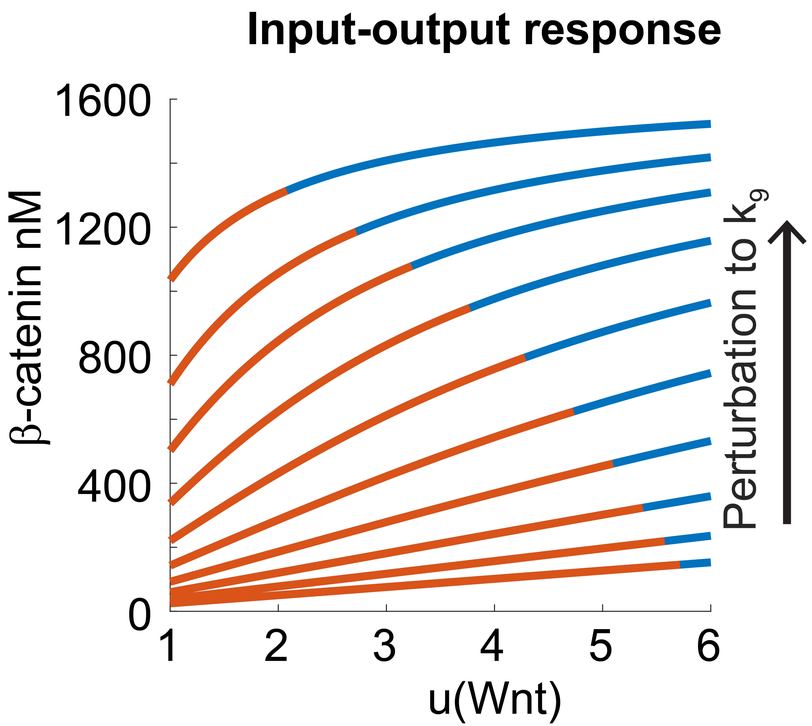

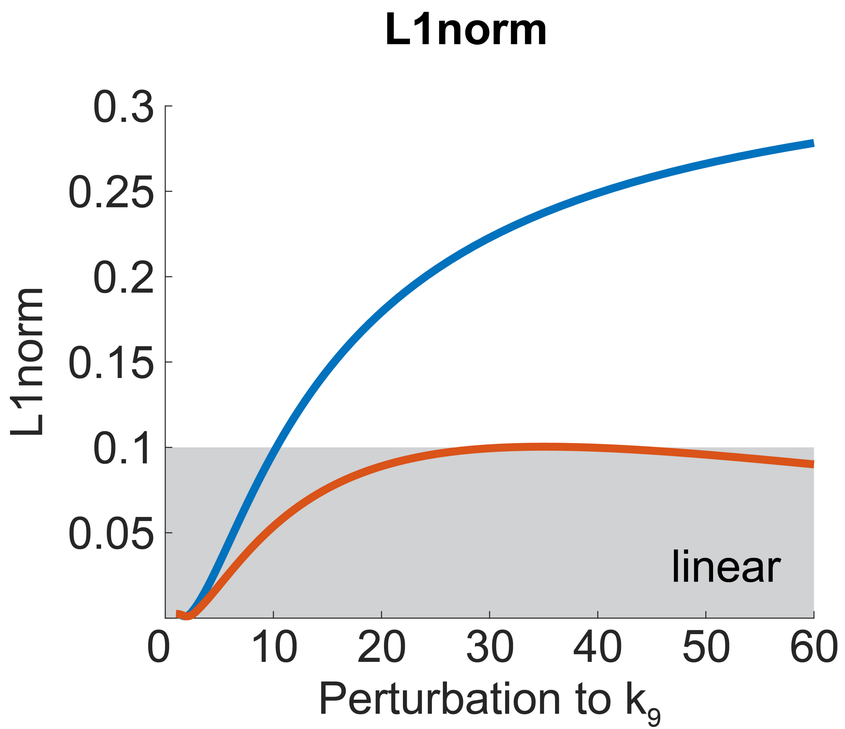

Wnt model

Wnt model with GSK3β dual function

Wnt model

$$u(Wnt) = 1 + k_3 \cdot [Dvl_a]/k_{-6}$$

Wnt model with GSK3β dual function

$$u(Wnt) = 1 + k'_3 \cdot [Dvl_a]/k_{-6}$$

$$k'_3 = k_3 \cdot \frac{k_9 \cdot [GSK3]}{k_r + k_9 \cdot [GSK3]}$$

Wnt Pathway

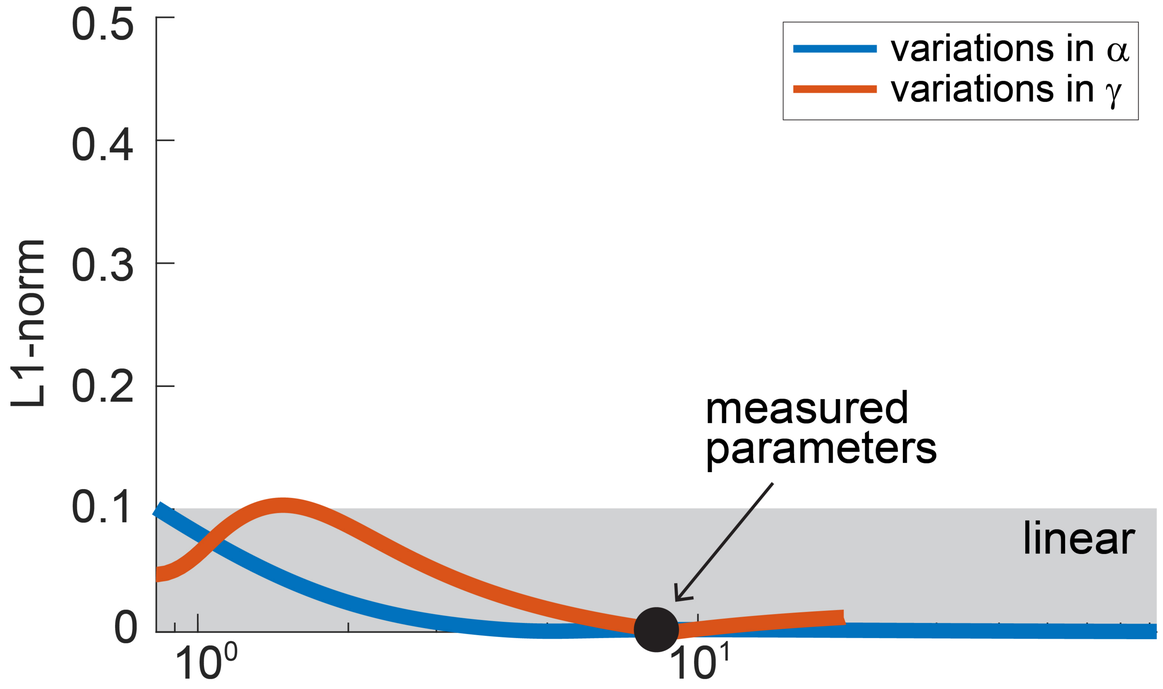

$$S = \frac{\alpha}{(1+\gamma)\cdot u}$$

ERK Pathway

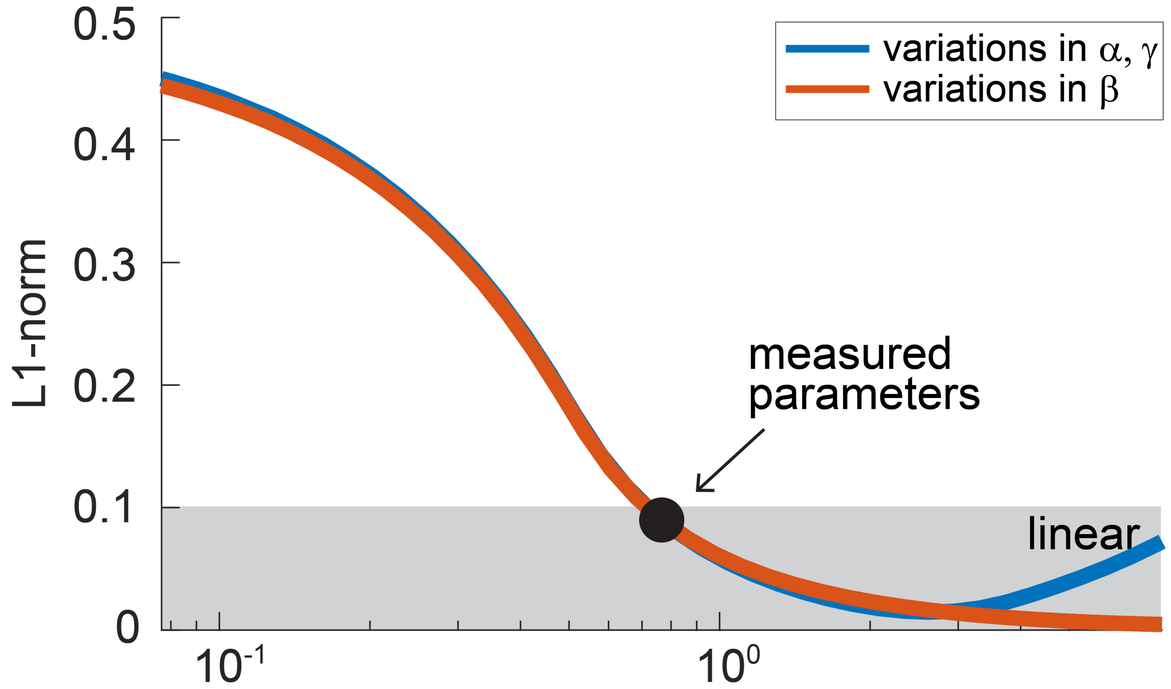

$$S = \frac{\beta[\mathrm{dpERK}]_s + \delta}{\alpha\cdot u} \cdot \frac{R_s}{\mathrm{Raf}_{tot}}$$

Tgfβ Pathway

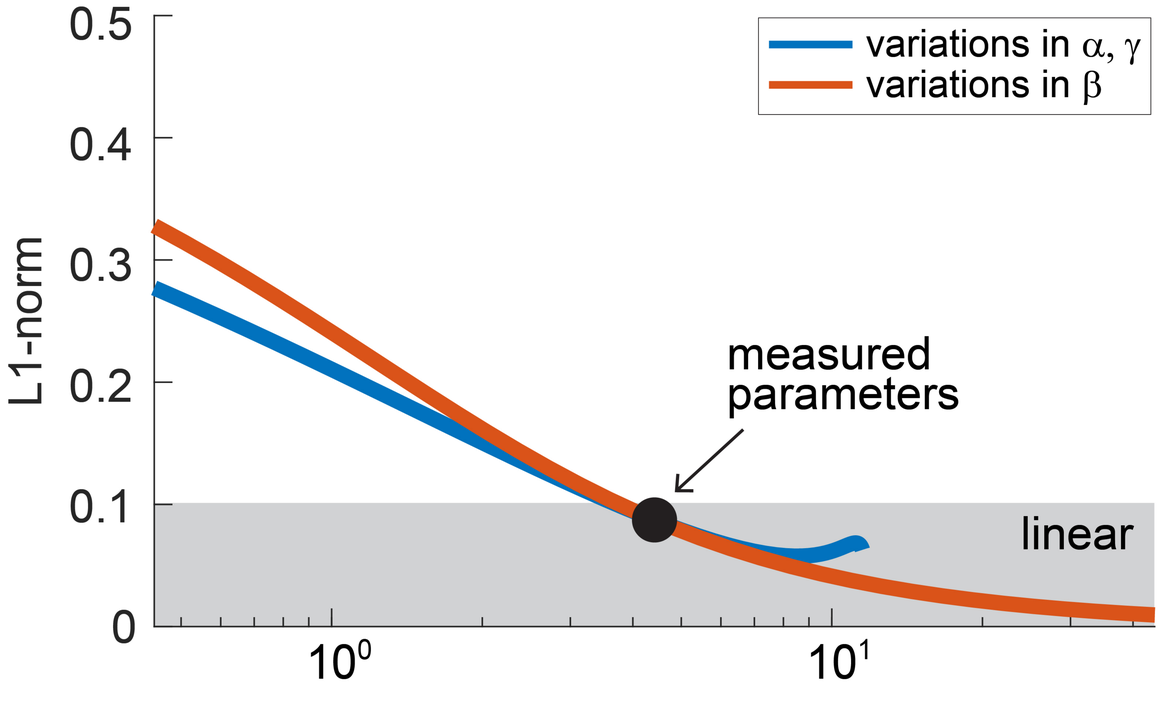

$$S = \frac{\beta}{(\alpha+\gamma)\cdot u}$$

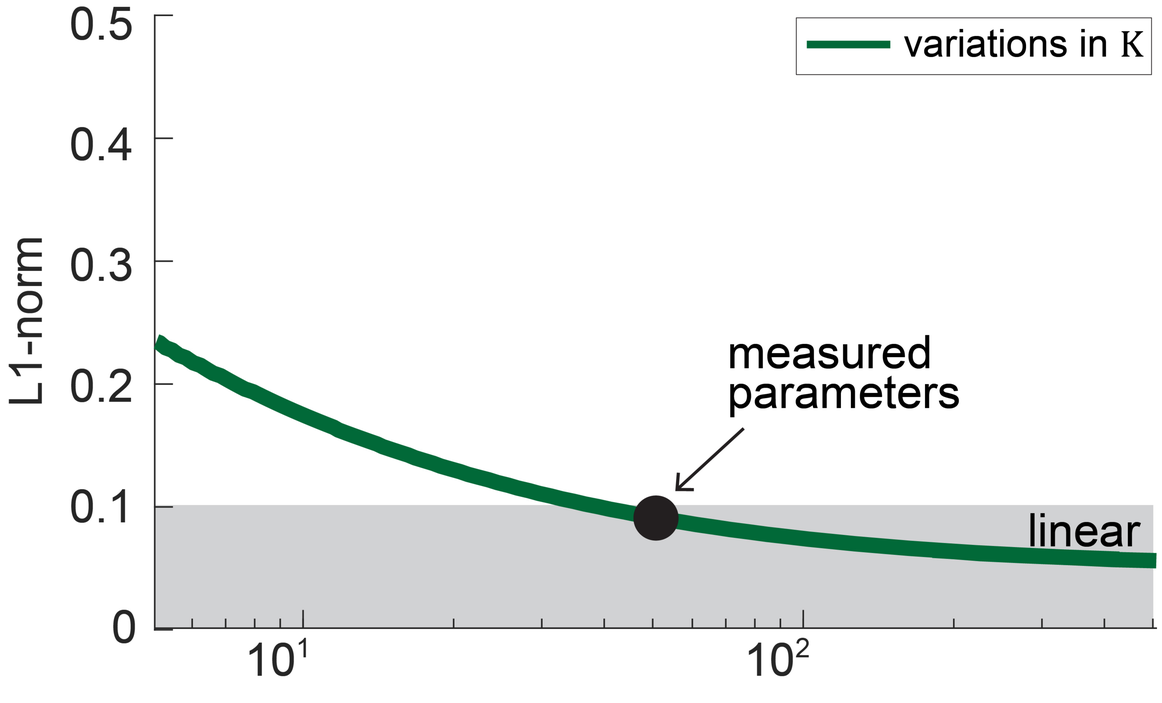

$$K = \frac{d\ln([\mathrm{dpERK}]_{ss})}{d\ln([\mathrm{pRaf}]_{ss})}$$

A

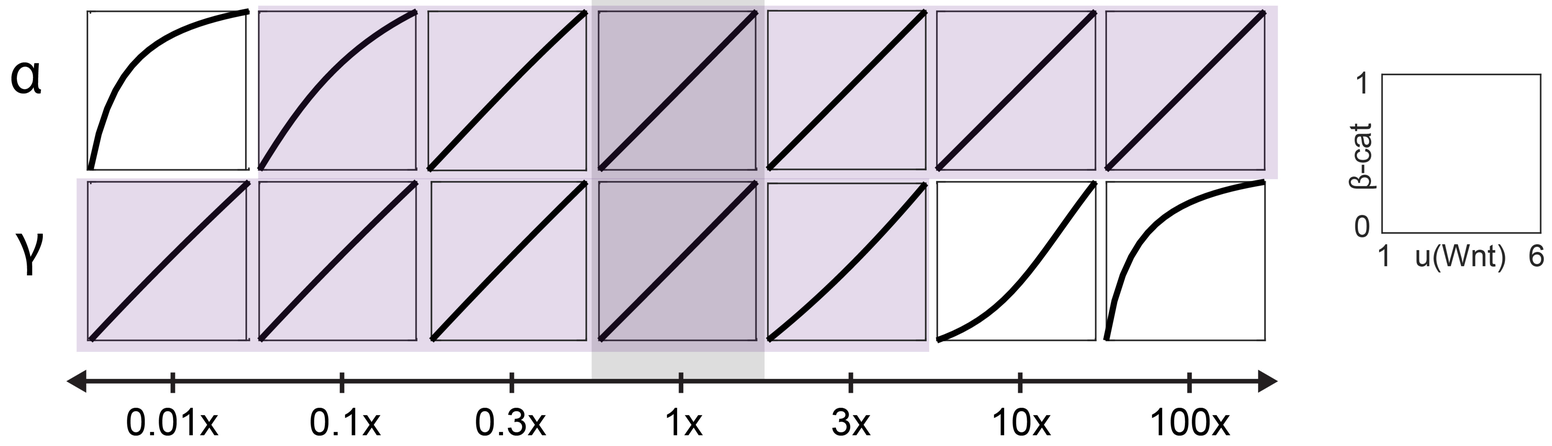
Wnt pathway
α
γ
0.01x
0.1x
0.3x
1x
3x
10x
100x
1
β-cat
0
1
u(Wnt)
6

B

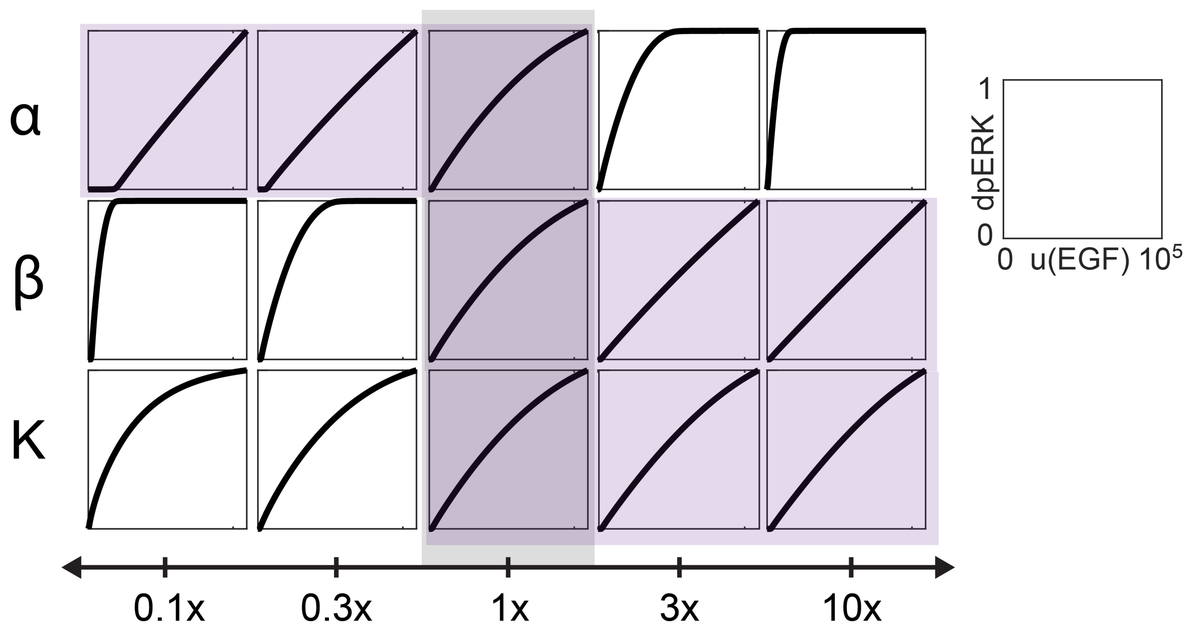
ERK pathway
α
β
κ
0.1x
0.3x
1x
3x
10x
1
dpERK
0
0
u(EGF)
10^5

C

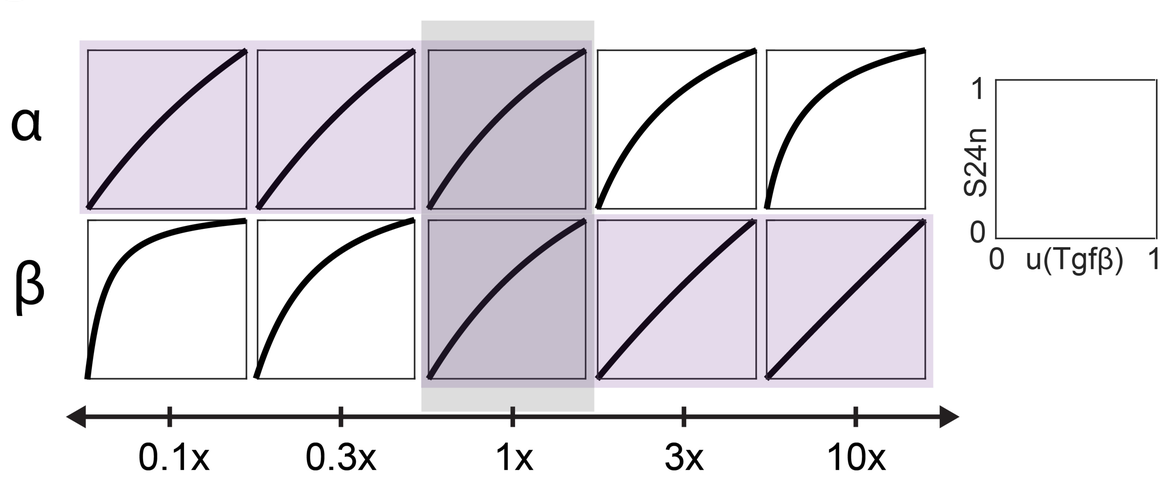
TGFβ pathway
α
β
0.1x
0.3x
1x
3x
10x
1
S24n
0
0
u(Tgfβ)
1

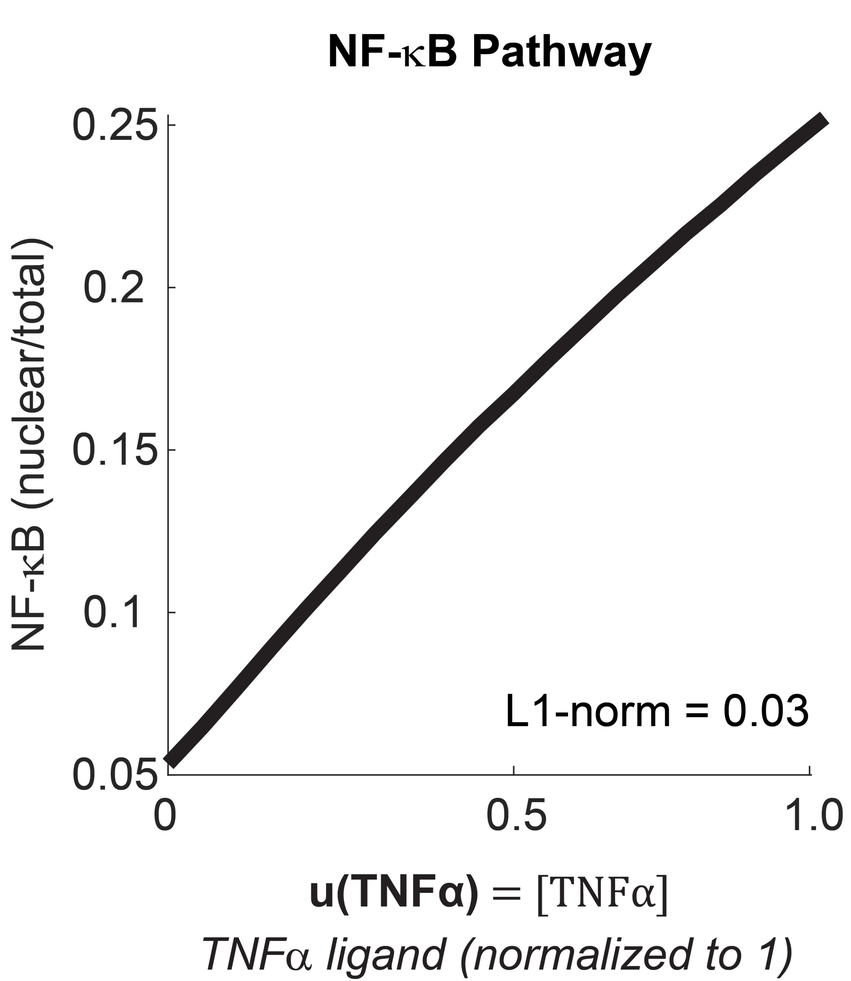
NF-κB Pathway
NF-κB (nuclear/total)
0.25
0.2
0.15
0.1
0.05
0
0.5
1.0
L1-norm = 0.03
u(TNFα) = [TNFα]
TNFα ligand (normalized to 1)

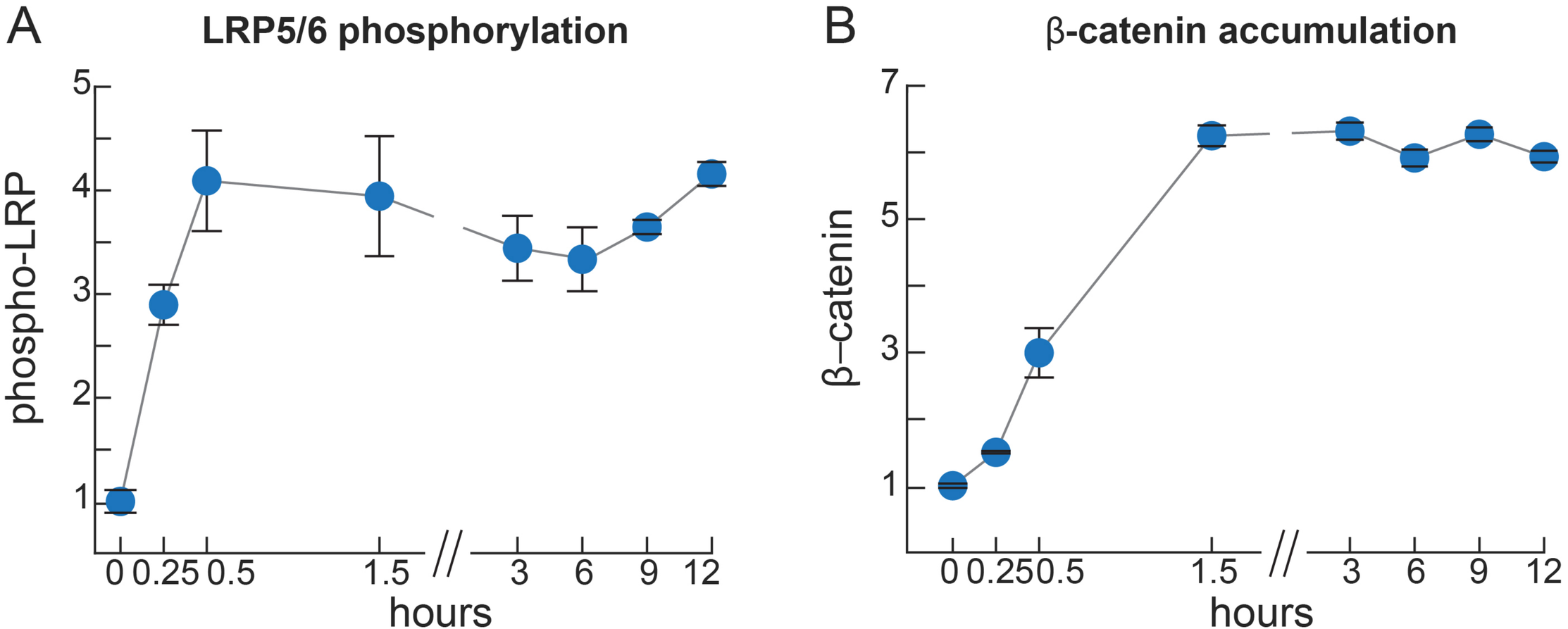
A
LRP5/6 phosphorylation
phospho-LRP
5
4
3
2
1
0 0.25 0.5 1.5 3 6 9 12
hours
B
β-catenin accumulation
β–catenin
7
5
3
1
0 0.25 0.5 1.5 3 6 9 12
hours

A. Wnt3A dose response for phospho-LRP5/6

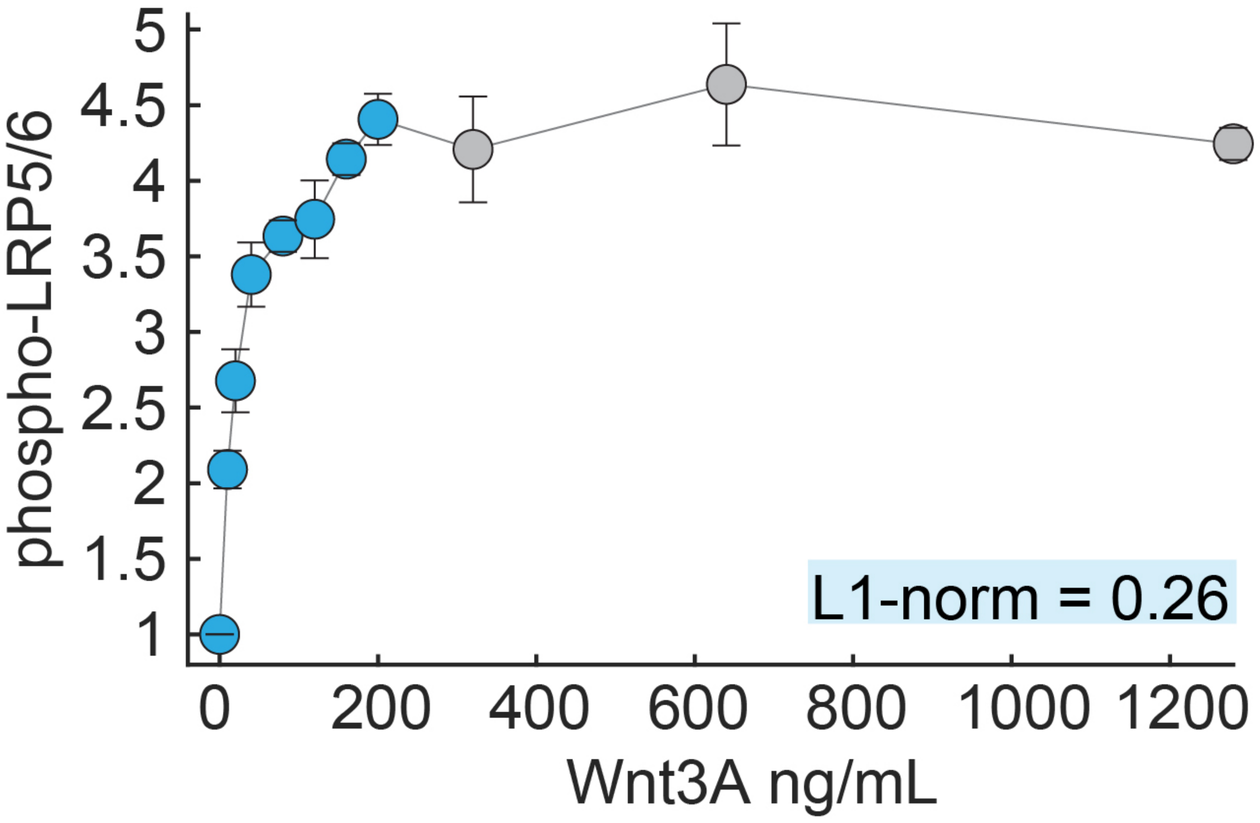

B. Wnt3A dose response for β-catenin

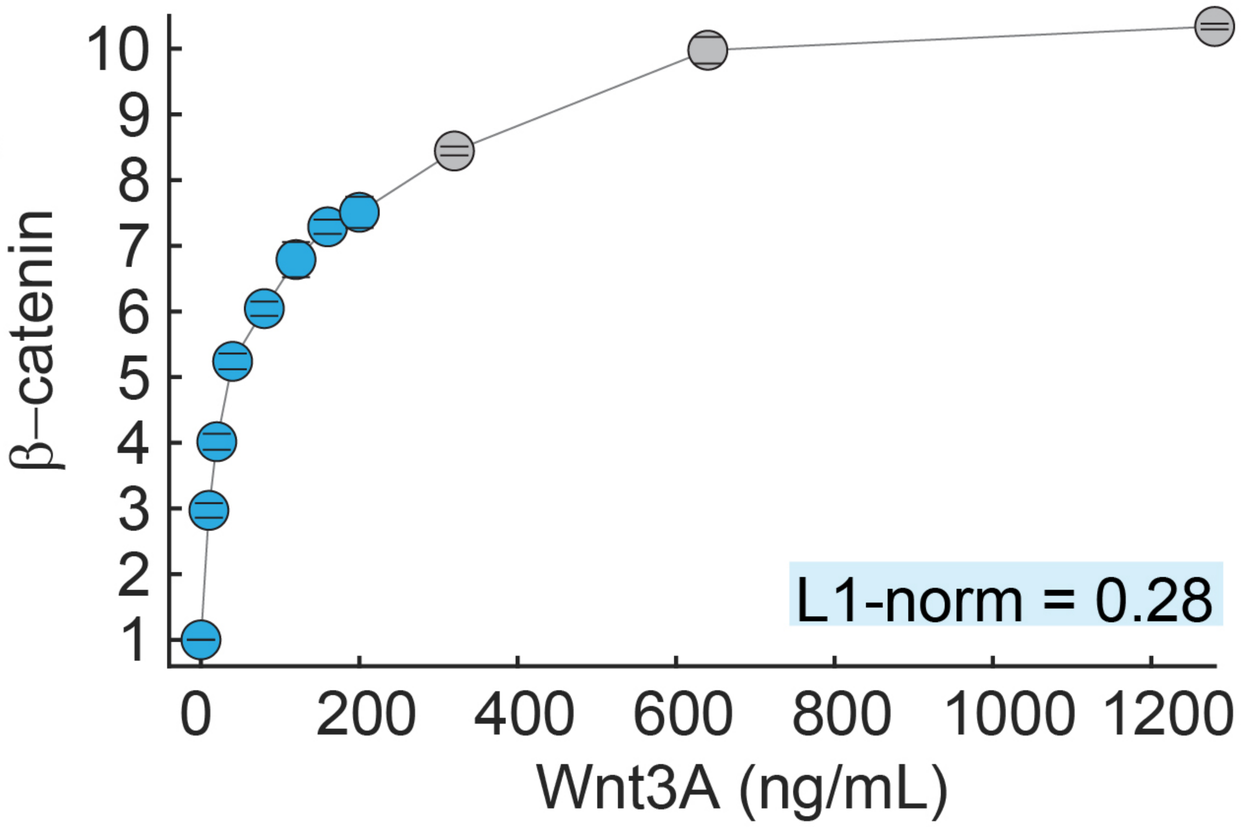

C. Wnt3A dose response for phospho-LRP5/6
1μM CHIR99021

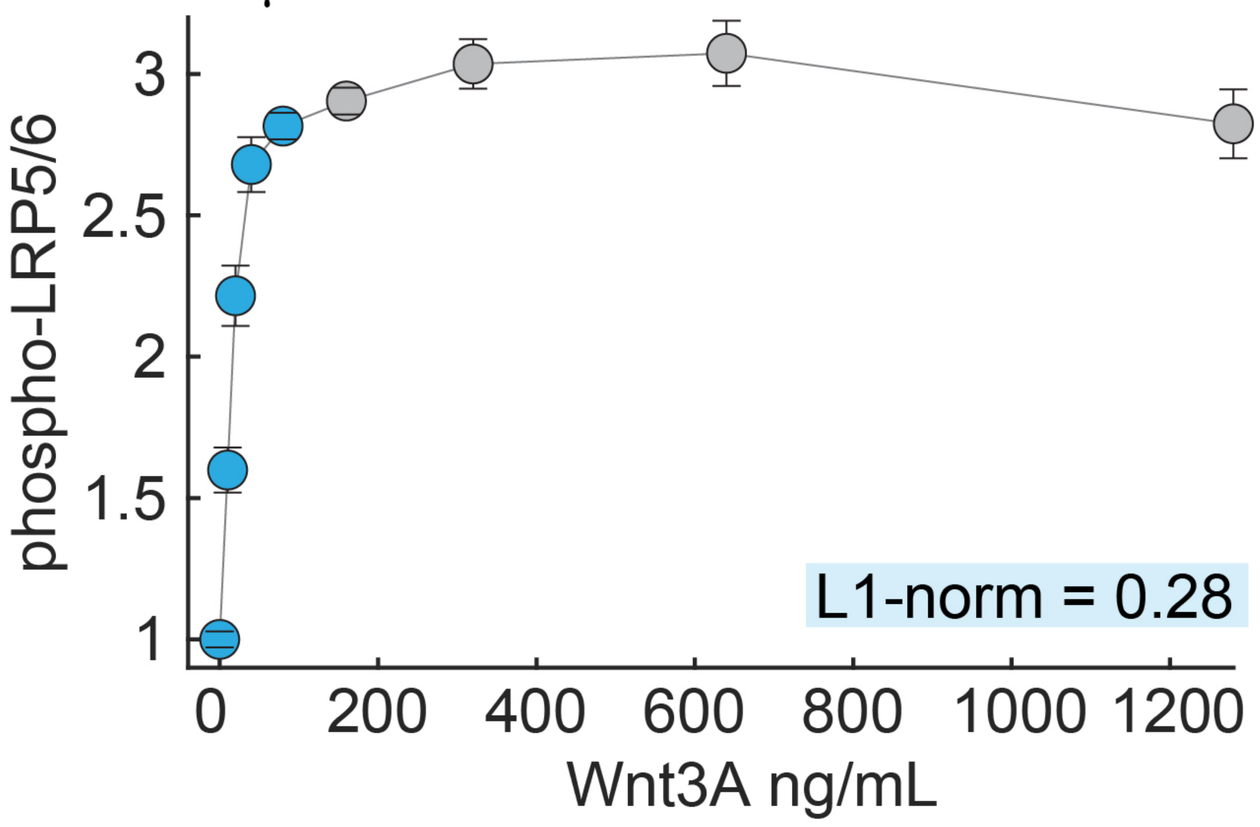

D. Wnt3A dose response for β-catenin
1μM CHIR99021

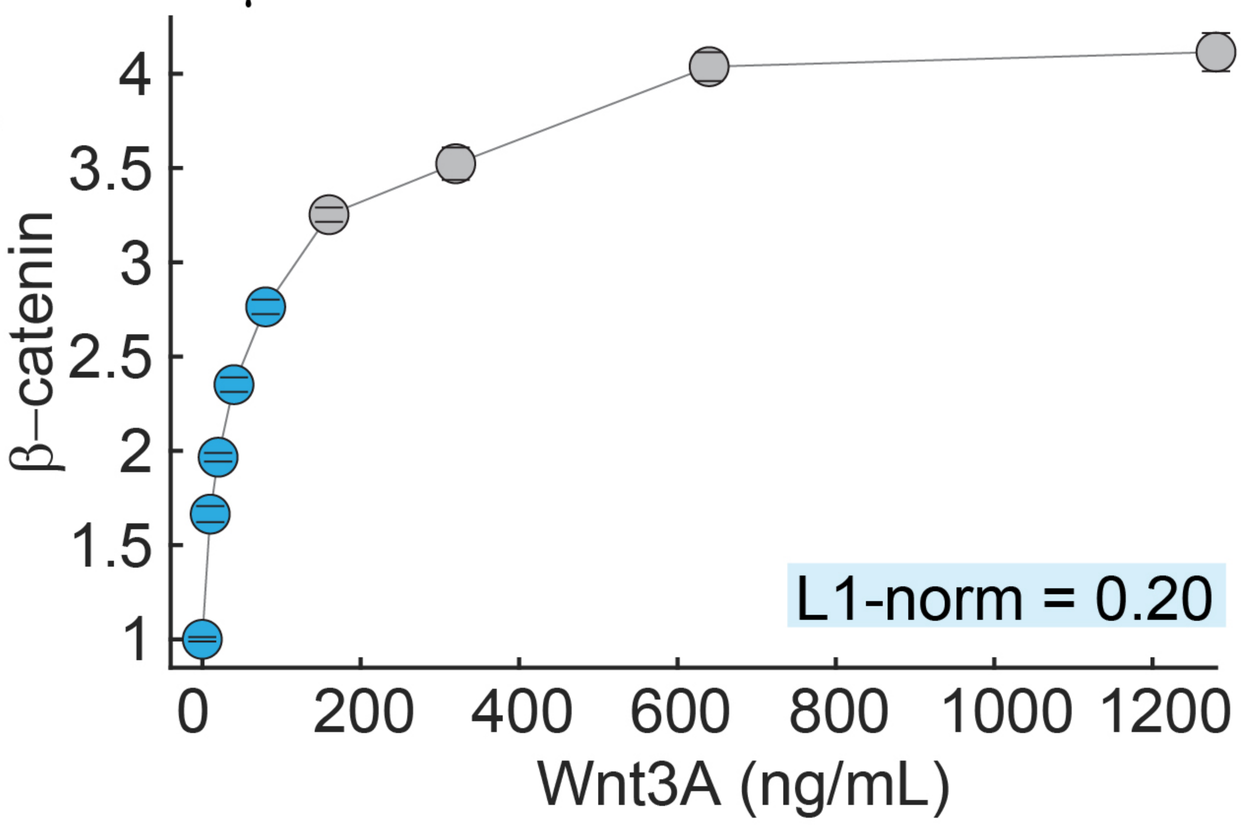

E. phospho-LRP5/6 level for 160 ng/mL Wnt3A

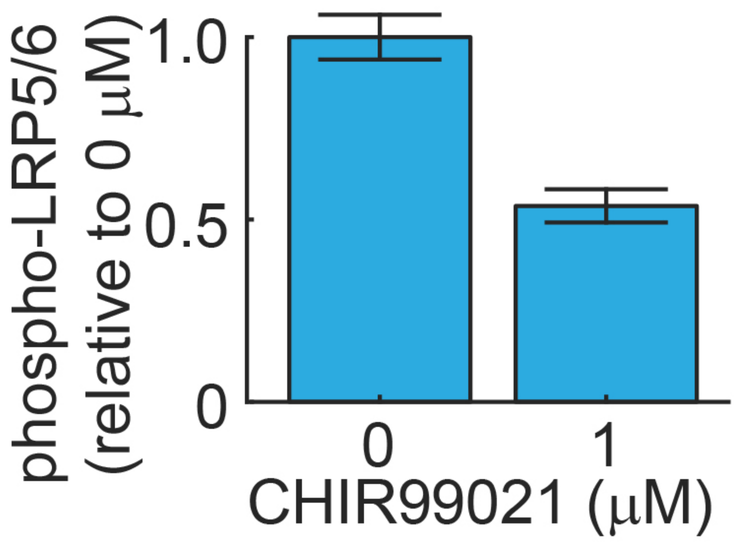

A. Timecourse of ERK activation

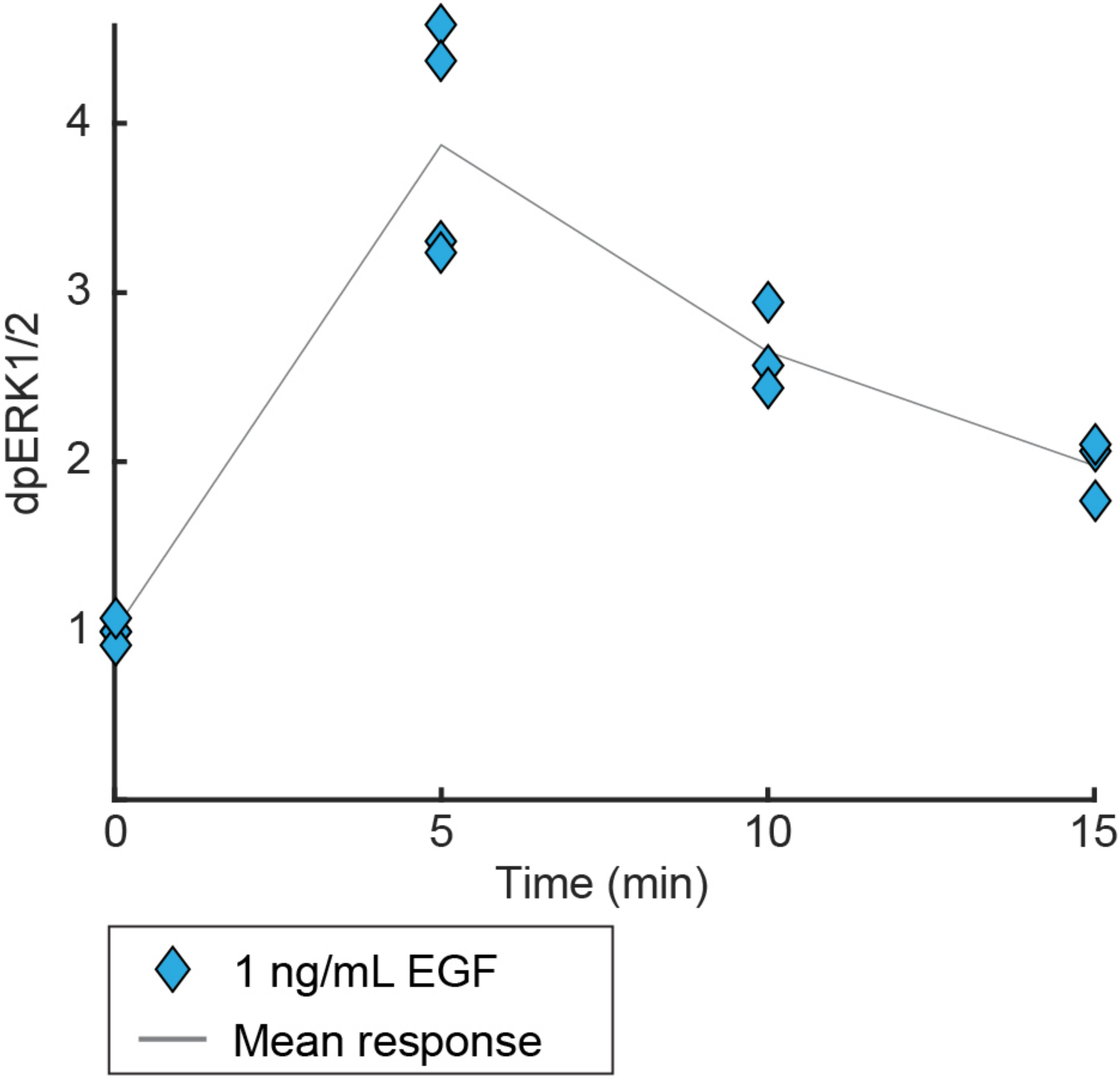

A

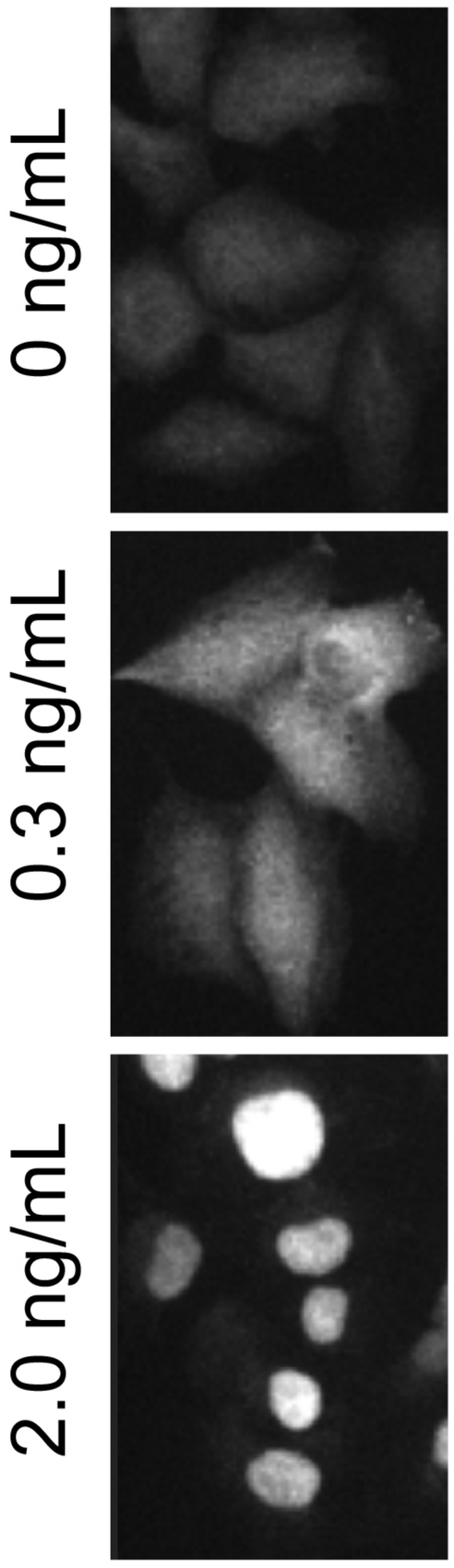
0 ng/mL
0.3 ng/mL
2.0 ng/mL

B

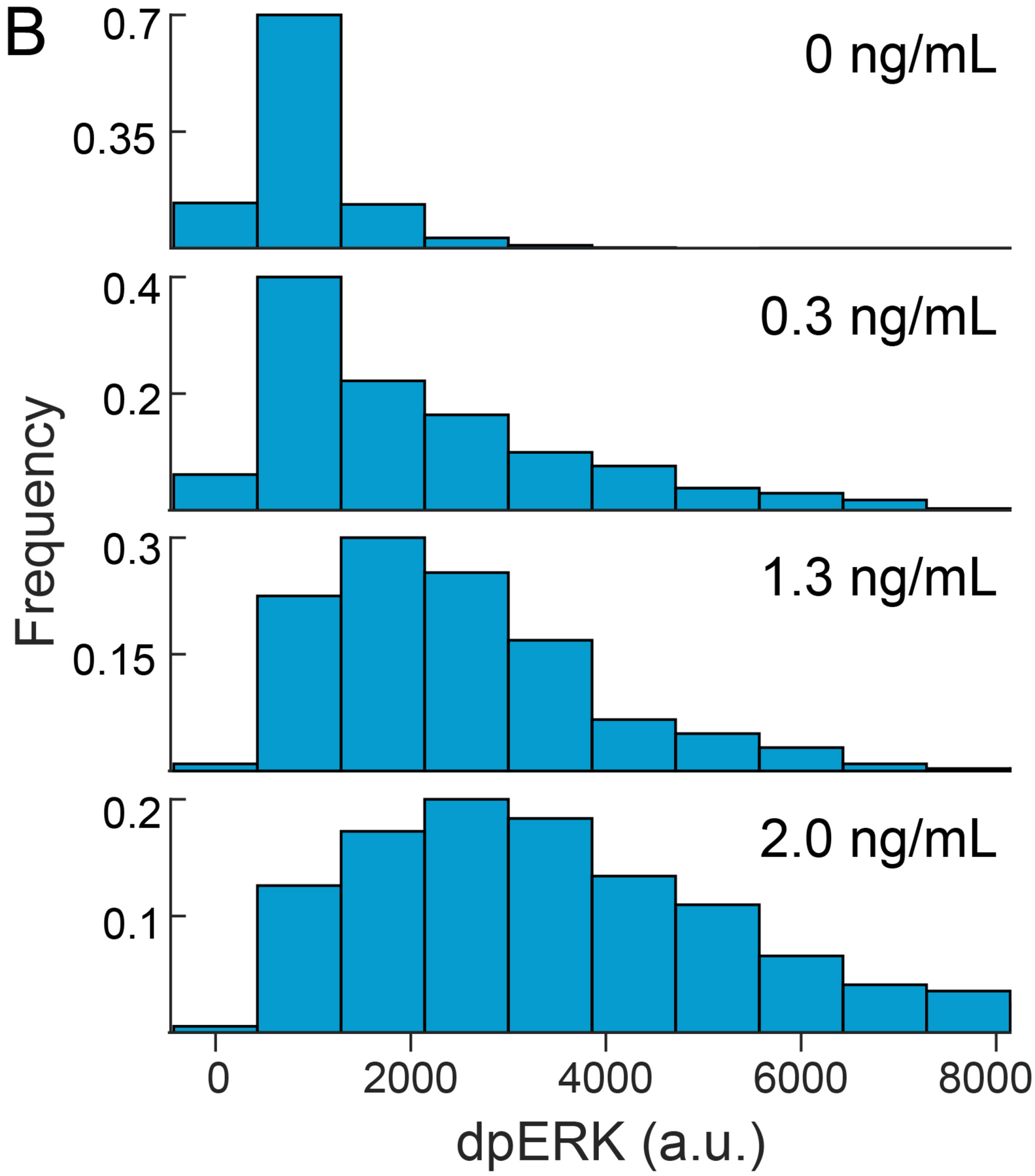
0.7
0.35
0 ng/mL
0.4
0.2
0.3 ng/mL
Frequency
0.3
0.15
1.3 ng/mL
0.2
0.1
2.0 ng/mL
0
2000
4000
6000
8000
dpERK (a.u.)

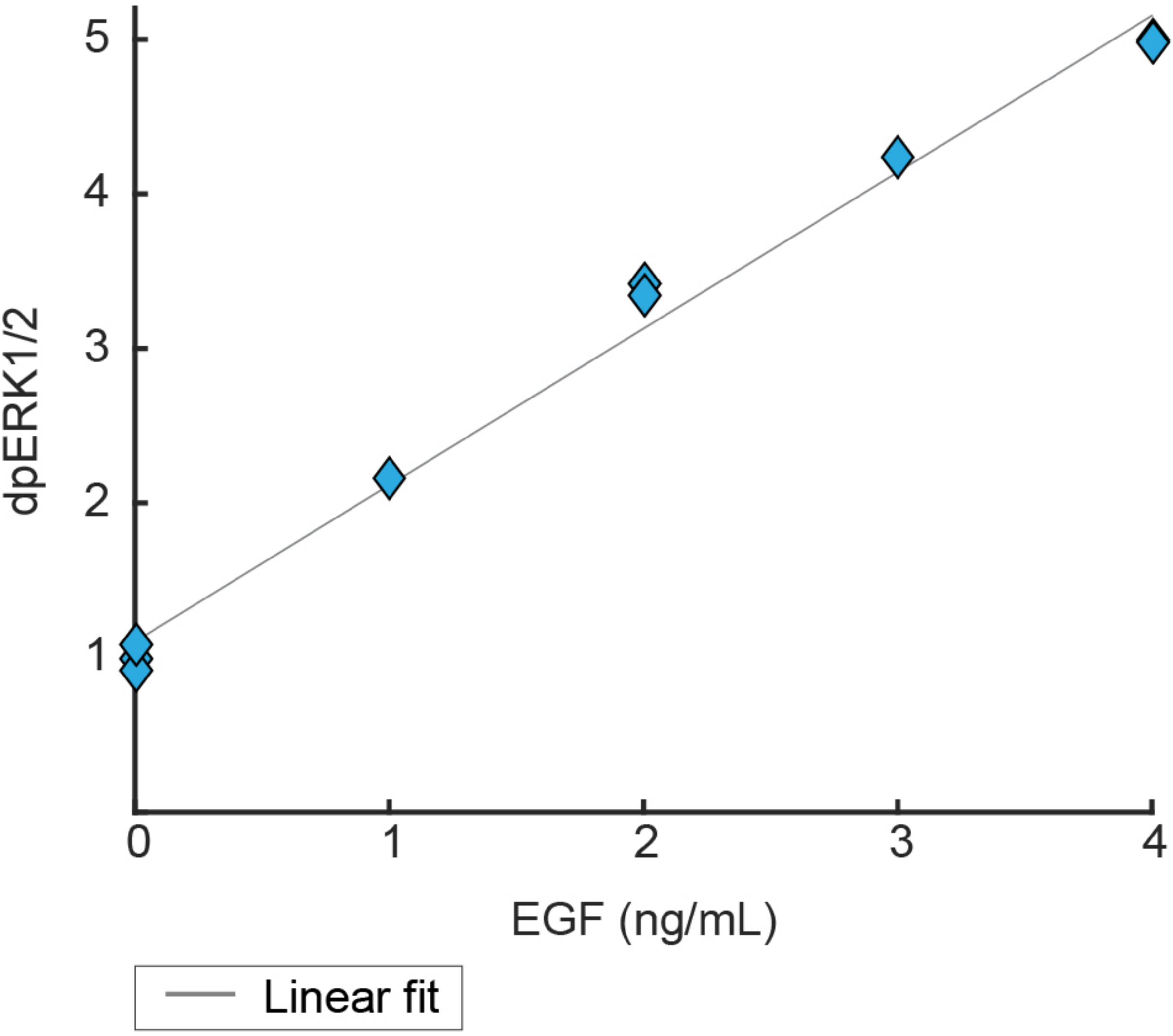
WT Raf-1 overexpression
dpERK1/2
5
4
3
2
1
0
1
2
3
4
EGF (ng/mL)
Linear fit

Raf S29/289/296/301/642A

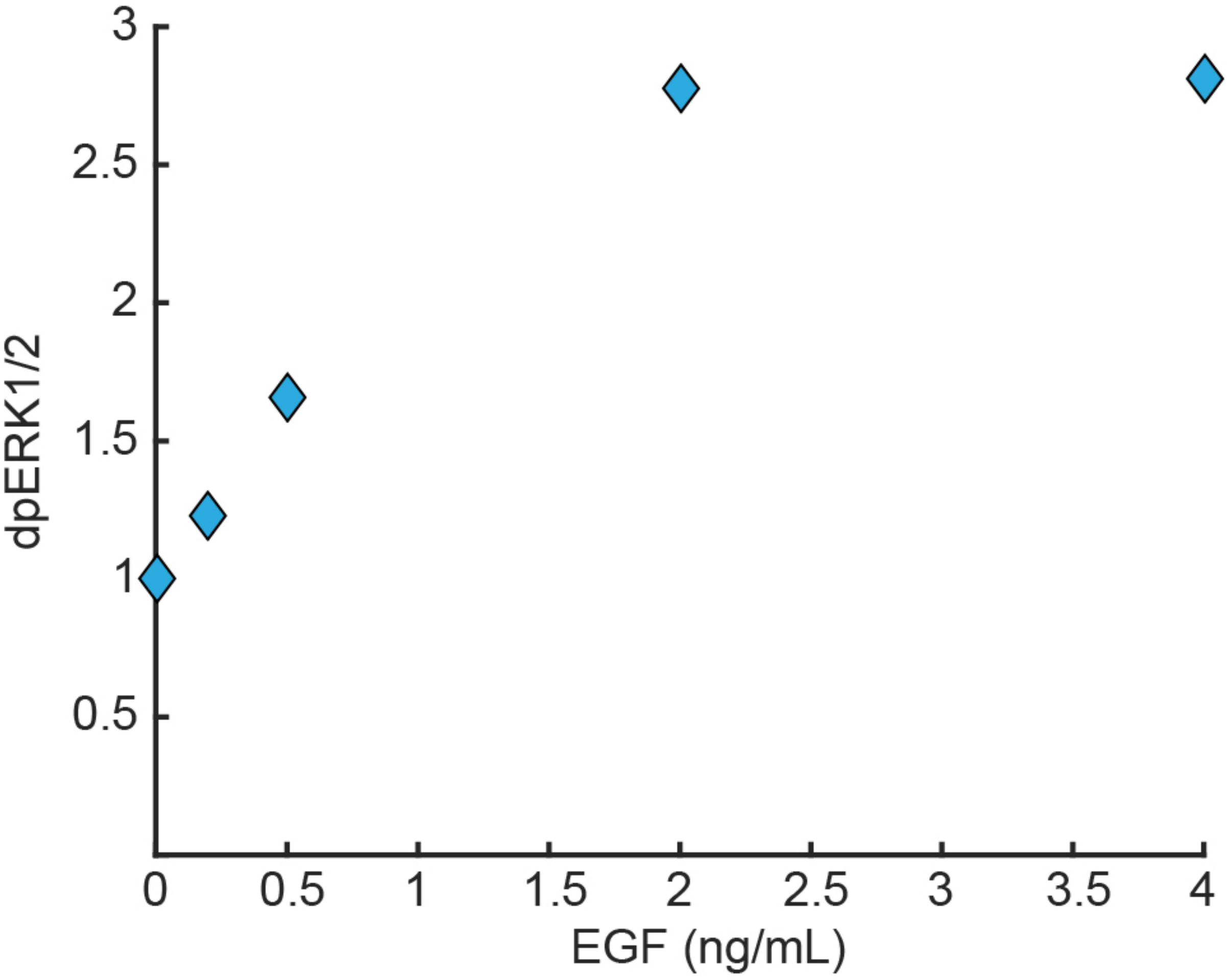

A. Single gel, lane-to-lane variability

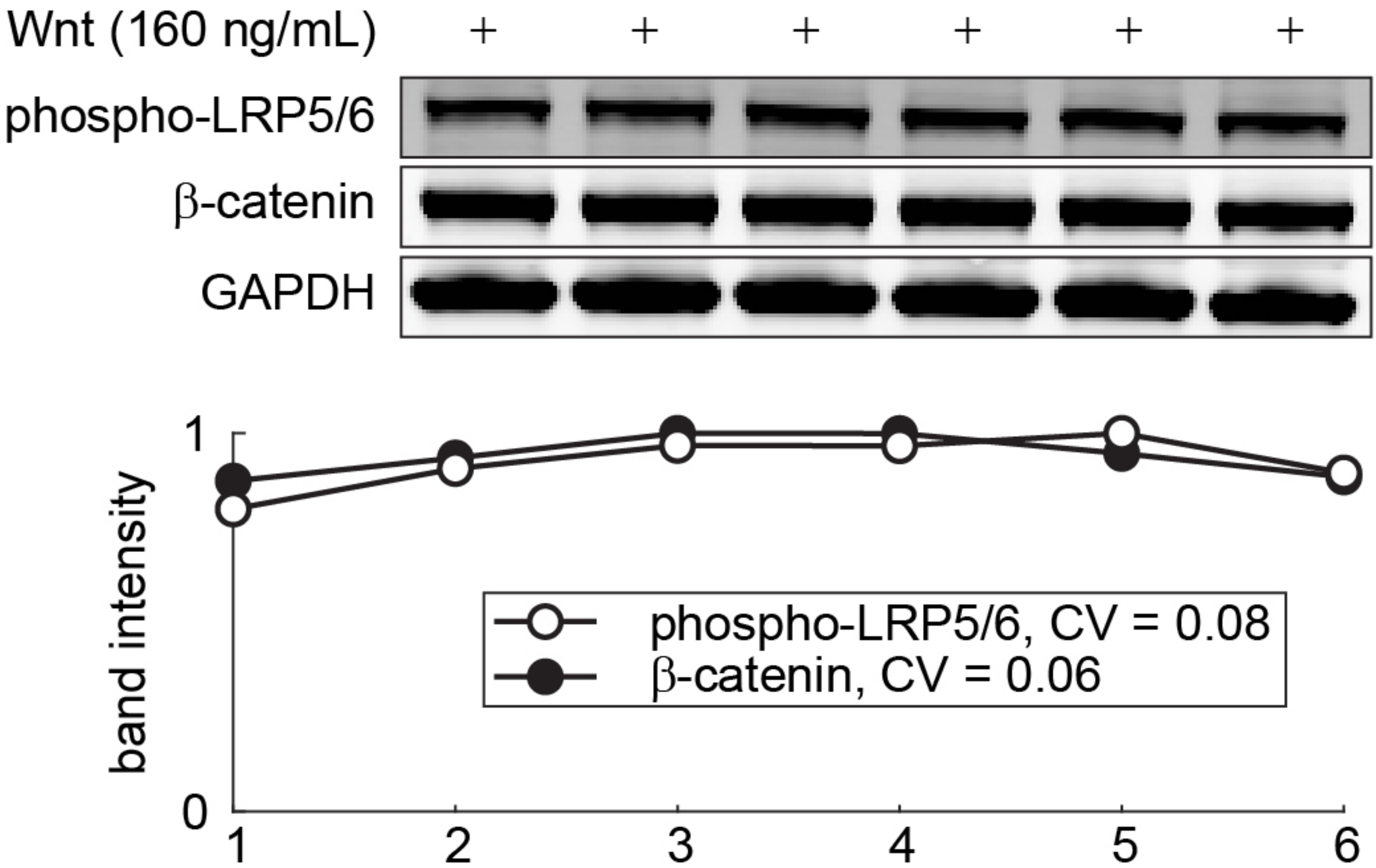

A. Multiple gels, gel-to-gel variability

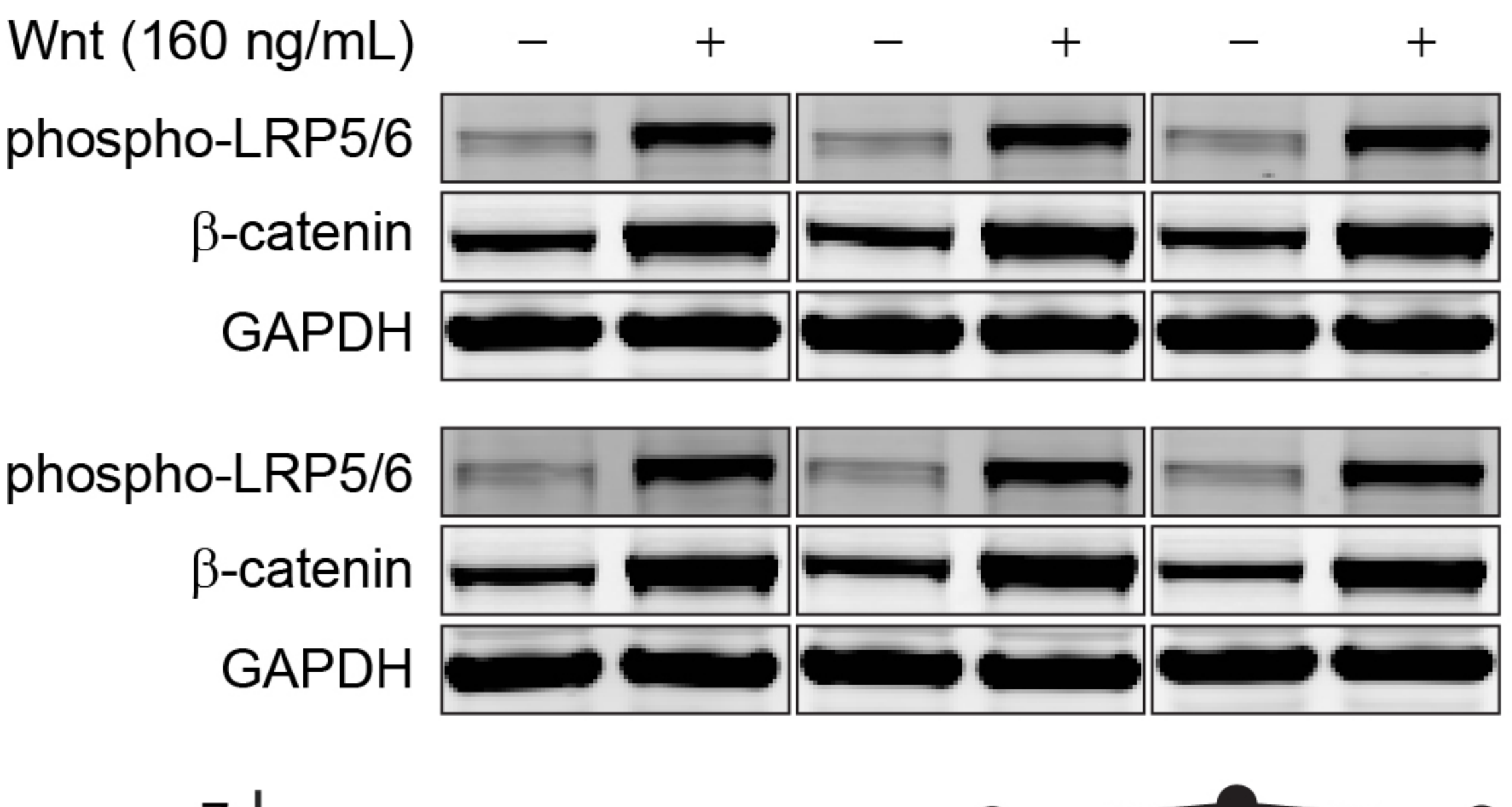

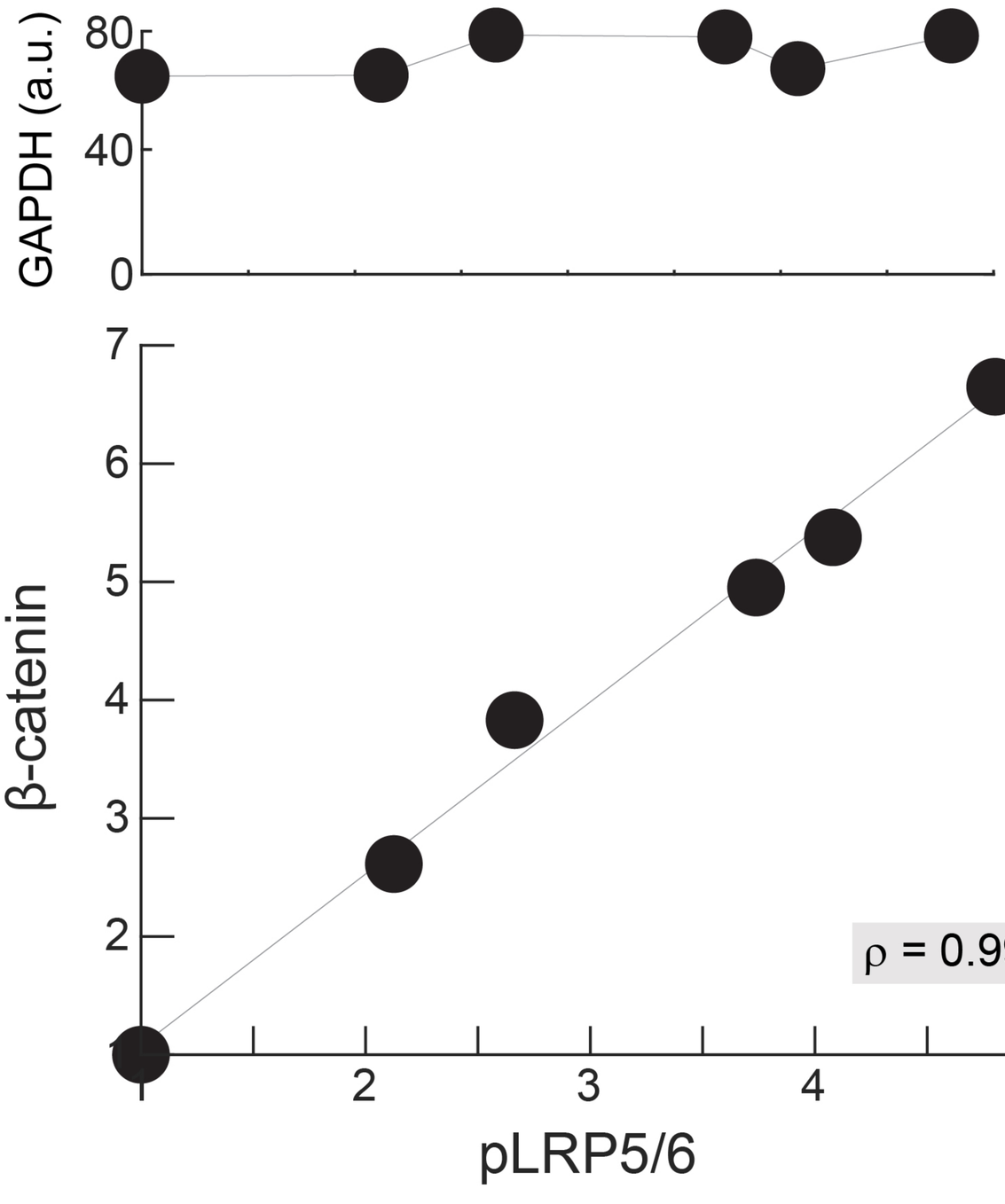
GAPDH (a.u.)
80
40
0

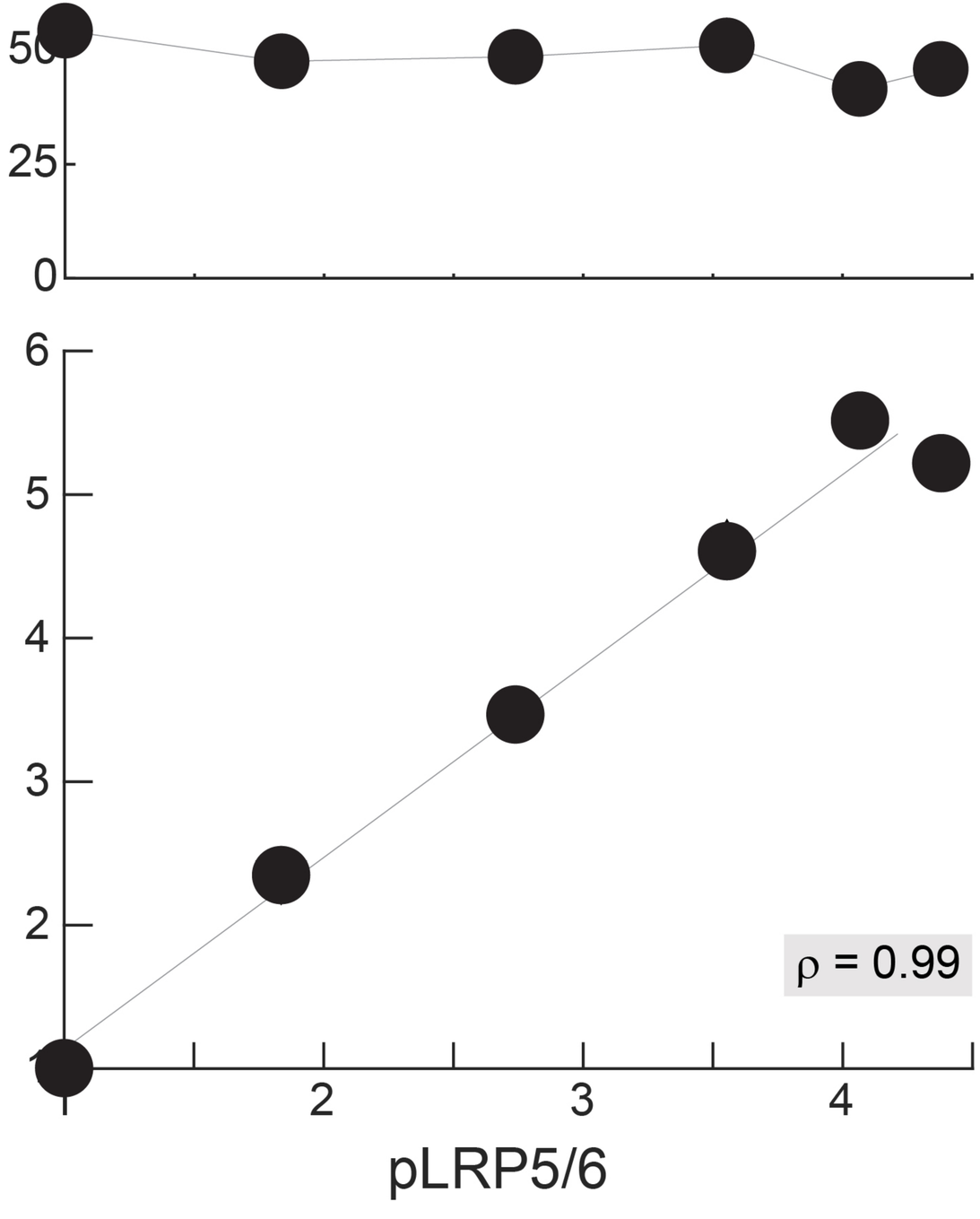
50
25
0

β-catenin
7
6
5
4
3
2
2
3
4
5
pLRP5/6
ρ = 0.99

6
5
4
3
2
2
3
4
pLRP5/6
ρ = 0.99

A. Wnt Pathway

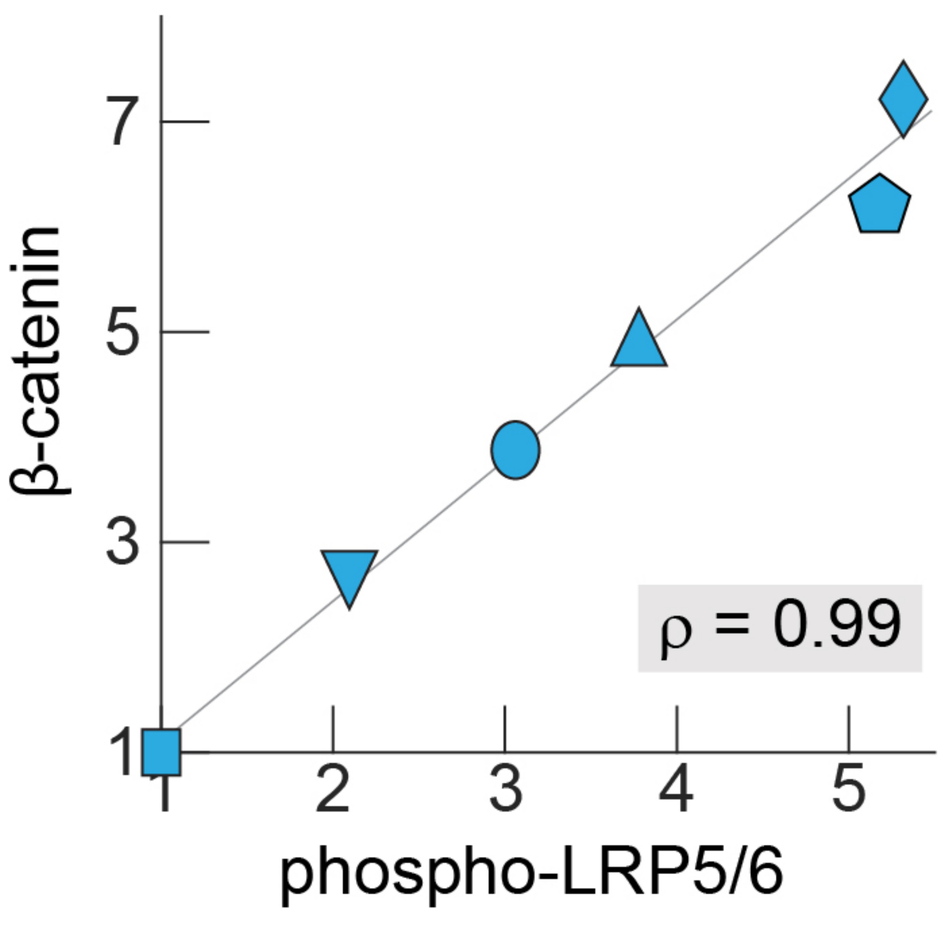

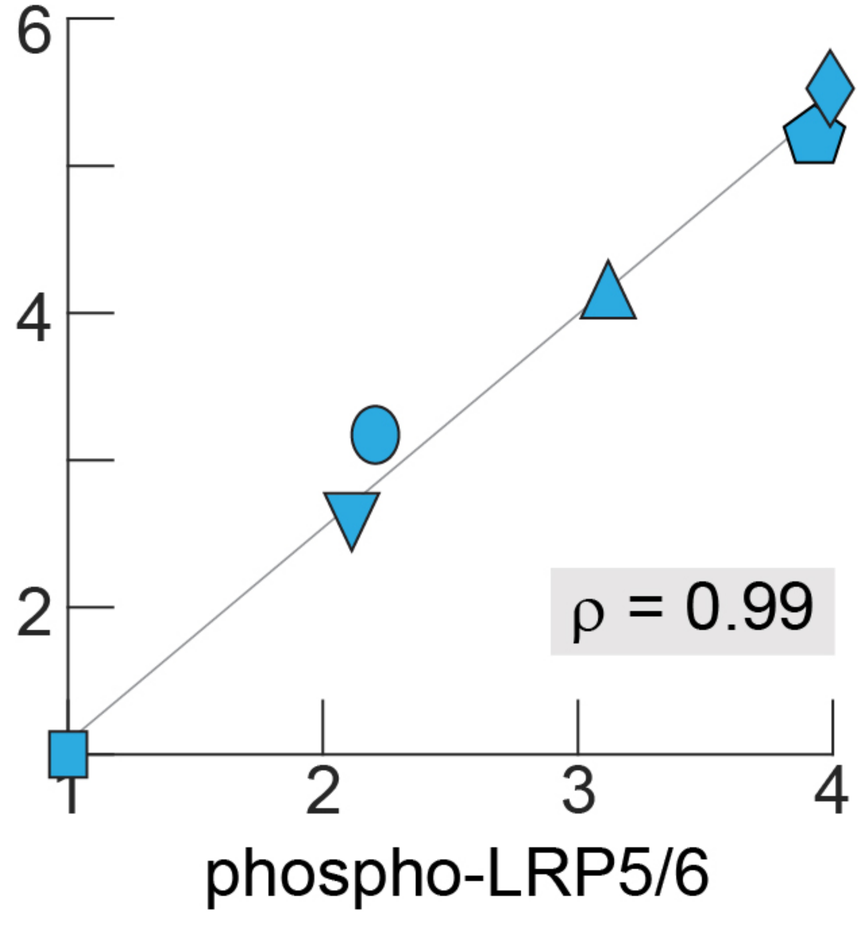

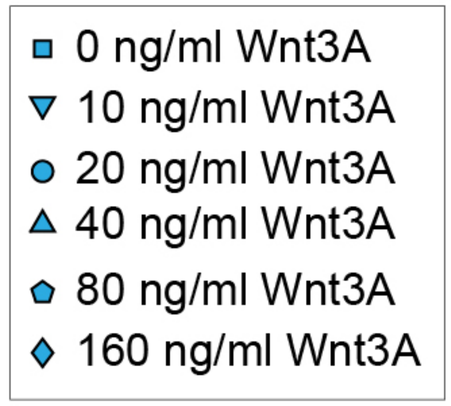
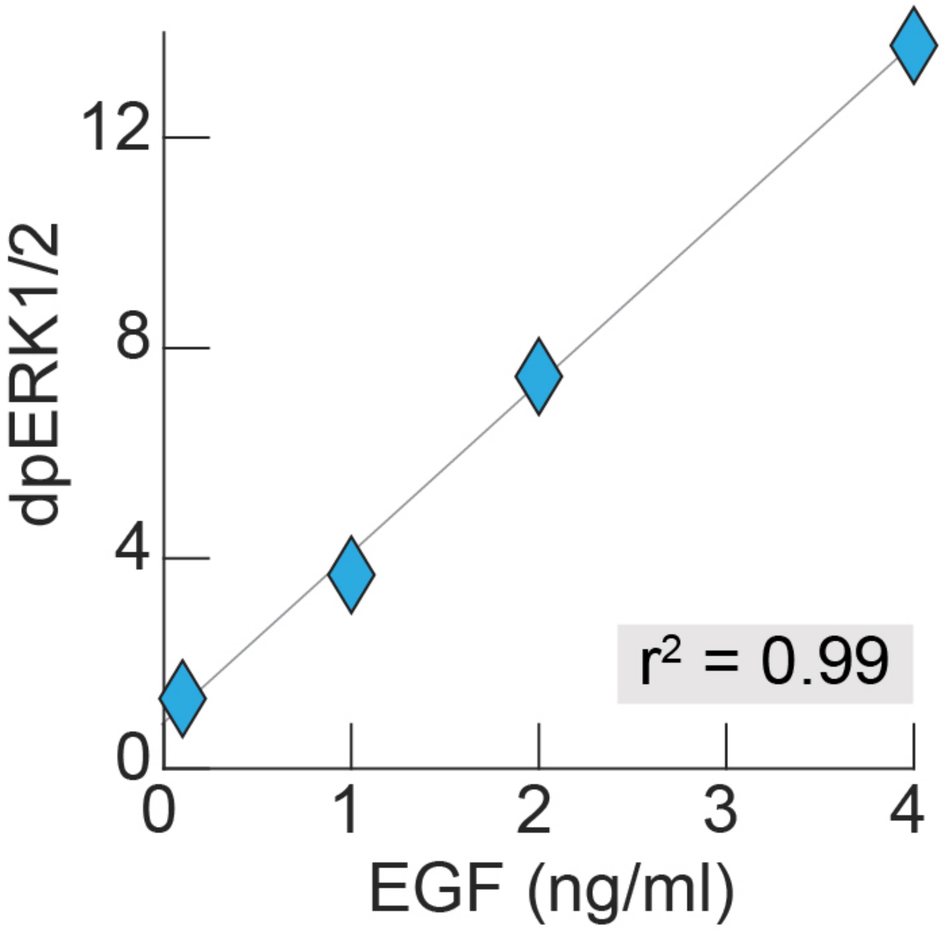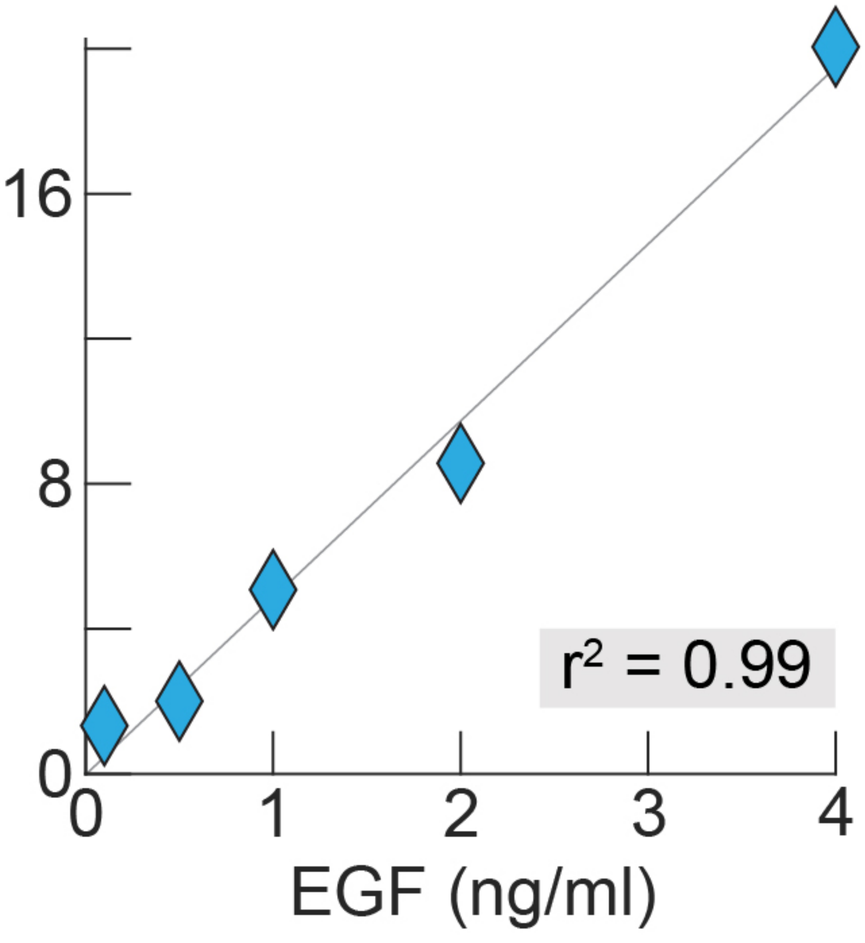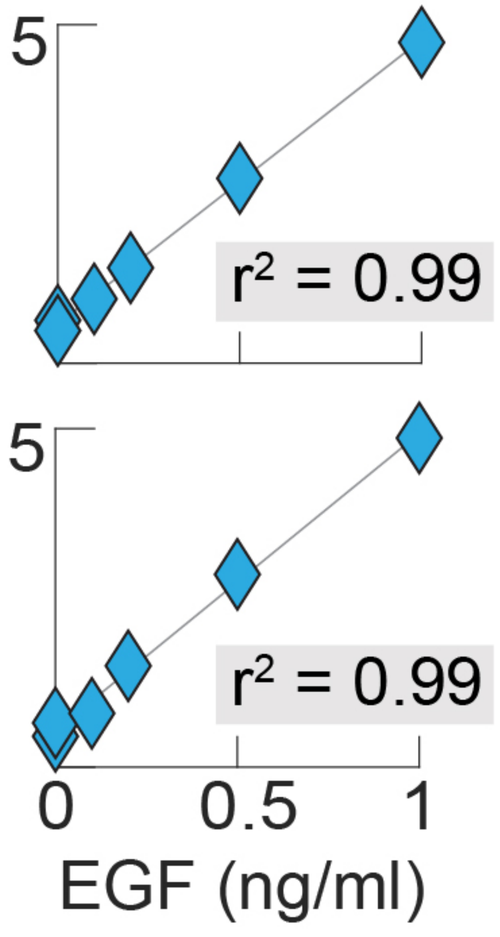
B. ERK Pathway